MULTIPLE GENERATIONS OF DOLOMITIZATION IN THE CATOCHE FORMATION OF PORT AU CHOIX, NEWFOUNDLAND

MICHAEL G. GREENE

MULTIPLE GENERATIONS OF DOLOMITIZATION IN THE CATOCHE FORMATION OF PORT AU CHOIX, NEWFOUNDLAND

by

© Michael G. Greene

A thesis submitted to the

School of Graduate Studies

In partial fulfillment of the

Requirements for the degree of

Master of Science

Department of Earth Science

Memorial University

March, 2008

St. John's, Newfoundland

ABSTRACT

The Catoche Formation of the St. George Group in the Port au Choix area consists of about 123 m of limestone overlain by 38 m of dolostone. Deposited on a shallow carbonate platform in subtidal to peritidal settings, the upper 38 m of the Catoche Formation has undergone multiple phases of dolomitization. A fabric-retentive micritic dolomite (D1) replaces limemuds. The preservation of mud laminae and near-micritic grain size implies that dolomitization began early after deposition. Dolomite 2 (D2) replaces peloidal packstone/grainstone and wackstone and exhibits two ranges of crystal sizes, subhedral to euhedral crystals that range from 50 to 120 μm and anhedral to euhedral crystals that range between 150 to 250 μm. Crystals belonging to D2 commonly have cloudy Fe-rich cores with clear Fe-free rims. Locally crystals have well developed faces and are associated with abundant intercrystalline porosity suggesting a limited supply of Mg^{+2} at the time of dolomitization. Overprinting early dolomite generations is a locally developed stylolite-related dolomite (D3). Crystals found along stylolites are generally subhedral to euhedral and range in size from 70 to 150 μm. A replacement and pore-filling euhedral to sometimes anhedral dolomite (D4) commonly occludes vugs and typically may reach several millimeters in size. Rare saddle-dolomites (D5), 300 to 600 μm in size, exhibit sweeping extinction and tend to occlude biomolds, veins but rarely lines vugs.

Trace element distribution shows an increase of Sr with depth for D1 and D2 suggesting a possible downward movement of the early dolomitizing fluids for the respective dolomite generations. Dolomite 1 has a Sr/Ca molar ratio that ranges from 0.0037 and 0.00094 suggesting an origin from a mixed meteoric/seawater source. Stable isotopes calculations yield a range of -10.7 to -6.4‰ SMOW and agree with a mixed meteoric/seawater source for the earliest dolomitizing fluid. Microthermometric measurements recorded from D4 indicate a temperature of formation ranging from 89.2 to 99.5°C suggesting deposition at significant depth. Oxygen isotope signatures for the dolomitizing fluid associated with D4 yield a range from -1.2 to 2.4‰ SMOW and suggest an origin derived from evolved diagenetic waters.

This work is dedicated to my parents,

Clarence and Linda Greene, for their love and

support.

ACKNOWLEDGEMENTS

The author wishes to express his sincere appreciation to Dr. Karem Azmy for his supervision at all stages of study and critical reading of the thesis. Thanks are extended to the Panatlantic Petroleum Systems Consortium (PPSC) for funding this project. Gratitude is expressed to Dr. Ian Knight from the Department of Natural Resources, Newfoundland and Labrador for field assistance, discussion and use of regional maps and logs. Alvin Harris from the Department of Natural Resources, Newfoundland and Labrador provided assistance handling and sampling core from the Springdale core-storage library. Mr. Erik French provided valuable field assistance and aided in the collection of samples used in this thesis.

Dr. Nigel Blamey from the National University of Ireland assisted in the collection of fluid inclusion data used in this study. The author also wishes to thank Allison Pye from the Stable Isotope Lab and Wilfredo Diegor from the LA-ICPMS Lab at Memorial University. Dr. John Hanchar provided assistance and equipment utilized for the cathodoluminescence study in this thesis. Mr. Steve Schwartz provided insightful discussion concerning the subject matter.

TABLE OF CONTENTS

LIST OF FIGURES

LIST OF TABLES

LIST OF PLATES

CHAPTER 1

INTRODUCTION

1.1 PURPOSE AND SCOPE OF STUDY

The St. George Group of Western Newfoundland consists mainly of peritidal carbonates of epeiric early Ordovician seas (Pratt and James, 1986). Deposition was paused by a major subaerial exposure resulting in the formation of the St. George Unconformity, which caused intensive karstification particularly in the uppermost part of the succession (Knight, 1991; Knight et al, 1991; Baker and Knight, 1993; Langdon and Mireault, 2004). These carbonates were affected later by significant diagenetic processes and multiphase dolomitization events (e.g., Haywick, 1984; Lane, 1990; Cooper et al., 2001). The occurrence of stratigraphically adjacent Upper Cambrian – Lower Ordovician organic-rich shales (Cow Head Shales, possible potential source rocks) and impermeable Middle Ordovician layers at the top of the sequence (Table Point Limestone, seal rock) as well as the structural framework developed by the Acadian orogeny (Cooper et al., 2001) makes the sequence a potential candidate for oil accumulations (e.g., Kerans, 1989). This is also consistent with the field observations of live kerogen seeps in the outcrops and oil production from earlier preliminary drillings (cf. Cooper et al., 2001).

The Catoche Formation is the focus of the current study. Earlier studies (Haywick, 1984; Lane, 1990; Knight, 1991; Knight et al, 1991; Baker and Knight, 1993) suggested that the Catoche Formation was affected by multiphase dolomitization mainly caused by diagenetic fluids of hydrothermal origin. The main objectives of this study are to:

1- Investigate the sedimentology and petrography of the Catoche dolomites

2- Investigate the diagenetic history and evaluate the reservoir potential of these carbonates

3- Investigate the geochemical attributes of the Catoche dolomite to better understand the influence of diagenesis on the porosity development.

1.2 GEOLOGICAL SETTING

1.2.1 *Location and Paleogeography*

The Lower Paleozoic St. George Group of Western Newfoundland extends approximately 400 km from the Port au Port Peninsula to Cape Norman on the Great Northern Peninsula (**Fig. 1.1**). The lower part of the Catoche Formation, the focus of this study, has been sampled from its well exposed outcrops in the Port au Choix area along the coast (Catoche reference section of Knight and James, 1987) due to easy access and completeness of the section. The upper part of the formation, approximately 40 m (**Figs. 1.2, 1.3 and 1.4**) was sampled from the Core PC 79-2 (477280E, 5616720N).

The Catoche Formation in Port au Choix consists of shallow water platform carbonates that were deposited on in an open-shelf, subtidal setting during the Arenig transgression over an epeiric platform (Knight et al., 1991). Lower basal limemuds are associated with possible storm-generated gravel bars and/or tidal deposits, and tidal muds (Knight and James, 1987). These limemuds are overlain by a lower energy, open, subtidal shelf setting carbonate sediments. The upper ~40m of the Catoche Formation is a series cyclic, shallowing upward, meter scale peloidal grainstone cycles interpreted as

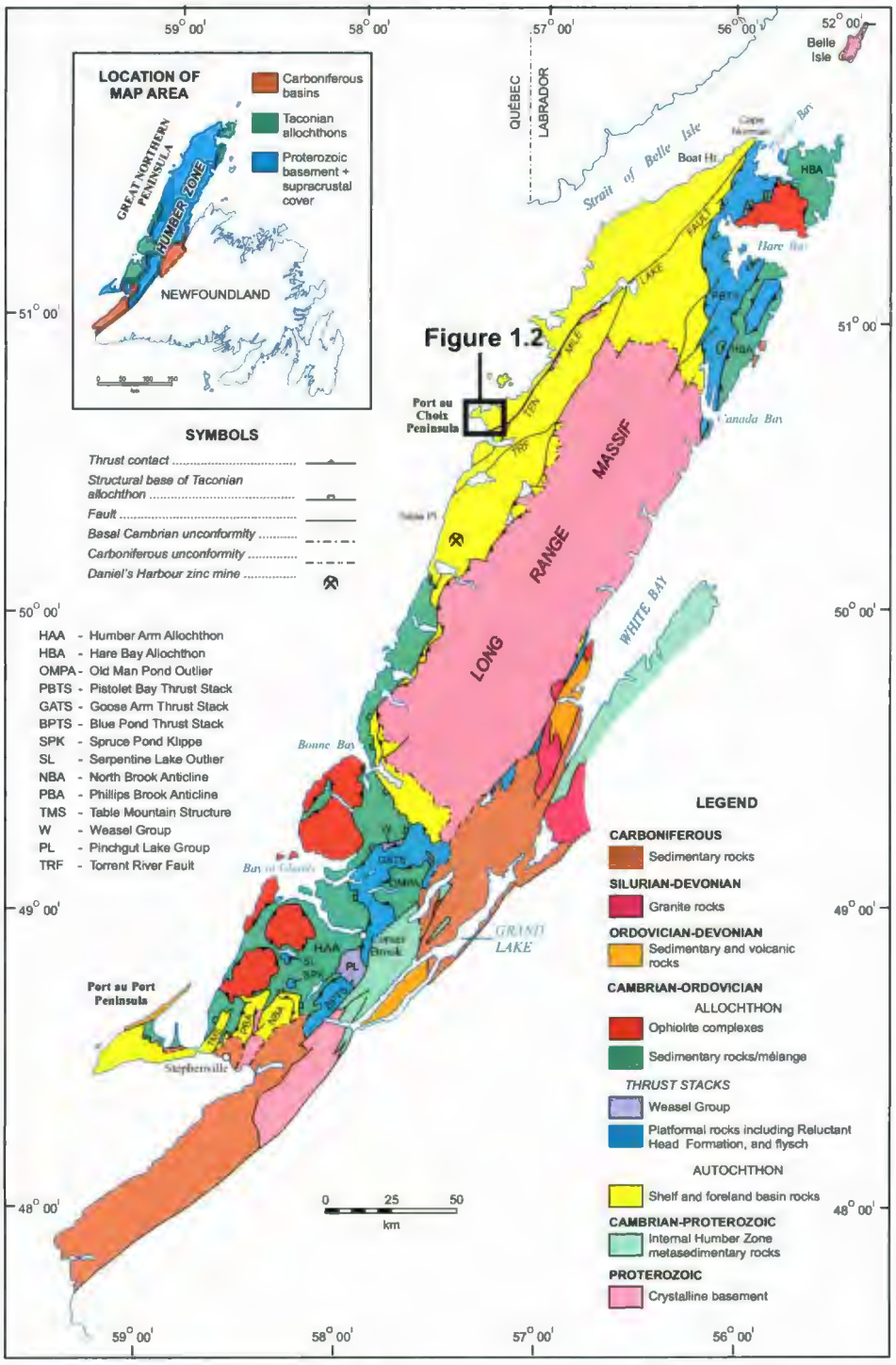

Fig. 1.1. Geological map of western Newfoundland displaying the study area on the Port au Choix Peninsula (Knight et al., 2007).

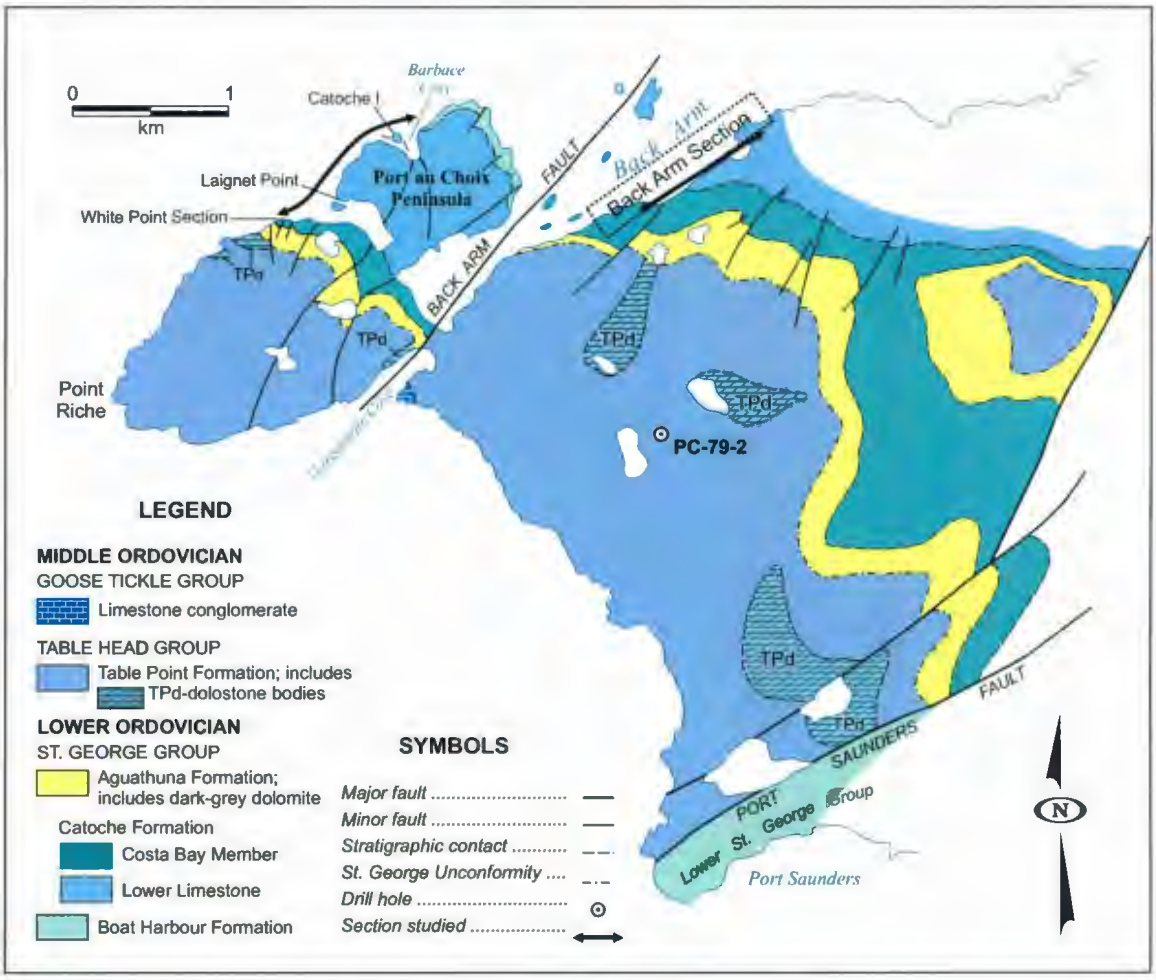

Fig. 1.2. Geological map of the Port au Choix Peninsula study area. Note location of Catoche outcrop on the northwest coast and drill-hole PC-79-2 further inland (Knight et al., 2007).

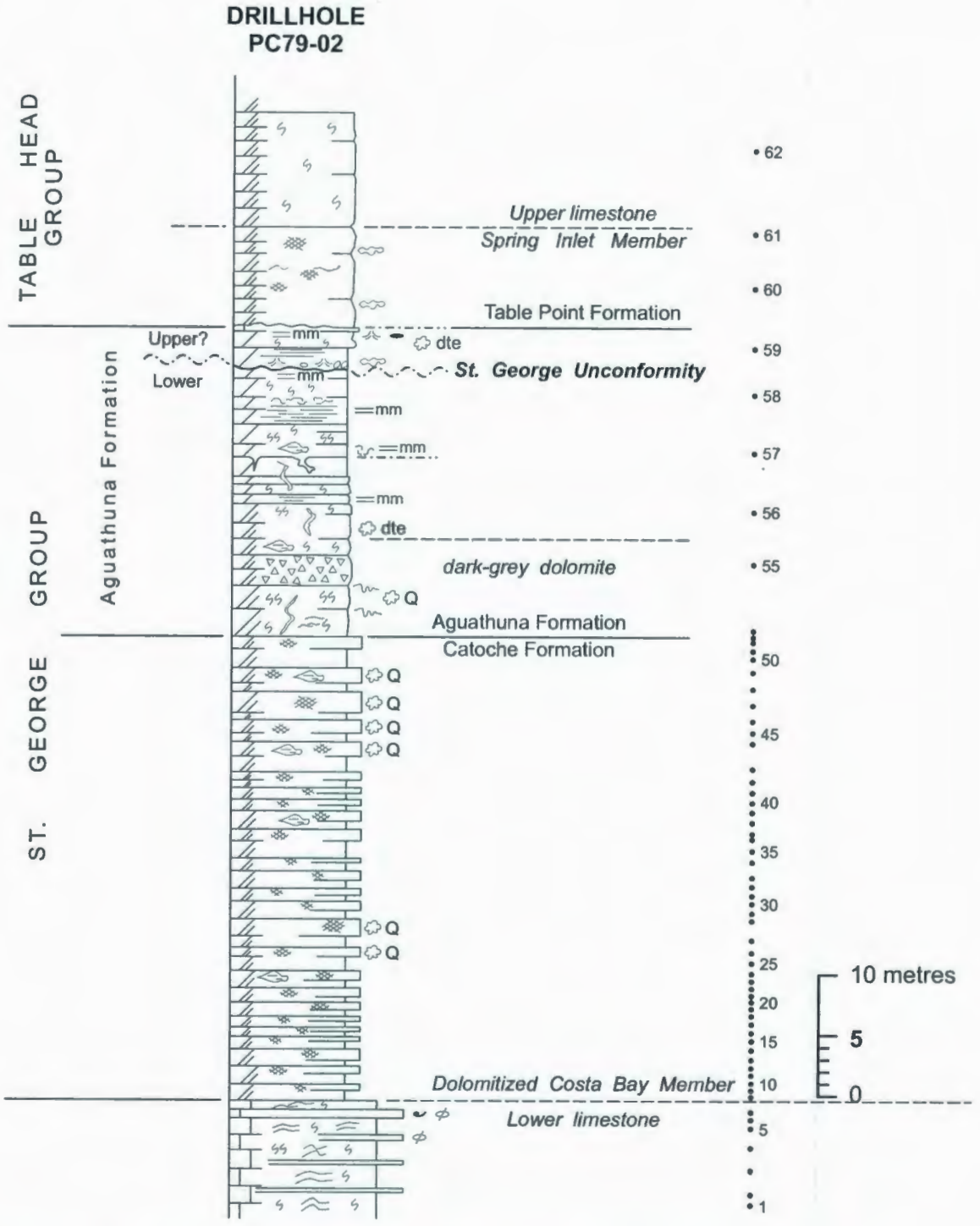

Figure 1.3. Detailed lithological log with sample locations of the Catoche Formation from Core PC79-02 (Knight et al., 2007).

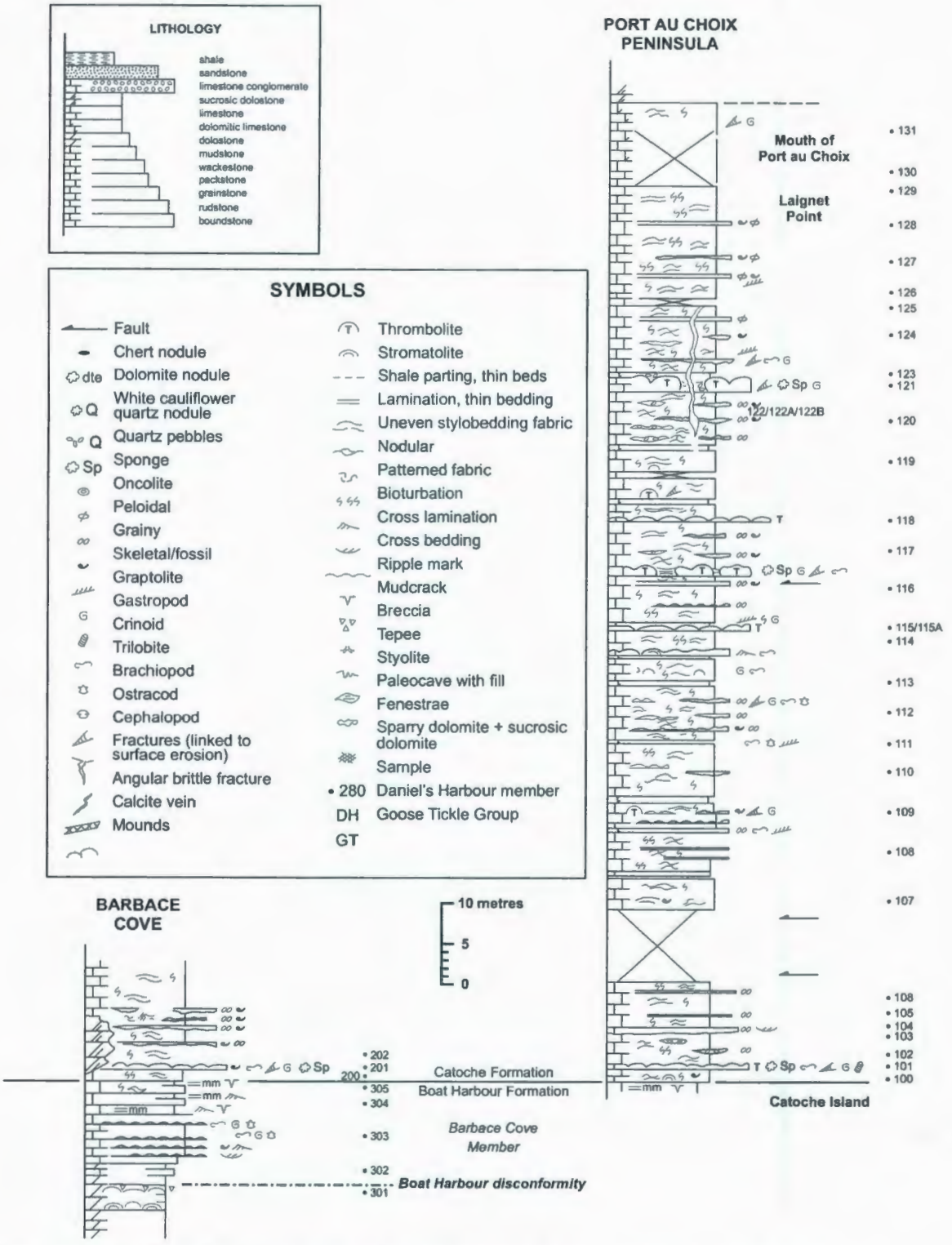

Figure 1.4. Detailed lithological log with sample locations of the Catoche Formation on the Port au Choix Peninsula (Knight et al., 2007).

peloidal sand shoals which have undergone extensive dolomitization (Knight, 1991; Knight et al, 1991; Baker and Knight, 1993, Knight et al, 2007).

1.2.2 *Geotectonics*

The Taconic and Salinic Paleozoic orogenies affected the Early to Middle Ordovician St. George Group sediments in western Newfoundland. The effect of the Taconic Orogeny (**Fig. 1.5**) is shown in the Cow Head Group (bed 10) which was deposited as gravity flows originating from the slope triggered by seismic shocks (James and Stevens, 1986) caused by an approaching foreland bulge associated with the closing of the Iapetus Ocean and convergence of Iapetus with Laurentia, coupled with highstand shedding of conglomerates on the continental margin slope (James et al., 1989 and Knight et al., 1991). On the platform, the relative subsidence slowed resulting in the deposition of peloidal sand shoals (Costa Bay Member). As a result of significant loading of material in the fore-arc trenches, the distal lithospheric response resulted in an upward deflection, or a foreland bulge. As the volcanic arc and its trench moved closer to Laurentia, the bulge migrated west across the slope and platform. During the late Ibexian, the platform edge was uplifted restricting circulation during the deposition of the Aguathuna Formation, which overlies the Catoche carbonates (**Fig. 1.6**). Synsedimentary northeast-trending faults formed at this time and local breccias developed below the surface of the platform in the already partially dolomitized Catoche Formation (Knight et al., 1991).

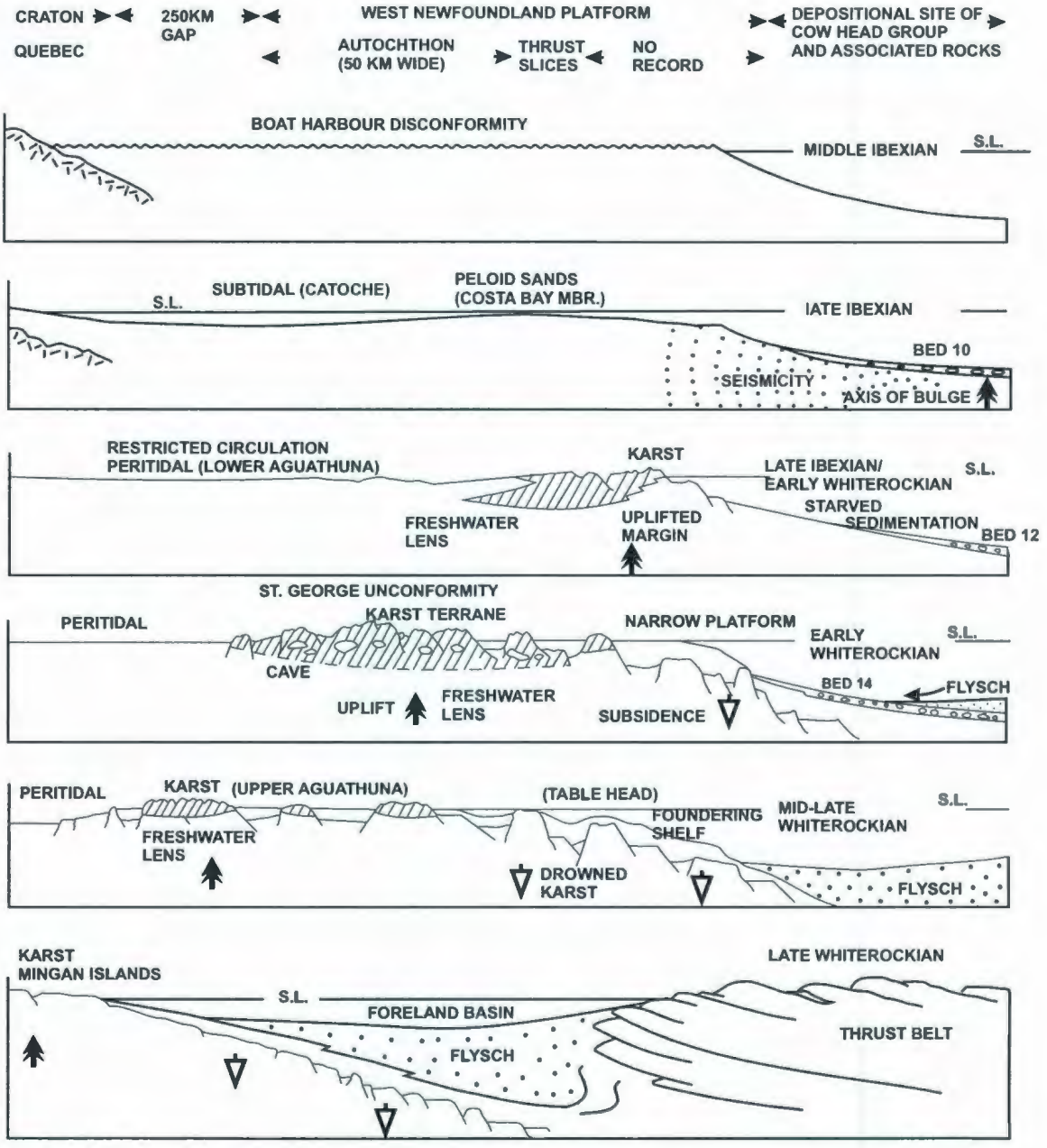

Figure 1.5. Simplified schematic of the effects of an encroaching periphal bulge on the Ordovician platform of western Newfoundland and Quebec (from Knight et al., 1991).

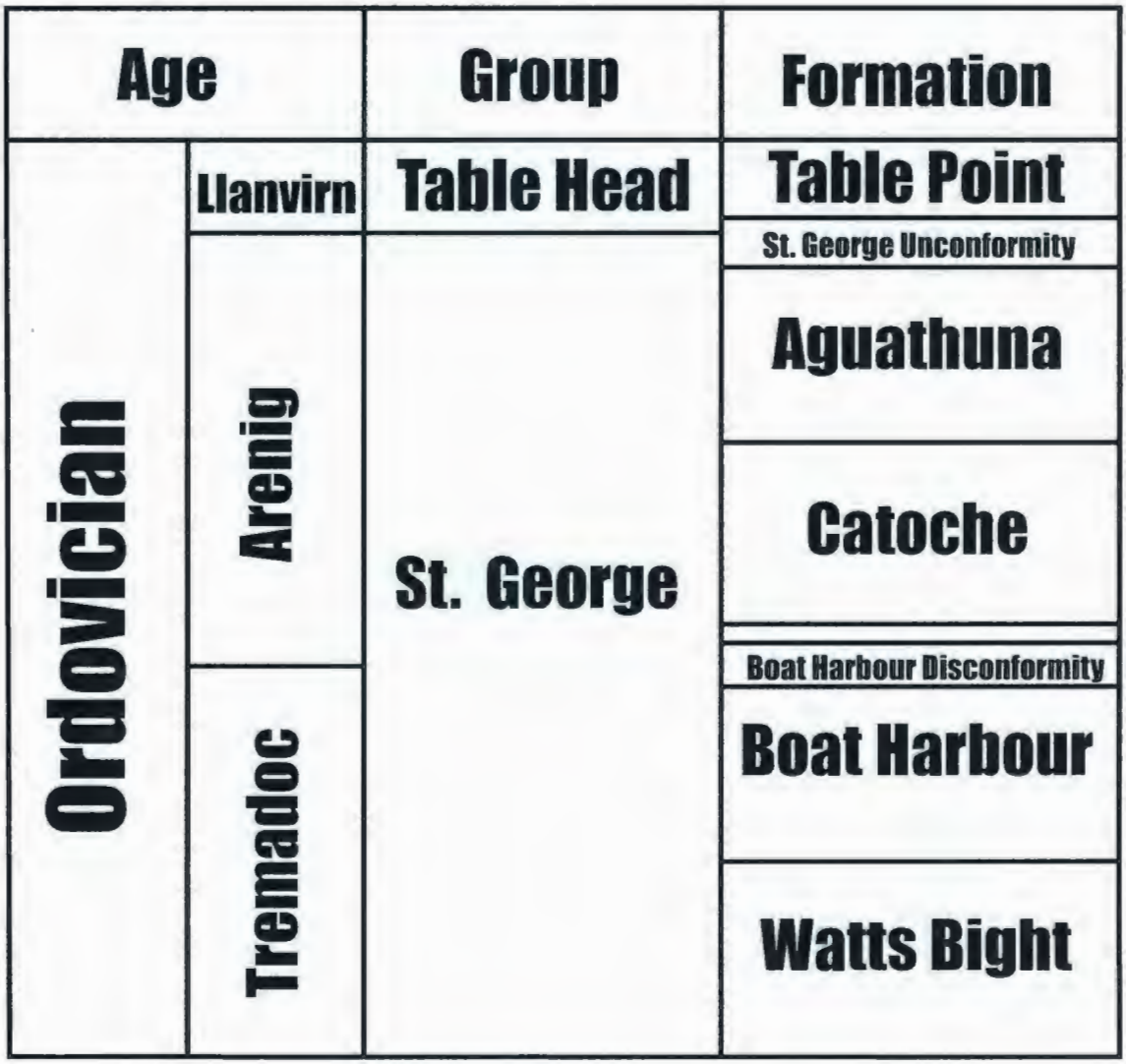

Figure 1.6. Simplified stratigraphic diagram of the St. George Group.

Uplift and further deformation of the platform is suggested to have occurred during the Salinic Orogeny in the Silurian and followed by a major erosion of the Taconic and Salinic flysch (Cawood et al., 1994; Knight, 1997).

1.2.3 *Reservoir Geology*

The major St. George unconformity is believed to have caused intense karstification and meteoric dissolution in the underlying layers of the Aguathuna and possibly down to the Catoche carbonates, which likely developed a significant porosity system. These pores worked as conduits for dolomitizing fluids, which affected the total porosity of the entire rocks. Catoche dolomites in the Port au Choix area have heterogeneous distribution of intercrystalline porosity and vugs, which causes high variability in ranges of the porosity and permeability characteristics of the rocks (Baker and Knight, 1993). Porosity measurements of samples from the BackArm section of Port au Choix range from 1.0% - 17.8% with horizontal permeabilities from 0.02mD to 317mD. Samples retrieved from the Pointe Blanche section yield porosity values of 6.8%-9.6% and horizontal permeability measurements of 0.19mD-224mD (Baker and Knight, 1993; Cooper et al., 2001). All samples that have peak porosity are from the dolomitized grainstones of the cyclic shallowing upward cycles. The concentration of fractures and brecciation strongly influences the reservoir characteristics where fractures can connect vugs and pores to create a very permeable network (Baker and Knight, 1993).

The Catoche Formation of the Port au Choix Peninsula is interpreted to be an exhumed oil field with common bitumen staining (Baker and Knight, 1993). The preserved porous beds of the shallowing upward cycles of the Costa Bay Member are believed to be laterally extensive; however vertical transmissivity is probably limited due to over dolomitized tight beds which are observed in the field and in thin-section. Devonian emplaced oil is believed to have migrated out of the reservoir after the integrity of the reservoirs was compromised during the inverted thick-skinned faulting of the Acadian Orogeny and the accompanying erosion of the Taconic/Salinic flysch cap rock (Knight, 1997 and Cooper et al., 2001).

1.2.4 *Reservior Stratigraphy*

The St. George Group consists of two major unconformity-bounded megacycles (**Fig. 1.6**). Both cycles consist of lower peritidal, middle subtidal, and upper peritidal sequences. The first megacycle initiated earlier in the latest Cambrian and is separated from the second megacycle by the mid-Boat Harbour Disconformity (**Fig. 1.6**). The second megacycle includes the upper member of the Boat Harbour Formation, the Catoche Formation and the Aguathuna Formation and is capped by the St. George Unconformity (Knight and James, 1987). Each cycle is a result of the interaction between relative rate of sea-level rise, subsidence and the relative rate of carbonate sedimentation. While the formation of the Boat Harbour Disconformity is attributed to a global sea-level fall, the formation of the St. George Unconformity is believed to be

primarily controlled by the Taconic tectonics resulting in significant uplift of the succession with eustatic sea level fluctuations having a lesser role (Knight et al., 1991).

The Lower Ordovician rocks of the St. George Group were likely deposited in a tidal flat island setting in shallow epeiric seas (Pratt and James, 1986). Deposition occurred on the former paleo-southern continental margin of the early Paleozoic Laurentia plate. It is argued that the main depositional controls for ancient shallow seas are tides and storms, suggesting that the shallowing-upward cycles may represent the accretion of low relief supratidal islands during relatively continuous subsidence. These islands and intertidal banks would be separated by open water with the distribution and physical characteristics of islands and banks controlled by prevailing wind, seasonal storms, tides and distance from the open ocean. The tidal flat islands in this model occur in a limited regional extent and their architecture and distributions are difficult to predict (Pratt et al., 1992). The areas of open water subtidal are the main zones of carbonate sediment generation. The Catoche Formation deposition occurred in subtidal areas associated with few islands.

In the Port au Choix area, the Catoche Formation is approximately 160m thick. The lower 120m consists of well-bedded, fossiliferous, bioturbated limestone with the top 40m comprised of pervasive dolostone. Intraclastic and bioclastic grainstone lenses and beds are common and thrombolitic mounds are present at several intervals in the lower limestones (Knight and James, 1987).

The sedimentary facies of the Catoche Formation indicate dominantly open shallow subtidal conditions relieved occasionally by high- and low-energy shoaling with

intertidal exposure. Thrombolitic mounds (**Fig. 1.4**) may have offered protection and allowed the accretion of broad shallow subtidal to low intertidal flats or banks as recorded in outcrop as thin-bedded lime mudstone and grainstone (Pratt and James, 1986). The upper most, Costa Bay Member (**Fig 1.3**), of the Catoche Formation consists mainly of meter scale grainstone cycles (Knight and James, 1987; Knight et al, 1991; Baker and Knight, 1993; Knight, 1997; Knight et al., 2007).

CHAPTER 2

METHODS AND THEORY

2.1 Sampling Protocol

Samples (110 hand specimens), covering over 210m-thick section, were obtained from outcrop and core (**Figs. 1.2, 1.3 and 1.4**). The sampled outcrop is located on the coast of the north-western side of the Port au Choix Peninsula whereas the core (PC 79-2, coordinates 477280E, 5616720N) is located about 2.5 km inland from the peninsula (**Fig 1.2**). Of the 110 samples collected, 81 were slabed, had thin-sections cut and stained using a mixture of potassium ferricyanide and alizarine red-S to facilitate identification of calcite and dolomite and visual estimations of Fe contents in the different generations of cements (Dickson, 1966). Thin sections were examined by a cold Cathodoluminoscope run at voltage of 12 kv, current intensity of about 700 microamps and 50 millitorr pressure.

2.2 Sampling and Analytical Methods for Geochemical Analysis

A total of 71 samples of different representative phases of calcites and dolomites were selected and sampled for trace element chemical analysis. Calcites consist of lime mud and later vein and biomold-filling calcite whereas dolomites included all generations (D1 to D5). The stylo-dolomite (D3) proved difficult to sample due to its nature and may have substantial contamination.

A portable hand microdrill and a microscope-mounted drill assembly were used to sample the different carbonate components. Samples were drilled, at a low rpm, from clean slabs that were washed with deionized water and dried overnight at 50°C. About 4.5 mg of powdered carbonate was used for trace element and isotope analysis. The samples were digested in 2.5% H_3PO_4 and analyzed for Ca, Mg, Sr, Mn, and Fe trace elements using a HP 4500plus at Memorial University of Newfoundland. Relative standard deviations (%) for Ca, Mg, Sr, Mn, and Fe are better than 5 %.

Oxygen isotopes were analyzed using a GasBench II connected to ThermoFinnigan Delta V plus at Memorial University in Newfoundland. The laboratory standards used were NBS-19 ($\delta^{18}O$ = - 2.20‰ and $\delta^{13}C$ = +1.95‰ PDB), L-SVEC ($\delta^{18}O$ = - 26.64 ± 0.25‰ and $\delta^{13}C$ = -46.6‰ PDB) and CBM ($\delta^{18}O$ = - 8.58 ‰ and $\delta^{13}C$ = +0.75 ± 0.06 ‰ PDB). Uncertainties of better than 0.1‰ (2σ) for the analyses were determined by repeated measurements of the standards.

For Sr isotope analyses, approximately 4 mg of sample powder was dissolved in 2.5N ultrapure HCl. After HCl evaporation, Sr was extracted with quartz glass ion exchange columns filled with Bio Rad AG50WX8 resin. Approximately 75–100 ng Sr was loaded on Re filaments using a Ta_2O_5–HNO_3–HF–H_3PO_4 solution. Measurements were performed with a Finnigan MAT 262 multi-collector mass spectrometer at the Institut für Geologie, Mineralogie und Geophysik, Ruhr Universität, Bochum, Germany (cf. Diener et al., 1996; Azmy et al., 1999). Sr isotope ratio measurements were completed using two standard reference materials, NIST (NBS) 987 and USGS EN–1,

which gave mean $^{87}Sr/^{86}Sr$ values over the analyses interval of 0.710236 ± 0.0000008 and 0.709151 ± 0.000008, respectively.

Fluid inclusions were observed using a Nikon microscope with a 40x Nikon objective lens. Microthermometry was performed on a Linkam THMS-600 heating-freezing stage and the calibration was checked using $TmCO_2$, TmH_2O and ThH_2O (-56.6, 0.0 and 374.1 °C). Accuracy in measurements around 0 and 100 °C is estimated between 0.1 and 0.2 °C.

2.3 Cathodoluminescence (CL) Theory

Minerals may display luminescence when excited by different types of radiation. Cathodoluminescence is the luminescence resulting from a bombardment of electrons sourced from a cathode. The bombardment of electrons causes low-energy electrons within the crystal to ascend to a higher-energy level. The transition from a higher to a lower level is impeded temporarily by defects in the crystal lattice, and as electrons leave the defects, energy is lost through the emission of photons. These photons have wavelengths in the visible light electromagnetic spectrum that cause the luminescence (Ozawa, 1990; Machel et al., 1991; Boggs Jr and Krinsley, 2006).

Defects within the crystal lattice of a mineral are commonly referred to as electron traps or luminescence centers. Two types of electron traps are extrinsic and intrinsic traps. Extrinsic centers, or impurity centers, are characteristic of the mineralizing fluid. Intrinsic centers are lattice imperfections or other defects due to non-

stoichiometric proportions, structural imperfections, or impurities causing a distortion of the lattice (Machel and Burton, 1991; Machel et al., 1991; Boggs Jr and Krinsley 2006).

The most important activator of the luminescence of minerals is Mn^{+2}. Activators are ions of various valances that substitute for cations in the host structure. Other common activators are Sm^{+3}, Pb^{+2}, and Ce^{+3}. Quenchers are impurity ions that suppress the emission of luminescence by activator ions. Common quenchers include Fe^{+2}, Fe^{+3}, Co^{+2}, and Ni^{+2}. The intensity of luminescence is commonly considered largely due to the ratio of the concentrations of Mn^{+2}/Fe^{+2} (Choquette and James, 1987; Machel and Burton, 1991; Machel et al., 1991).

Common cathodoluminescence applications in carbonate rocks include a quick relative percentage of minerals present in a sample, the identification of different generations of cements, observations regarding zonations of crystals reflecting evolving pore fluids and crystal growth, and identification of microfractures and microbrecciation that otherwise are difficult to observe using traditional petrographical techniques (Pagel et al., 2000).

2.4 Trace Elements

The progressive diagenetic evolution of marine carbonates is accompanied by changes in the original trace element concentrations reflecting the nature of the diagenetic fluids. Changes in original mineralogy and chemistry occur as a result of the stabilization of metastable phases, aragonite (A) and high-Mg calcite (HMC), into stable low-Mg calcite phases (LMC).

Aragonite and HMC dominate the mineralogy of recent carbonates while LMC is the major constituent of ancient limestones. A shift to LMC occurs during burial due to post-depositional redistribution of Mg. LMC consists of 0-5 mole % $MgCO_3$, IMC (intermediate-Mg calcite) contains between 5-8 mole % $MgCO_3$, and HMC contains between 8-28 mole % $MgCO_3$ (Milliman, 1974). The decrease in mole % $MgCO_3$ in ancient carbonates is due to the post-depositional stabilization of metastable phases through the dissolution-precipitation process carried out by pore waters (Bathurst, 1975; Brand and Veizer, 1980; Veizer, 1983).

Stabilization on of an original metastable carbonate assemblage to a stable assemblage is accomplished through corresponding textural, mineralogical and chemical changes. Common trace elements found to substitute in the $CaCO_3$ lattice are Sr^{2+}, Mn^{2+}, Mg^{2+}, Fe^{2+}, Pb^{2+}, Zn^{2+}, and Na^{+}.

The original carbonate phase, precipitated in chemical equilibrium with seawater, will incorporate trace elements and stable isotopes from the ambient sea water. Distribution coefficients govern the trace element distribution between the liquid phase (diagenetic fluid) and the solid phase ($CaCO_3$) according to the following equation:

$$(m_{Mc}/m_{Ca})_s = D\,(m_{Mc}/m_{Ca})_w$$

where D is the distribution coefficient for the trace element, m is the molar concentration, Me is the trace element, and s and w signify the solid phase (CaCO3) and the liquid phase (diagenetic fluid) respectively. For trace elements in which D>1 (e.g., Fe and Mn) the precipitated phase will contain, with respect to calcium, a higher Me concentration than the liquid phase and vice versa (Brand and Veizer, 1980).

Trace element analysis aides in (1) providing geochemical characteristics of dolomites and dolomitizing fluids, (2) determination of the diagenetic environment and nature of the system under which dolomitization occurred, (3) evaluation of controls on dolomitization and its relationship to porosity.

2.5 Stable Isotopes

The process of dolomitization requires large volumes of water to supply the Mg needed. The oxygen isotopic composition of the resulting dolomites is totally buffered by the isotopic composition of the dolomitizing fluid (Land, 1983). The ratios of the resultant dolomites therefore reflect the temperature and the isotopic composition of the ambient fluid in which these dolomites were formed.

The isotopic composition of marine carbonates is equilibrated with the intervening diagenetic porewater of different isotopic composition through a wet dissolution-precipitation process (Bathurst, 1975) which results in repartitioning of these stable isotopes and the redistribution of the trace elements (Brand and Veizer, 1981; Veizer, 1983; Al-Aasm and Veizer, 1986).

The isotope exchange between the carbonate phase and the diagenetic fluid usually results in the enrichment of ^{12}C and ^{16}O isotopes in the stabilized LMC and can be expressed by the following equation:

$$^{13}C^{18}O_3^{-2} + H_2{}^{16}O + {}^{12}CO_2 \longleftrightarrow {}^{12}C^{16}O_3^{-2} + H_2{}^{18}O + CO_2$$

The isotopic composition of O is measured by mass spectrometry and is expressed relative to standard mean ocean water (SMOW) (Hoefs, 1997). The use of a standard

permits values to be reported in terms of a parameter called delta (δ), which for O is defined by the equation:

$$\delta^{18}O = 1000((^{18}O/^{16}O)_{sample} - (^{18}O/^{16}O)_{standard})/(^{18}O/^{16}O)_{standard}$$

The $\delta^{18}O$ values of the carbonate samples are reported relative to the PDB standard which is from a belemnite from the Cretaceous Pee Dee Formation of South Carolina. The isotopic composition of O is always expressed in terms of enrichment or depletion of ^{18}O (Faure and Mensing, 2005).

Several factors influence the distribution of oxygen and carbons isotopes during diagenesis are (Brand and Veizer, 1981; Anderson and Arthur, 1983; Faure and Mensing, 2005):

(1) The stability of the original carbonate phase relative to the diagenetic environment;

(2) The openness of the system (the water/rock ratio);

(3) The isotopic composition of both seawater and the evolving diagenetic water;

(4) The fractionation factor of an isotope between the fluid and carbonate mineral;

(5) The temperature and salinity of ambient seawater and the diagenetic fluid;

(6) Regional changes in the ^{18}O composition of meteoric waters due to latitude, altitude and seasonal variations;

(7) Secular variations in the ^{18}O composition in global seawater;

(8) Biological fractionation of isotopes in biological carbonates.

The main objectives of the study of the isotope composition of the Catoche dolomites are to: (1) evaluate the isotopic shifts during progressive dolomitization and in

conjunction with trace elements and petrographic data; and (2) estimate the nature of the environment that dominated the process of diagenesis during dolomitization.

5.3 Strontium Isotopes

The four naturally occurring stable isotopes of strontium are ^{88}Sr, ^{87}Sr, ^{86}Sr, and ^{84}Sr, of which ^{87}Sr is radiogenic and formed by the β-decay of naturally occurring ^{87}Rb (Faure and Mensing, 2005). The isotope composition of Sr of modern seawaters is recorded during the formation of biogenic and inorganic marine calcite/aragonite. Residence time of strontium in the oceans is about 2.6×10^6 years while mixing time for the ocean is roughly 1000 years (Faure and Mensing, 2005). As a result the ratio of $^{87}Sr/^{86}Sr$ is isotopically homogenous throughout the ocean at any given time. Although the strontium isotopic ratio is homogenous throughout the ocean, the ratio has changed with time reflecting the waxing and waning of continental and mantle fluxes (Veizer et al., 1999; Faure and Mensing, 2005). These variations are due in part to changes in the inputs of Sr derived from a volcanic source, causing the $^{87}Sr/^{86}Sr$ ratio of seawater to decline. In contrast to the declining $^{87}Sr/^{86}Sr$ ratio of seawater are the increases of the $^{87}Sr/^{86}Sr$ ratio throughout the Phanerozoic. The increase in the $^{87}Sr/^{86}Sr$ ratio is argued to be the effect of weathering of sialic continental rocks which is enhanced particularly by collisions of continents during episodes of orogeny (e.g., Faure and Mensing, 2005 and more references therein).

CHAPTER III

PETROGRAPHY OF THE CATOCHE FORMATION

3.1 Petrography of Catoche Formation Lithofacies

The petrography of the Catoche has been investigated by earlier authors (Knight, 1991; Haywick, 1984; Baker and Knight; 1993; and Lane, 1990). However, the current investigation provides a higher-resolution and detailed description of the rocks that are more beneficial to petroleum geoscience.

3.1.1 Bedded, Bioturbated Mudstone to Grainstone Lithofacies

These units represent open, subtidal, low-energy shelf deposits of muddy and fine scale grains. Ubiquitous burrowing and diverse benthonic shelly fauna are commonly observered throughout the first 90 to 100 m (Knight, 1991; Baker and Knight, 1993; Knight et al., 2007). Samples studied here have been observed as partially to entirely recrystallized mud to grainstones. Skeletal components occur in varying proportions as pelloids, algal aggregates, and fragments of gastropods, trilobites and brachiopods.

Although relict textures and grains are present, algal or peloidal calcic mud has been intensely recrystallized to microspar or pseudospar (**Plates 3.1 and 3.2**). The calcite microspars are equigranular and exhibit curved and embayed crystal boundaries.

Burrows and ichnofossils are abundant in the mudstones and wackstones (**Plates 3.2, 3.3 and 3.4**), sometimes composing as much as 30% of the observed sample. In most instances, the burrows have been partially to completely dolomitized. The dolomite

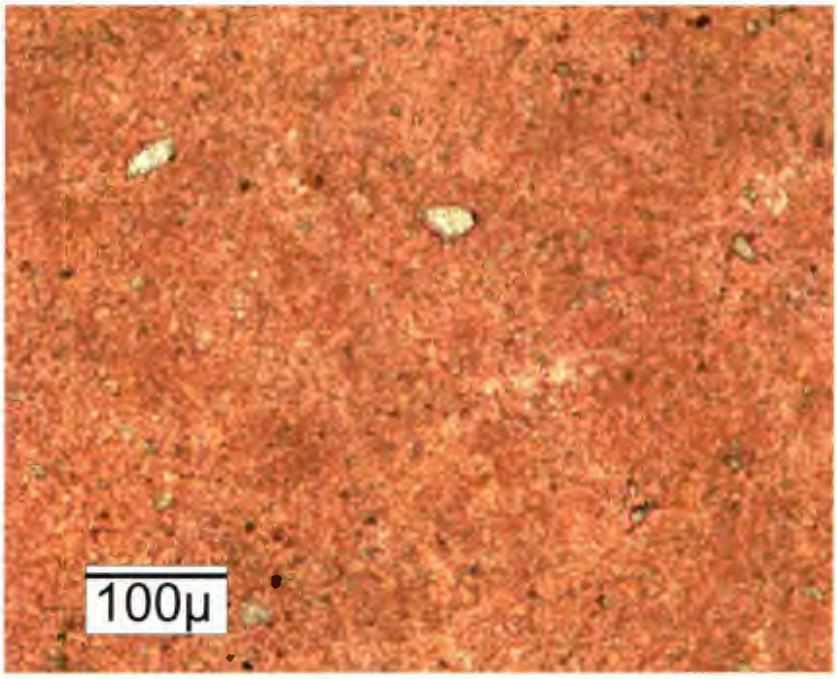

Plate 3.1. Typical recrystalized mudstone of the Catoche Formation (TS - MG 100).

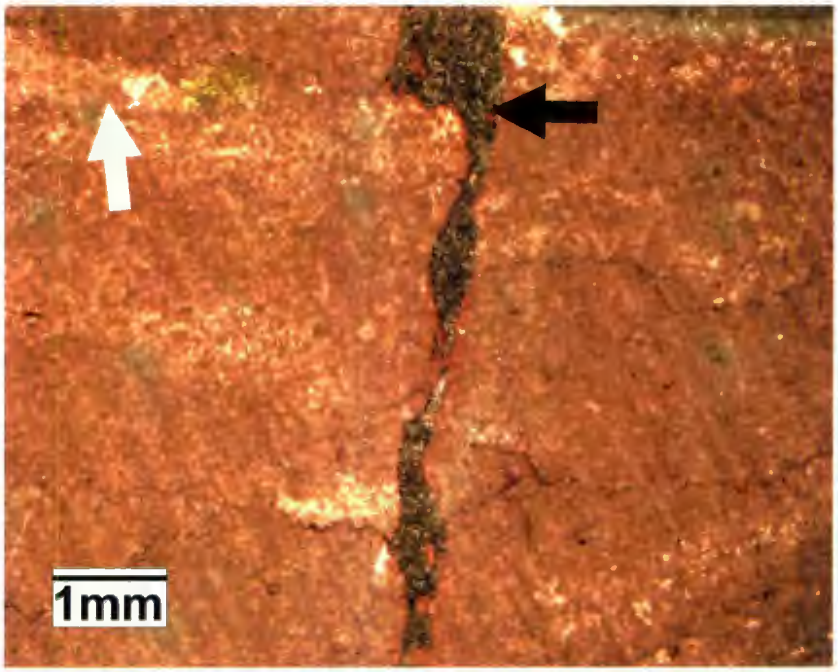

Plate 3.2. Recrystalized mudstone. Lighter (coarser) areas are possible former burrows (white arrow). An irregular fracture is filled with Fe-rich dolomite (black arrow) (TS - MG 100).

Plate 3.3. Typical dolomitized burrows in a lime mudstone present in the Catoche Formation in the St. George Group.

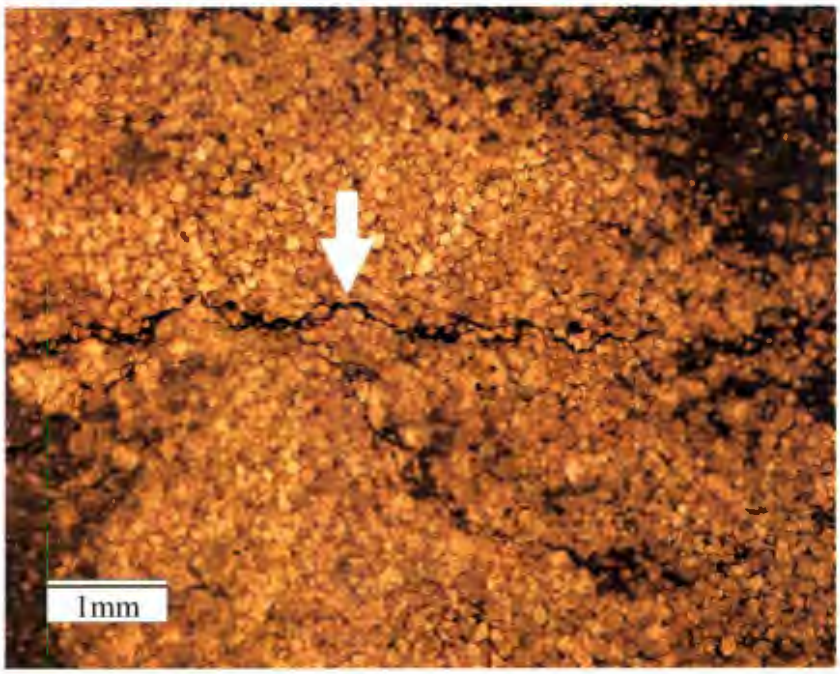

Plate 3.4. Photomicrograph of dolomitized burrow. Dolomitized burrow predates stylolization (white arrow) (TS - MG 125).

crystals range in size from 70 to 150 μm and are subhedral to anhedral but rarely euhedral (**Plate 3.4**). The cloudy cores of these crystals stain blue, indicating a relative high Fe content, while the rims are clearer and stain light blue, suggesting lower relative Fe. Commonly associated with these dolomites is insoluble material that appears orangish-brown in thin section.

Sample 108 (retrieved from the Port au Choix section from approximately 30 m above the base of the formation) is a floatstone comprising of replaced brachiopods set in a peloidal pellet matrix (**Plates 3.5, 3.6, 3.7, and 3.8**). The brachiopod shells have been replaced with a generation of calcite followed by a coarse saddle dolomite. The calcite is coarse blocky and averages approximately 500 μm in size. The dolomite displays strong cleavage sweeping extinction under cross-polarized light (**Plate 3.7**). It is commonly of mm scale, anhedral in shape and uniformably turbid. The dolomite crystals exhibit a deep blue colour after staining (**Plate 3.6**) indicating a high relative Fe content and appear dull red to non-luminescent under the cathodoluminoscope (CL) (**Plate 3.8**).

Stylolization is widespread throughout the muddy members of this lithofacies (**Plate 3.2**). The stylolites are low amplitude (1.5 mm), horizontal to subvertical, hummocky to irregular and commonly anastomosing. The stylolites form parallel to bedding and are in many cases associated with characteristic euhedral dolomite (**Plate 3.9-3.10**). Relative timing for each generation of stylolite was not determined due to a lack of cross-cutting features. The dolomite crystals range is size from 60 to 120 μm and average about 80 μm. The stylo-bounded dolomites are anhedral to commonly subhedral

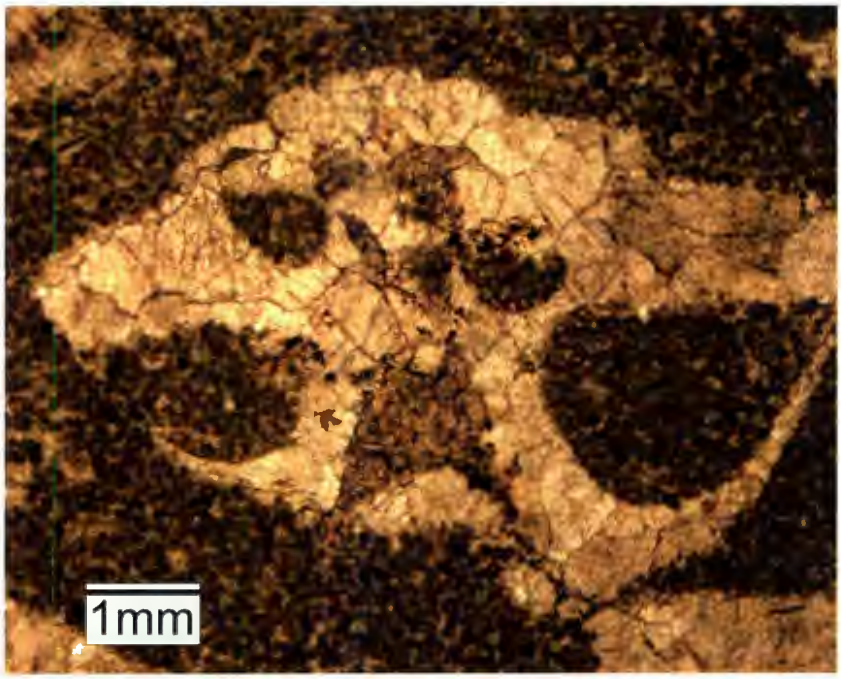

Plate 3.5. Photomicrograph of a recrystallized brachiopod. Internal chambers are infilled with matrix grains creating geopetal structures. The coarse crystals are late equant calcite. Replacement saddle dolomities are common but not present in this photo (TS - MG 108).

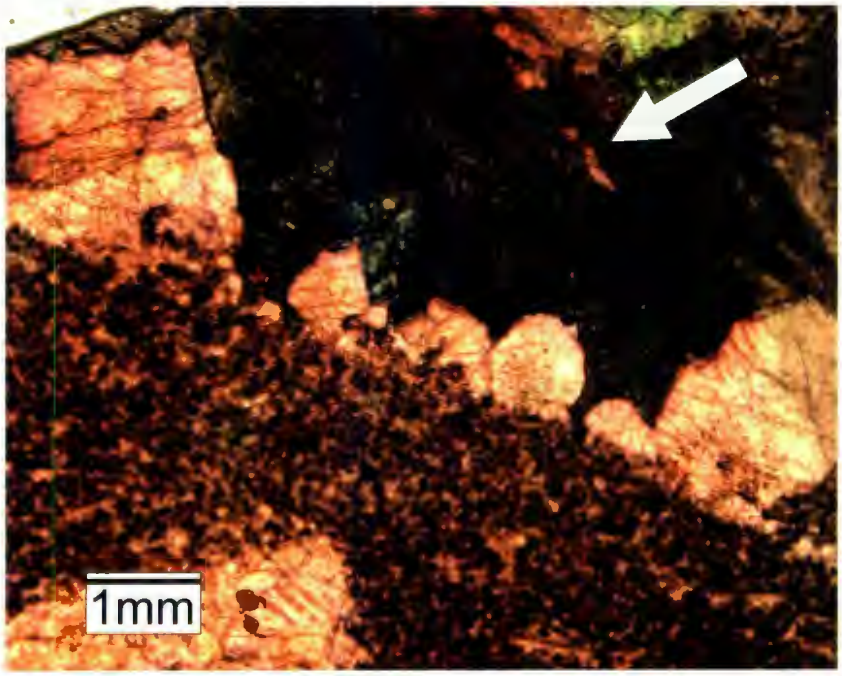

Plate 3.6. Photomicrograph of replacement saddle dolomite. Staining reveals a high relative Fe-content. Remnant calcite within dolomite suggest replacement of precursor late equant calcite (white arrow) (TS - MG 108).

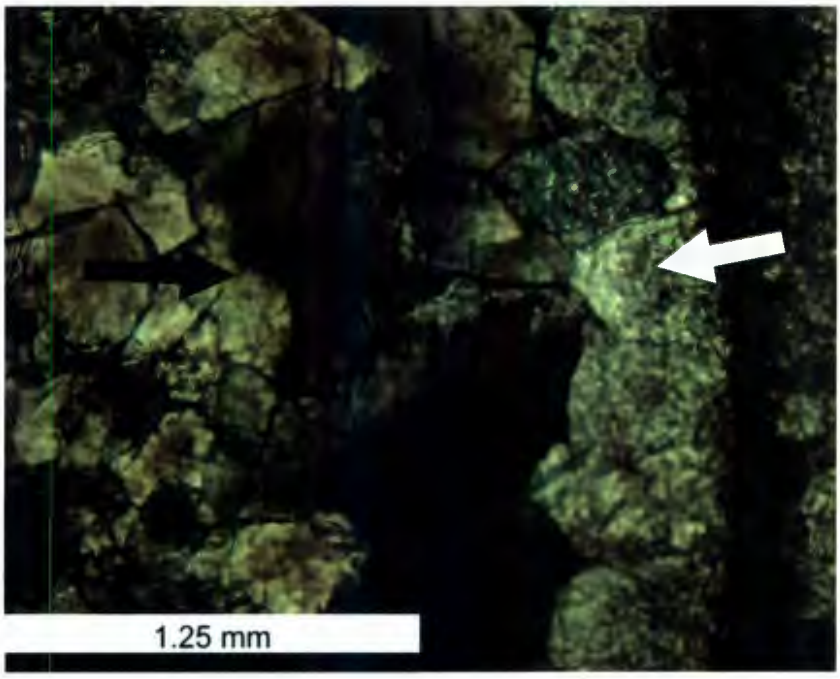

Plate 3.7. Photomicrograph of replaced brachiopod under cross-polarized light. Replacive calcite (whte arrow) and saddle dolomite (black arrow) (MG 108).

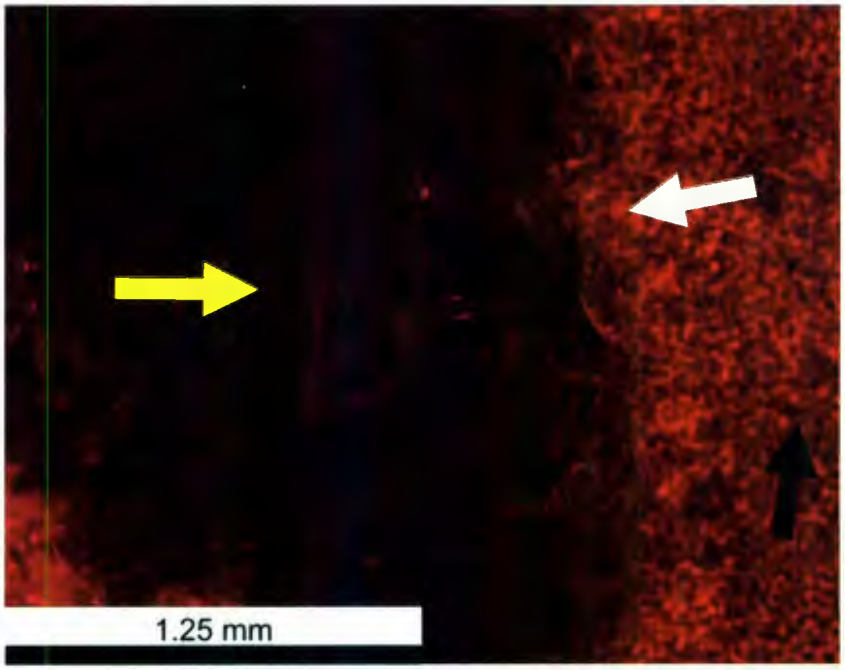

Plate 3.8. Photomicrograph of recrystallized brachiopod. Calcite crystals (white arrow) and surrounding matrix (black arrow) have a similar orange-red luminescence. Saddle dolomite (yellow arrow) is dark red to non-luminescent and contians fracture which are slightly brighter (TS - MG 108).

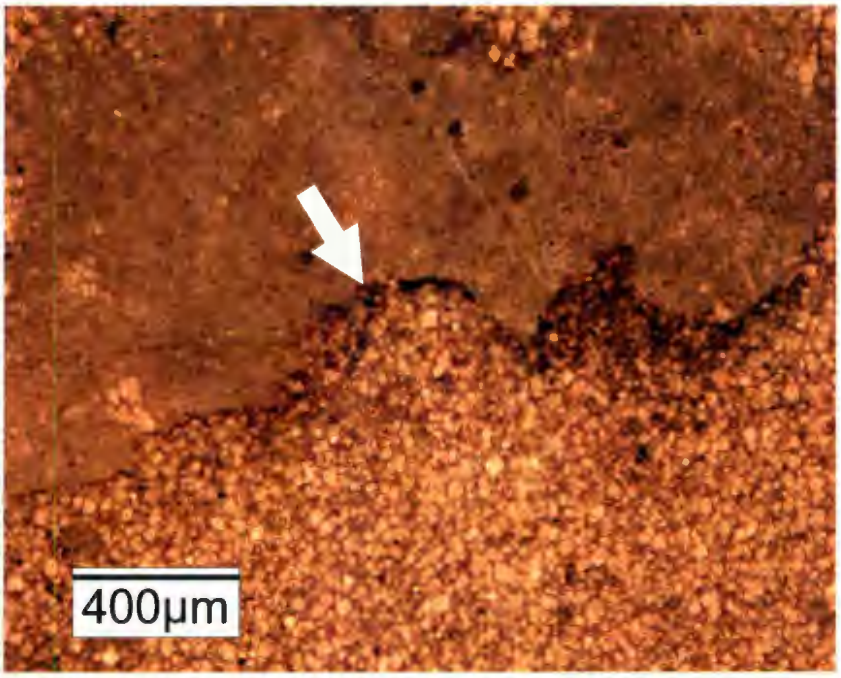

Plate 3.9. Photomicrograph of stylo-bounded dolomite. The stylolite (white arrow) marks a sharp boundary between the original lime mud and diagenetic dolomite.

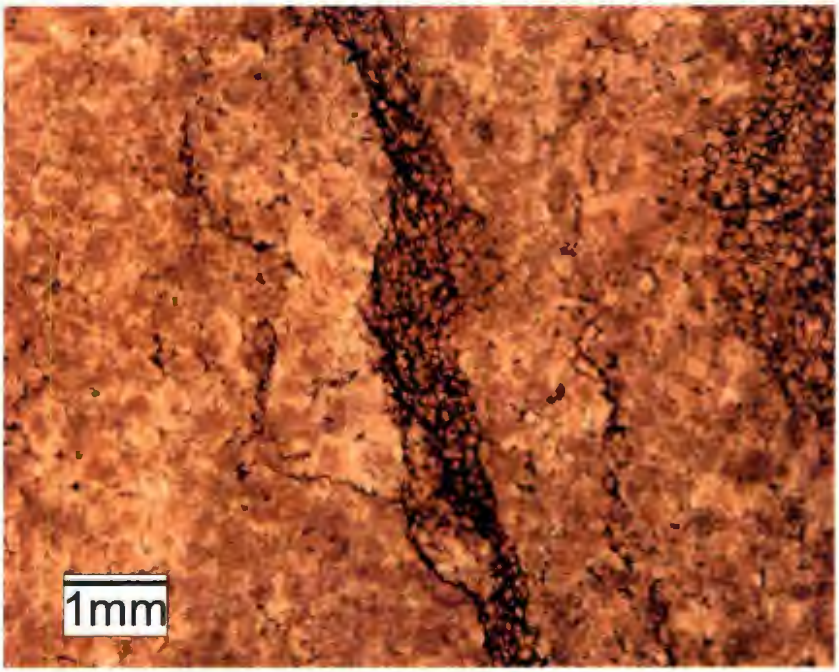

Plate 3.10. Photomicrograph of a stylo-associated dolomite cutting an earlier generation of replacement dolomite (TS - MG 126).

and rarely euhedral in shape. Similar to the burrow related dolomites, these crystals exhibit cloudy cores with clear rims.

3.1.2 Packstone and Grainstone Lithofacies

Packstone and grainstone lithofacies were most likely deposited as storm-generated gravel bars and/or tidal-channel deposits as lenses with scoured bases and wavy tops (Knight, 1991; Baker and Knight, 1993; Knight et al., 2007). Skeletal grains are composed of about 80% peloids and algal aggregates with skeletal fragments of trilobites, crinoids and brachiopods (**Plate 3.11**).

The mud present in the packstones of this lithofacies has been recrystallized to microspar and occasionally pseudospar with crystals of equant shape and irregular grain boundaries. Early equant calcite spar (50-250 μm) is present lining grains and filling pores (**Plate 3.12**). The crystal boundaries of these cements are usually irregular and embayed. A coarser (80-500 μm) and later generation of calcite spar, fills both pores and fractures present in this lithofacies (**Plate 3.6**). The late generation calcite spar stains light red suggesting low relative Fe content.

3.1.3 Intraclastic Rudstone Lithofacies

The intraclastic rudstones are interpreted to possibly represent subtidal channel deposits (Knight, 1991; Knight et al., 2007). The skeletal grains of this lithofacies consist mainly of algal mud aggregates and peloidal mud clasts (75-85%) with the remainder of the facies consisting of fragmented skeletal material of trilobites, brachiopods and

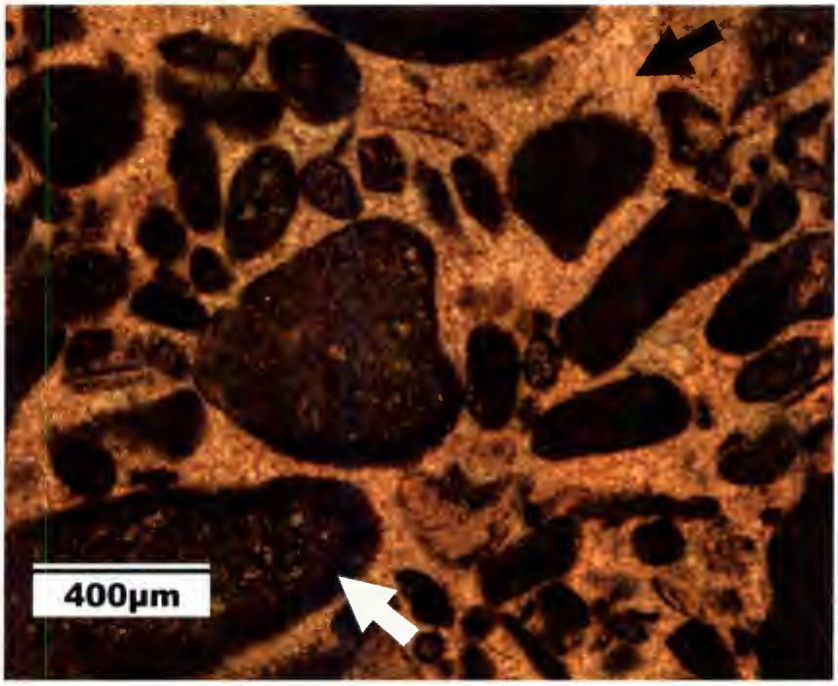

Plate 3.11. Packstone/Grainstone Lithofacies. Common micritic envelopes (white arrow) are developed. Black arrow points to calcite microspar of possible recrystallized mud origin (TS - MG 100).

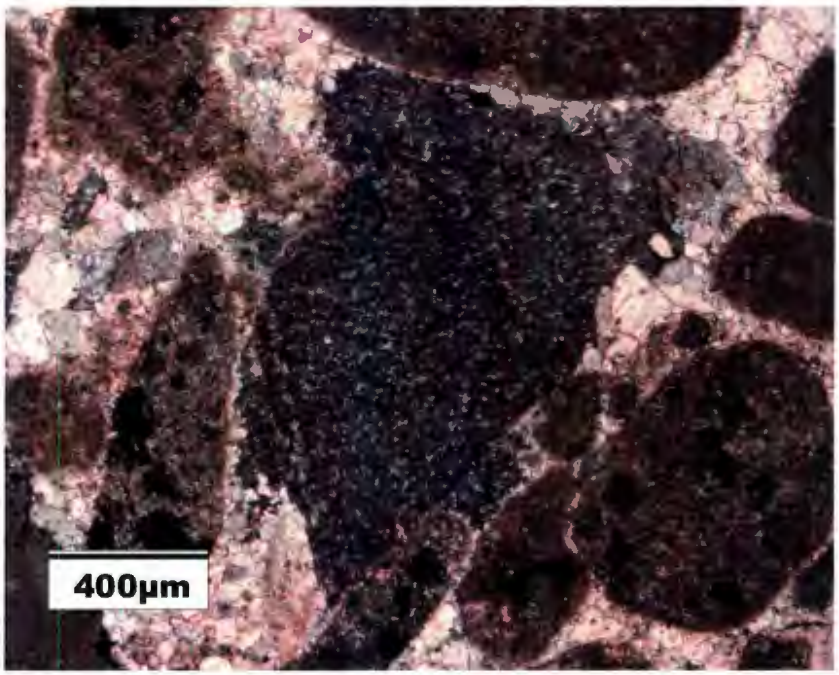

Plate 3.12. Photomicrograph of syntaxially cemented crinoid fragment under cross-polarized light (TS - MG 100).

crinoids. The clasts are well rounded, usually elongated, show a rough imbrication and range in size from 150 μm to 2 cm in length with an average size of 300 μm (**Plates 3.12, 3.13, 3.15 and 3.16**). Preferential dolomitization has affected about 50% of the clasts while the matrix remained unaffected.

Rare bladed calcite cements were observed nucleating from several grains. Syntaxially cements over crinoids are common up to 1mm in size and postdate the bladed cement. All calcites appear orangish-red under CL (**Plate 3.14**).

Micritic envelopes commonly surround clasts and resist alteration by recrystallization or dolomitization while dolomite has replaced many clasts inward of the envelopes. Complete micritization of several grains sometimes occur.

Dolomite crystals range in size from 75 to 150 μm and average about 100 μm. Crystal shape is commonly an- to subhedral and rarely euhedral and is uniformably cloudy. These dolomites exhibit dull red luminescence under CL (**Plate 3.14**).

3.1.4 Cryptalgal Boundstone Mound Lithofacies

Boundstone mounds and mound banks formed within the photic zone and very shallow subtidal settings in the Port au Choix area (Knight, 1991). Five occurrences of mounds are found in the Port au Choix section and exhibit two different growth forms. High relief, spherical mounds (**Plate 3.17**) and lower relief linear mounds are both common. Linear mounds trend north-south to northeast-southwest suggesting a similar orientation for storms and/or tidal currents (Knight 1991, Knight et al., 2007).

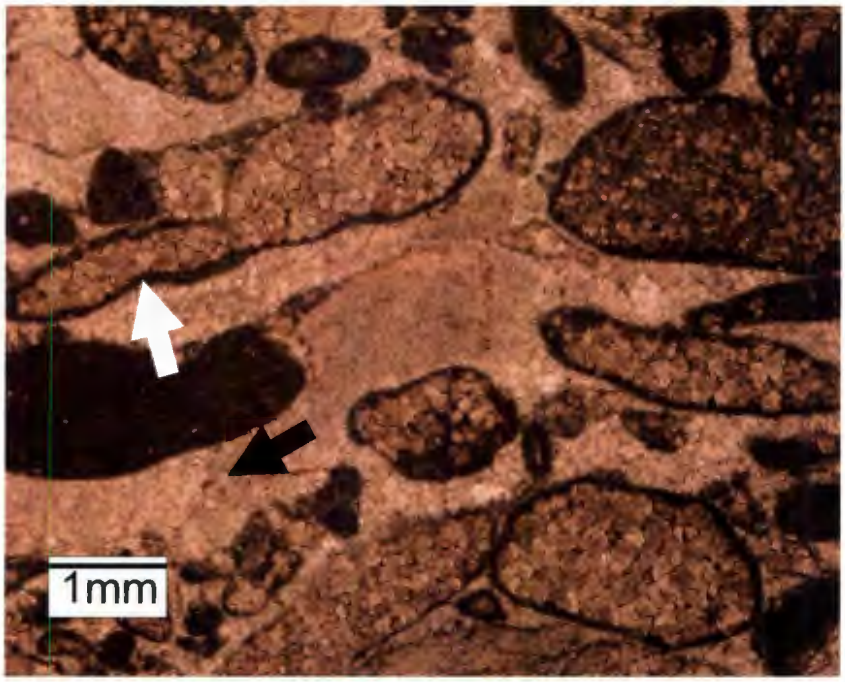

Plate 3.13. Intraclastic Rudstone lithofacies. Micritic envelopes are resistant to preferential dolomitization (white arrow). Calcite cement crystals are much coarser the the packstone/grainstone lithofacies (black arrow) (TS - MG 104).

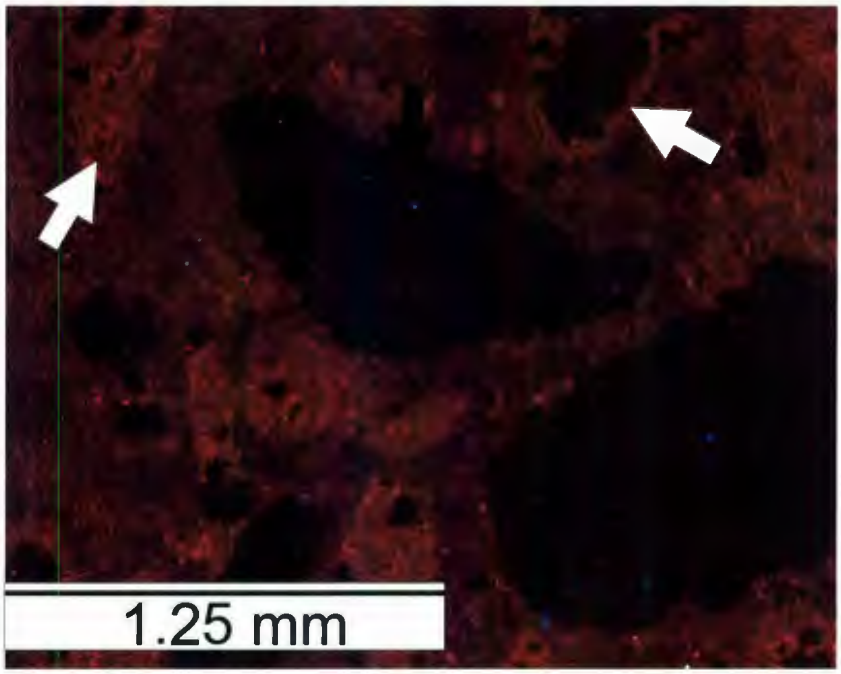

Plate 3.14. Cathodoluminesence of intraclastic rudstone lithofachies. Preferentially dolomitized peloids (black arrow) appear dark red to non-luminescent. Micritic envelopes and completely dolomitized grains have orange-red luminescent (white arrows). Calcite cements between grains appear redish-orange.(TS-MG 104).

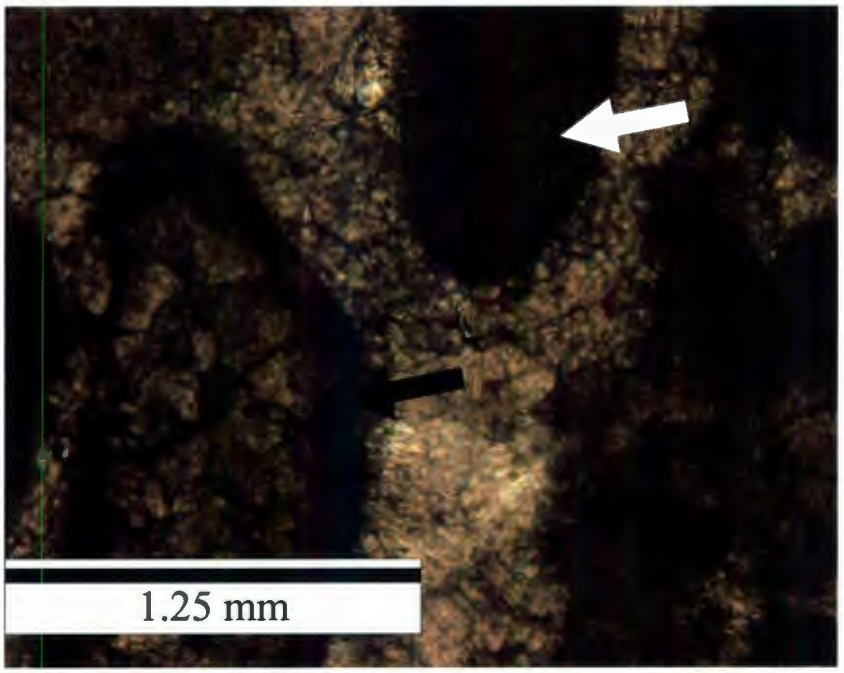

Plate 3.15. Typical peloids within the Catoche Formation. The white arrow points to a completely micritized grain while the black arrow points to a grain featuring a micritic envelope with the remainder of the grain preferentially dolomitized (SP MG 104).

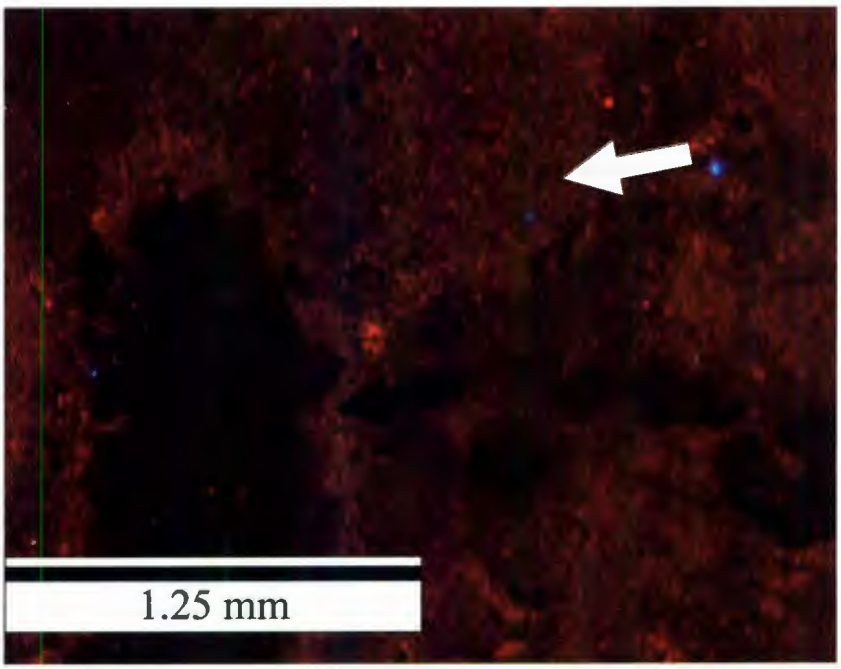

Plate 3.16. A photomicrograph of the same sample as above under cathodoluminesce. Micritized grains and micritic envelopes have dull to medium reddish-orange luminescence (SP MG 104).

Plate 3.17. Meter scale, high-relief mounds of the Catoche Formation of western Newfoundland.

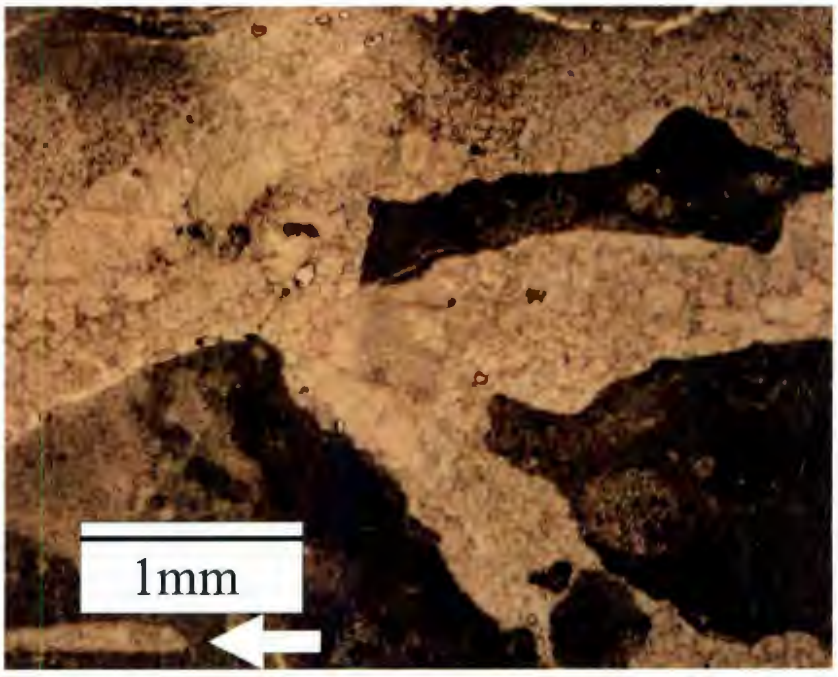

Plate 3.18. Photomicrograph of calcite cemented boundstone mound. White arrow points to cemented boring (burrow?) (TS - MG 115).

Petrography reveals a high degree of organic boring and precipitation of calcite cements in voids (**Plate 3.18**).

3.1.5 Diagenetic Dolostone

The diagenetic dolostones were sampled entirely from the core (PC 79-2) at approximately 1 m intervals. Significant porosity is developed in the upper 40 m of the Catoche in contrast with the lower 120 m where porosity is rare to mostly absent. Porosity exists as intercrystalline, vug and stylo-porosity (**Plates 3.19 to 3.22**). Dolomitization has completely obliterated all primary texture making identification of primary depositional lithofacies difficult in the Port au Choix location, but other workers have identified the precursor textures as meter scale peloidal sand shoals.

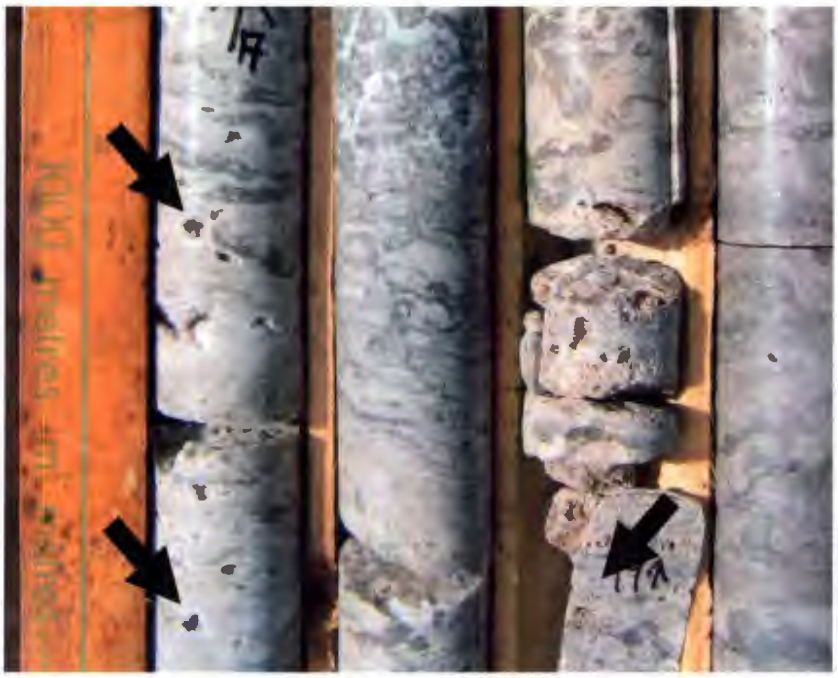

Plate 3.19. Core PC-79-2. The top 40m of the Catoche consists of diagenetic dolomite. Vugs (black arrow) are common throughout the dolostone.

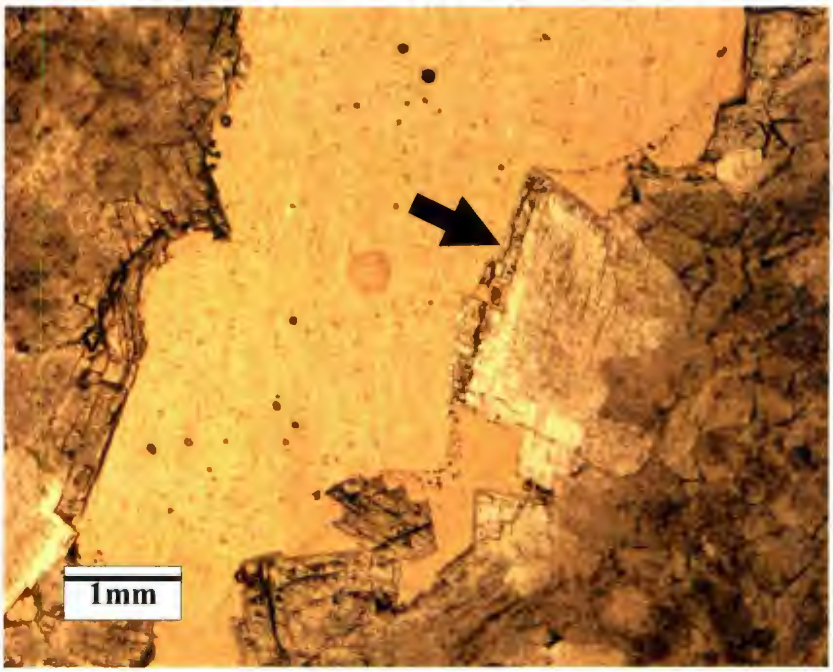

Plate 3.20. Photomicrograph of a vug within the Catoche Dolostone. The vuggy pore has been slightly enlarged due to leaching or dissolution of dolomite (black arrow) (TS - MG 35).

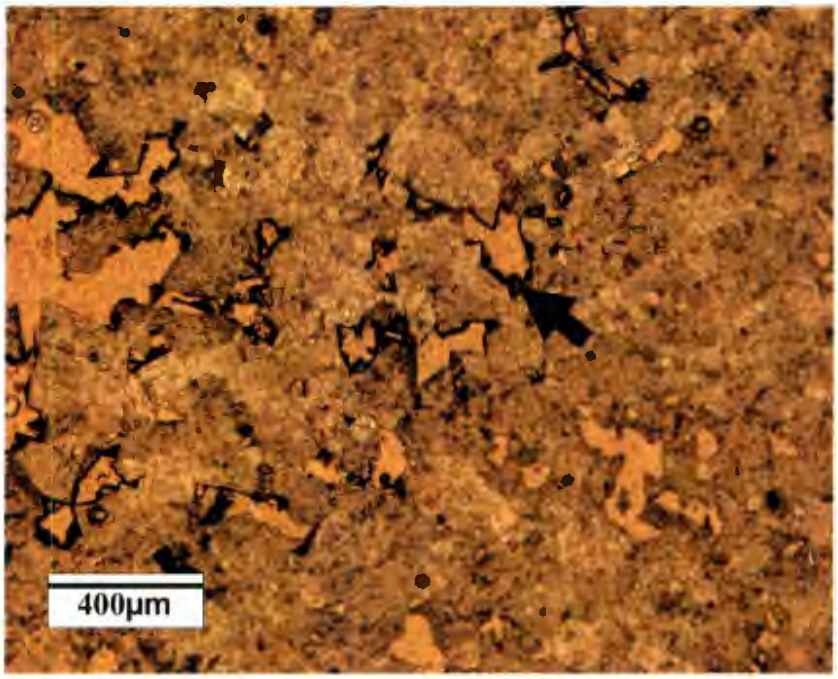

Plate 3.21. Photomicrograph of intercrystalline porosity in the Catoche Dolomites. Pores are lined with bitumen (black arrows) (TS - MG 13).

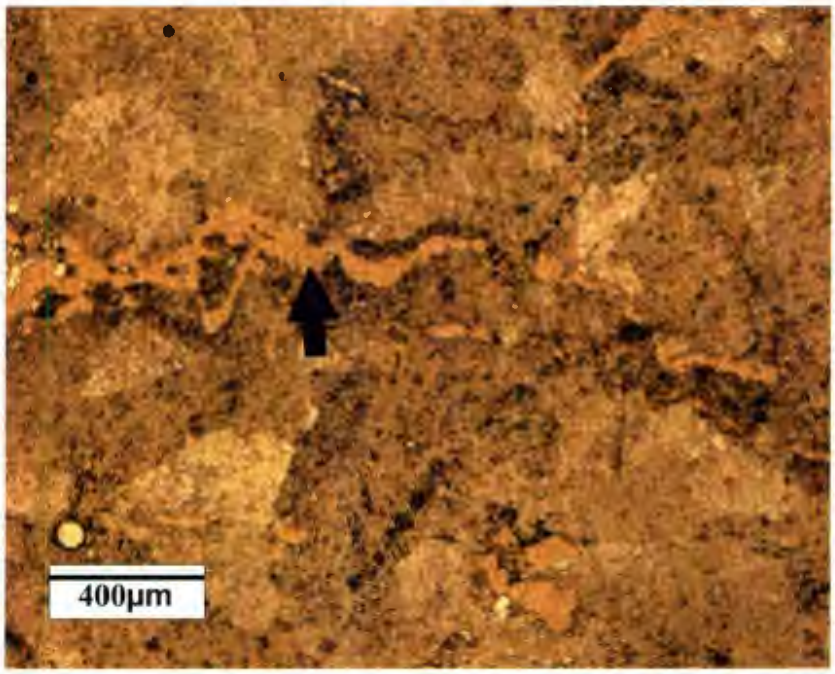

Plate 3.22. Photomicrograph of stylo-porosity (black arrow). Stylo-porosity may significantly increase effective porosity and act as counduits for fluid flow (TS - MG 43).

CHAPTER IV

DIAGENESIS

4.1 Definition

Diagenesis refers to all physical, biological, and chemical changes that occur, before the realm of metamorphism, to a sediment following deposition (Choquette and James, 1987). Diagenesis begins on the seafloor after deposition and continues throughout the entire burial history of the rock (Bathurst, 1975; Choquette and James, 1987; James and Choquette, 1988; James and Choquette, 1988; Tucker and Wright, 1990; Tucker, 2004; Flügel, 2004). Geochemical changes during burial include a replacement of unstable aragonite and high-Mg calcites (HMC) with stable low-Mg calcites (LMC) (Bathurst, 1975). Original stable isotope signatures progressively shift towards signatures of the altering fluids (Veizer, 1983).

4.2 Diagenetic environments of carbonates

Carbonate diagenesis occurs in near-surface marine and meteoric environments, and also in the shallow/deep burial environment (**Fig. 4.1**). The diagenetic environment can be identified by observing the type of cementation, microbial micritization, neomorphism, dissolution, cementation, compaction features and dolomitization (Bathurst, 1975; Tucker, 2004; James and Choquette, 1988; Choquette and James, 1987, Flügel, 2004).

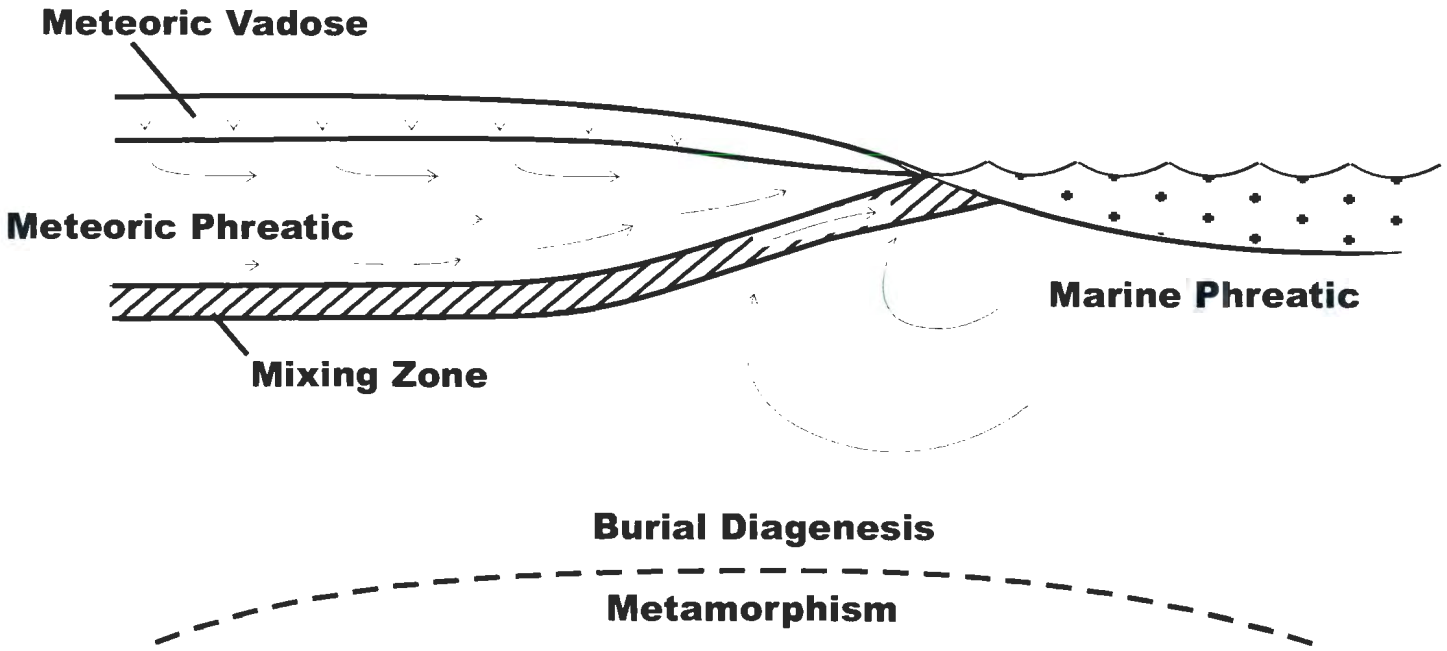

Figure 4.1. A schematic diagram outlining the main diagenetic zones involved in carbonate diagenesis.

4.2.1 Marine environment

Marine diagenesis is the earliest stage of diagenesis and starts on the sea floor or a few inches below the sediment/sea floor interface. Pore waters in this environment are commonly supersaturated with respect to $CaCO_3$. Common diagenetic processes are occurring in the marine realm include dissolution (in the deep marine environment), cementation and micritization (Bathurst, 1975). There are 3 main subenvironments of marine diagenesis

1. **Active marine phreatic** – an area of active circulation of marine waters inducing precipitation of marine cements. Aragonite and high-Mg calcite (HMC) precipitate directly from seawater as botryoidal, isopachous fibrous and needle form and as micrite and fibrous to bladed isopachous crusts.
2. **Stagnant marine phreatic** – characterized by low energy and little pore fluid activity limiting cementation. Microbial boring and formation of micritic envelopes and micritic grains are common in the stagnant marine phreatic zone.
3. **Burial marine phreatic zone** – as marine sediments and associated pore waters are progressively buried, temperature and pressure increase (James and Choquette, 1988).

4.2.2 Meteoric environment

The meteoric diagenetic environment can be divided into 3 distinct settings

1. **Meteoric vadose zone** – above the water table and open to the atmosphere, the meteoric vadose zone consists of a zone of infiltration which lies directly below the sediment/atmosphere interface and the zone of gravity percolation which lies above the water table and below the zone of infiltration.
2. **Meteoric phreatic zone** – this zone lies below the water table, where meteoric water fills pores and waters are actively moving. Dissolution and corrosion are active at the water-air interface where the development of caves and cavities with solution sculpted walls is common.
3. **Mixing Zone** – a transition zone composed of active mixed marine-meteoric waters. Mixing zones can be the site of intense limestone alteration including dissolution and precipitation of dolomite (James and Choquette, 1988).

4.2.3 Burial environment

The burial diagenetic environment is defined as of the zone between near surface diagenesis and the onset of low-temperature metamorphism (Choquette and James, 1987). Intrinsic factors affecting burial diagenesis include mineralogy, grain size and texture, organic matter, cements and dolomitization, porosity and permeability and porewater chemistry. Extrinsic factors influencing diagenesis at burial conditions include temperature, pressure, time and fluid flux. The burial diagenetic realm is commonly divided into two sub-environments.

1. **Shallow burial environment** – this diagenetic environment refers to the first few meters to tens of meters of burial and typically precipitate cements of low-Mg micrite and equant microspar.
2. **Deep burial environment** – typical cements include clear coarse equant spar, coarse dolomite and poikilitic calcite (Choquette and James, 1987).

4.2.4 Diagenetic environment of Catoche Formation

The Catoche Formation carbonates were deposited in a warm shallow marine environment and the diagenetic features observed through the petrographic analysis suggest that the sediments have gone through a wide spectrum of marine, meteoric and burial diagenesis.

4.3 Cement Petrography

4.3.1 Bladed Cements

Rare bladed calcite cements grow normal to the substrate and range in length from 150 μm to 600 μm with length to width ratios of about 2.5:1 (**Plates 4.1 and 4.2**). Staining suggests a low relative Fe^{+} content. Crystal faces are euhedral and terminations are prismatic.

4.3.2 Drusy (to Equant) Mosaic

The most common calcite cement in the Catoche carbonates is drusy to equant, pore-filling and pore-lining, calcite (**Plates 3.12 and 4.3**). Individual calcite crystals

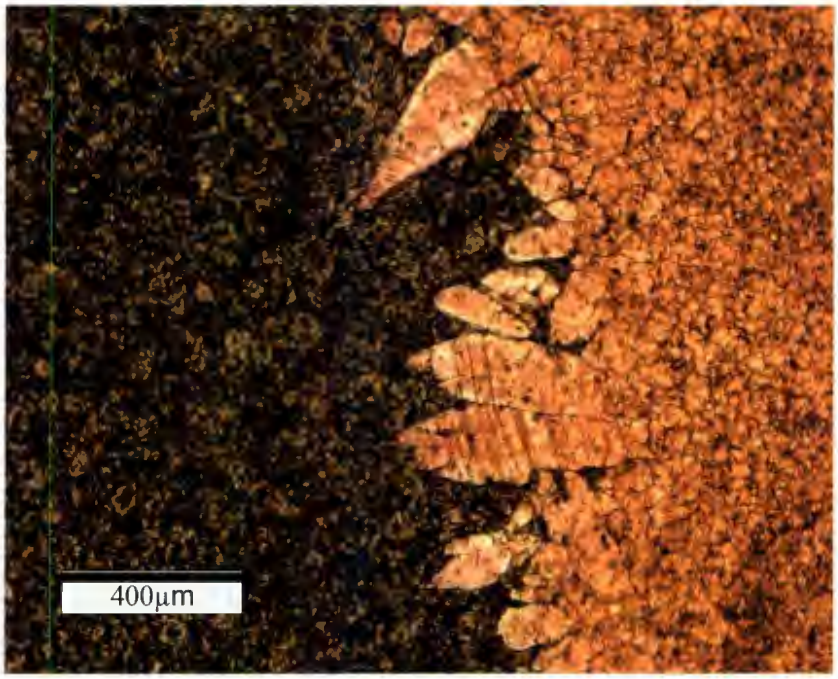

Plate 4.1. Rare blade calcite cements growing normal to the substrate. Crystal terminations are prismatic and length to width ratios are usually <3:1. Staining suggests a relative low Fe-content (TS MG - 123).

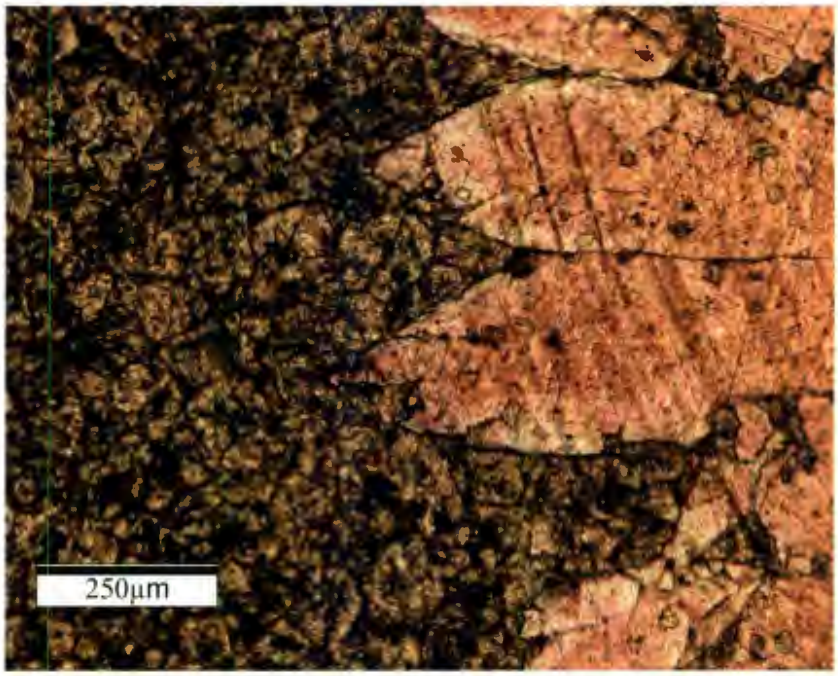

Plate 4.2. A magnified view of the bladed calcite cement from the previous plate. D2 clearly post-dates the cemcnt (TS MG - 123).

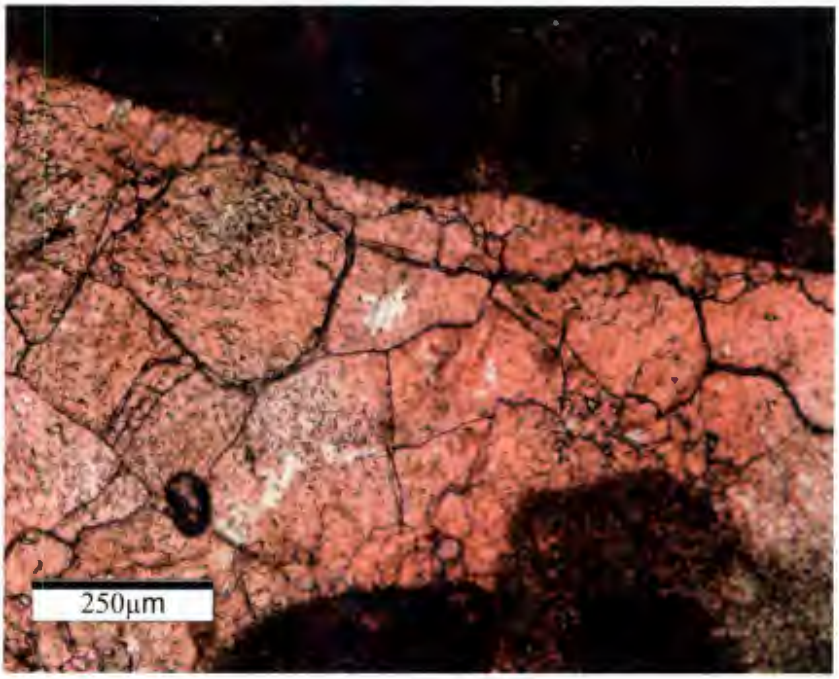

Plate 4.3. Coarse equant calcite cements occluding porosity in a peloidal grainstone. Staining reveals a relatively low Fe-content. Crystals are generally anhedral with irregular surfaces.

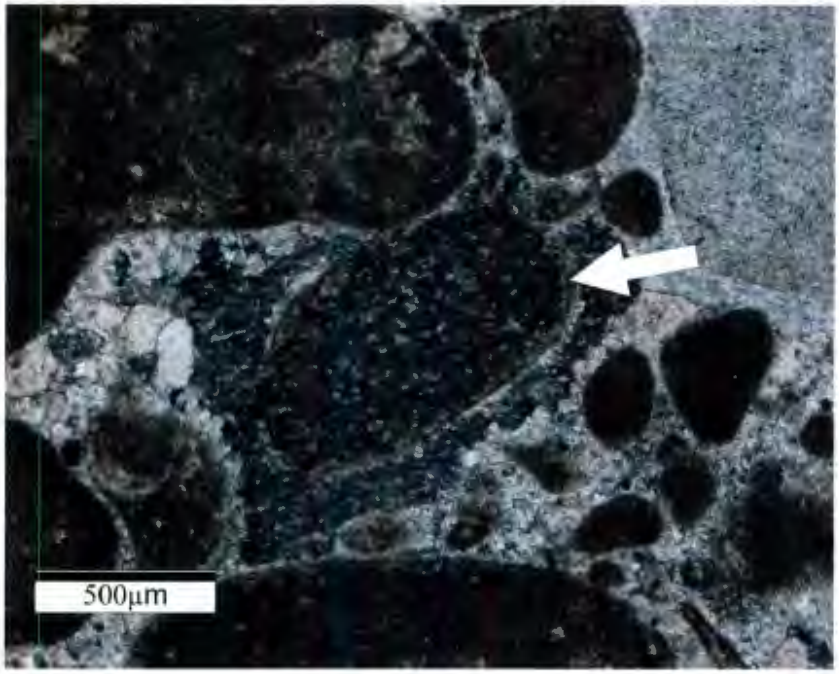

Plate 4.4. A syntaxial overgrowth around an echinoderm fragment. The echinoderm fragment has a micritic envelope (white arrow) that predates the syntaxial overgrowth.

range in size from 20 μm to 400 μm with smaller crystals lining pores and skeletal grains with crystal size increasing toward the center of the occluded pore. Crystals are usually sub- to anhedral. They stain pale red to pink (Dickson, 1966) suggesting relatively Fe^{+} free calcite and precipitation in an oxidizing environment. Equant cements exhibit dull luminescence. Earlier equant calcites tend to have a slightly greater intensity than that of calcite cements next to the pore walls.

4.3.3 Syntaxial Cements

Substrate controlled syntaxial cements are frequent within grainstones of the Catoche Formation (**Plates 3.12 and 4.4**). The cement is an overgrowth of an echinoderm fragment and distinctly forms in optical continuity with the grain. Crystals are commonly of the mm size. The echinoderm fragment has a partial micritic envelope that predates the formation of the syntaxial cement (**Plate 4.4**). Crinoids and other skeletal fragments appear dull under cathodoluminescence.

4.3.4 Dolomite 1

Dolomite 1, dolomicrite to dolomicrosparite, ranges in size from 5 to 35 μm and typically exhibits a nonplanar mosaic with irregular intercrystalline boundaries in a tight packed configuration (**Plates 4.5 and 4.6**). This dolomite appears to mimic the precursor depositional texture of lime mud and exhibits dark to medium luminescence under CL.

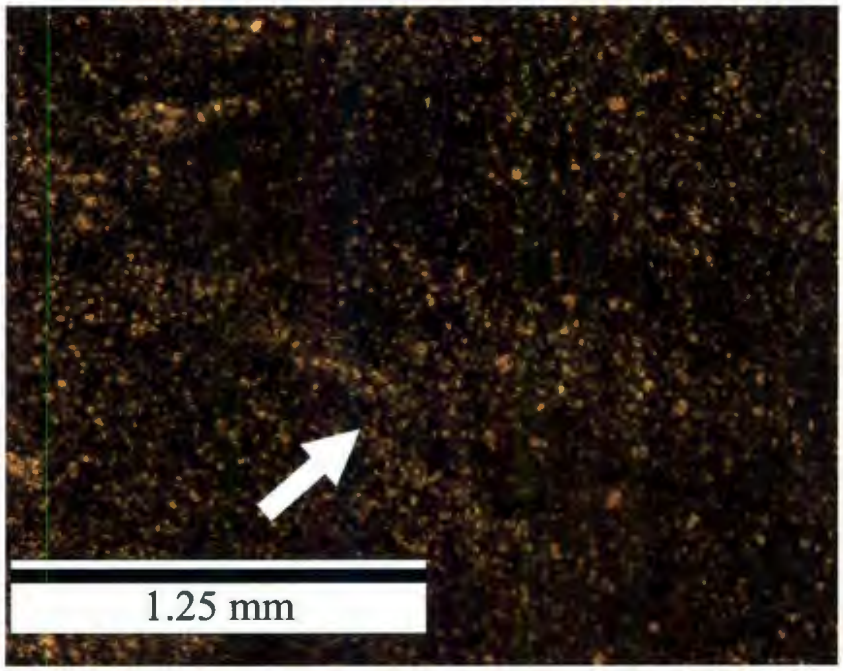

Plate 4.5. Photomicrograph of dolomicrite under plane-polarized light. Faint laminations are visible and likely represent former laminations in the precursor lime-mud (TS MG -402).

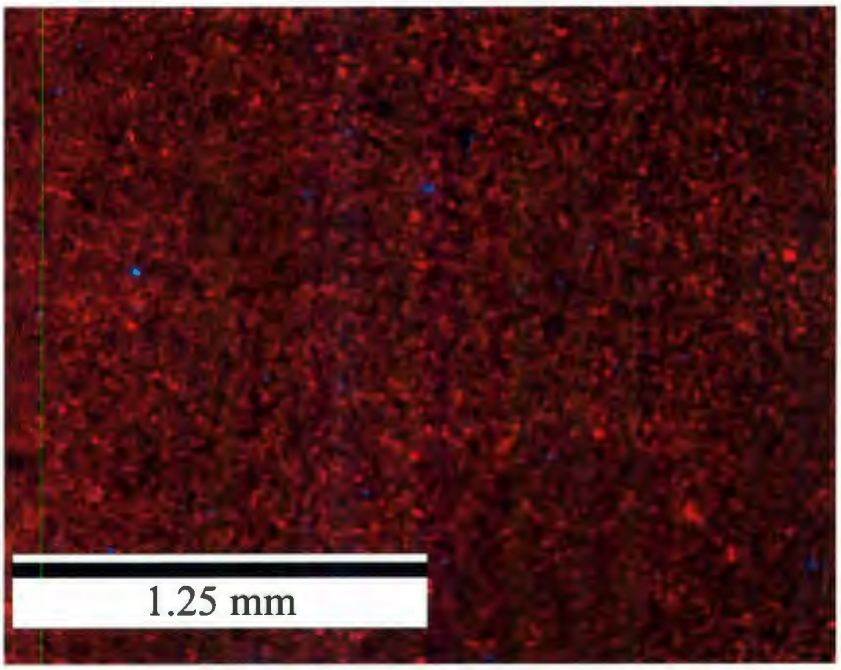

Plate 4.6. Photomicrograph of the same position as above but under cathodoluminescenc. Dolomicrite displays medium to dull red luminescence (TS MG - 402)

4.3.5 Dolomite 2

Dolomite 2 exhibits two ranges in crystal sizes, a subhedral to euhedral, 50 to 120 μm and an anhedral to euhedral 150 to 250 μm (**Plates 4.7 and 4.8**). The crystals have Fe-rich, cloudy cores with Fe-poor clear rims. The inclusion rich, cloudy cores may represent peloids or other allochems which were subsequently replaced by dolomitization. The "ghosts" of the peloids, or the cores of the dolomite crystals, have a bright to medium luminescence under CL while the rims of the crystals consistently display a dull luminescence (**Plate 4.8**). Dolomite 2 (D2) also occurs within burrow walls in mud and wackestone.

4.3.6 Dolomite 3

Dolomite 3 (D3) is a fabric destructive dolomite associated with, and usually bounded by, stylolites (**Plates 4.9 and 4.10**). The stylolites are brownish-red in thin-section and are irregular and swarming. The crystals are sub- to euhedral and range from 70 to 150 μm. Dolomite 3 (D3) displays a medium-red luminescence under CL but no compositional or sector zoning is apparent.

4.3.7 Dolomite 4

Dolomite 4 (D4) lines and fills pores and vugs and is very diverse in size, ranging from 200 μm to over 1 mm (**Plates 4.11 and 4.12**). There are two distinct crystal shapes of D4, an anhedral to subhedral type and a euhedral type. The euhedral pore-filling dolomite is usually associated with considerable intercrystalline and vuggy porosity while

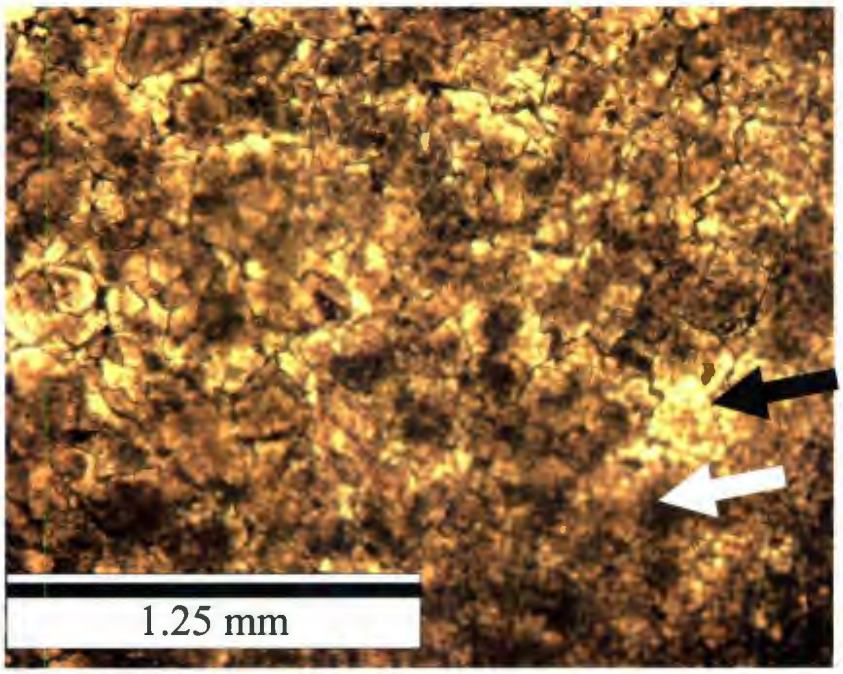

Plate 4.11. Ghosts of peloids under plane polarized light in a dolostone (white arrow). Ghosts appear dark and intergranular areas appear clear (black arrow). The dolomite crystals of the D2 generation (TS MG - 126).

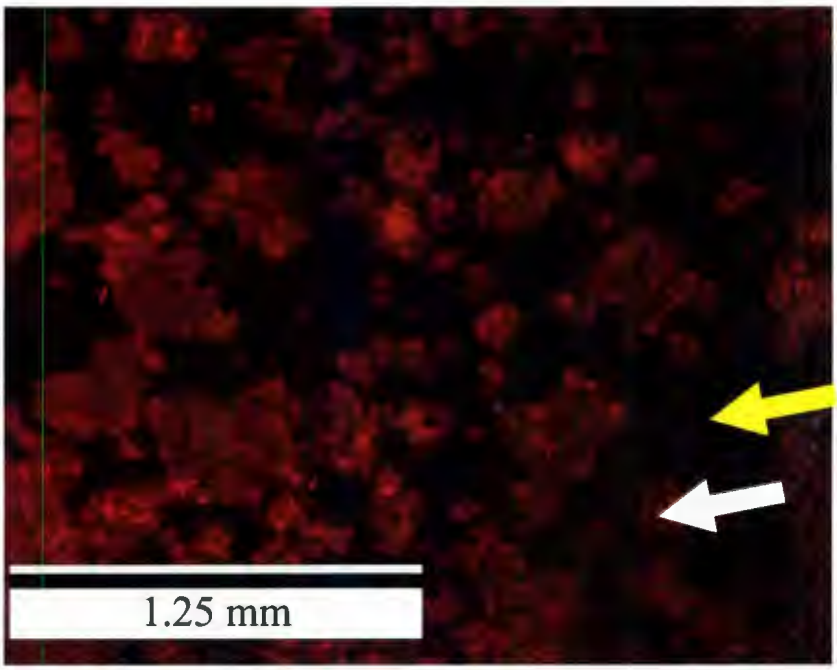

Plate 4.12. Ghosts of peloids under cathodoluminesence appear medium to bright red (white arrows) and intergranular areas display a dark to nonluminescent red (yellow arrow). Dolomite crystals (D2) have replaced the precursor grains and generally have medium red luminescent cores with dull red to non-luminescent rims (TS MG - 126).

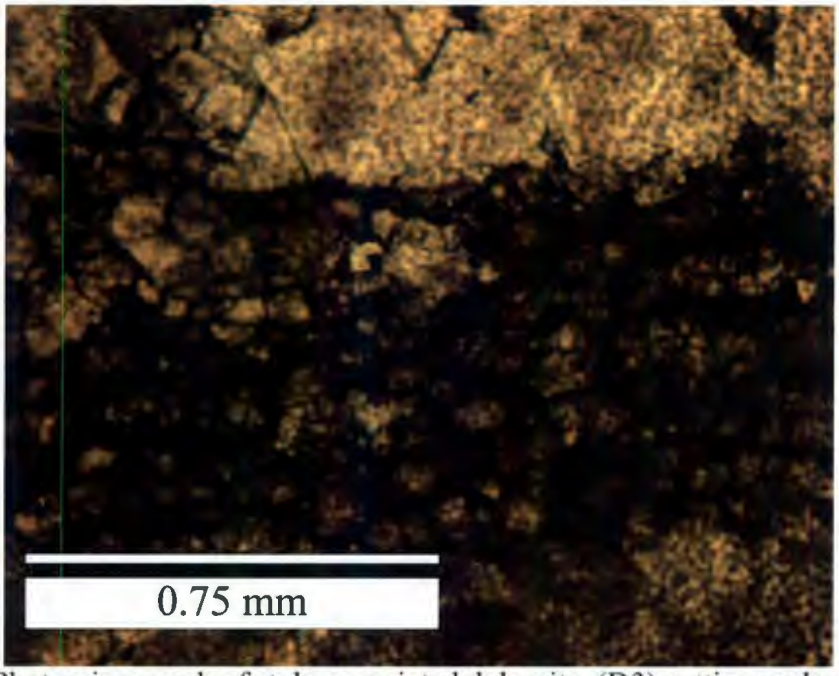

Plate 4.9. Photomicrograph of stylo-associated dolomite (D3) cutting replacive dolomite (D2) under plane-polarized light. D3 is controlled by stylolite formation and associated with organic matter. D2 commonly has cloudy core and well defined crystal surfaces (TS MG 126).

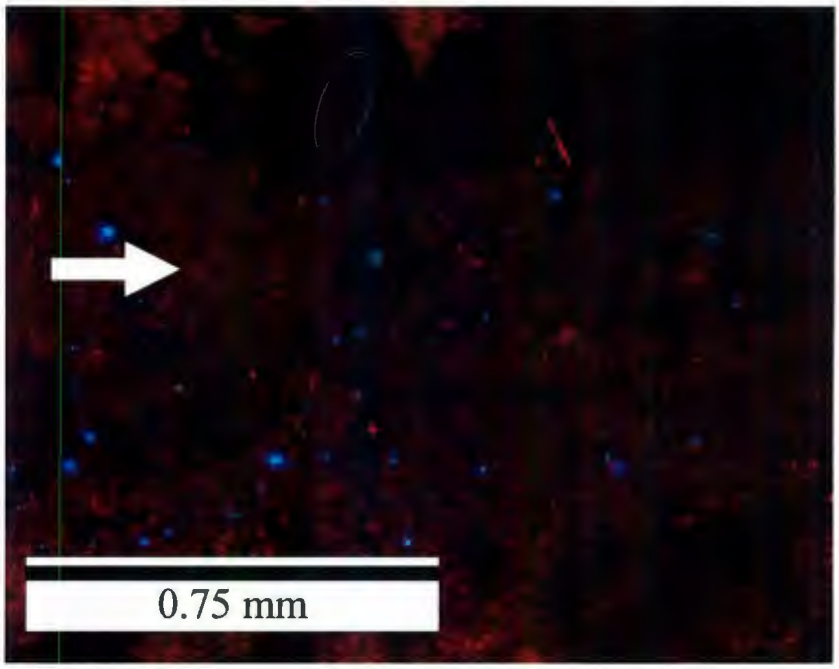

Plate 4.10. Photomicrograph of the above sample under cathodoluminescence. D2 has slight to dull red luminescence at its core (circle) and a dull to non-luminescentzone before the well formed crystal edge and a zone of bright to medium red luminescence. D3 commonly displays medium to dull red luminescence (white arrow).

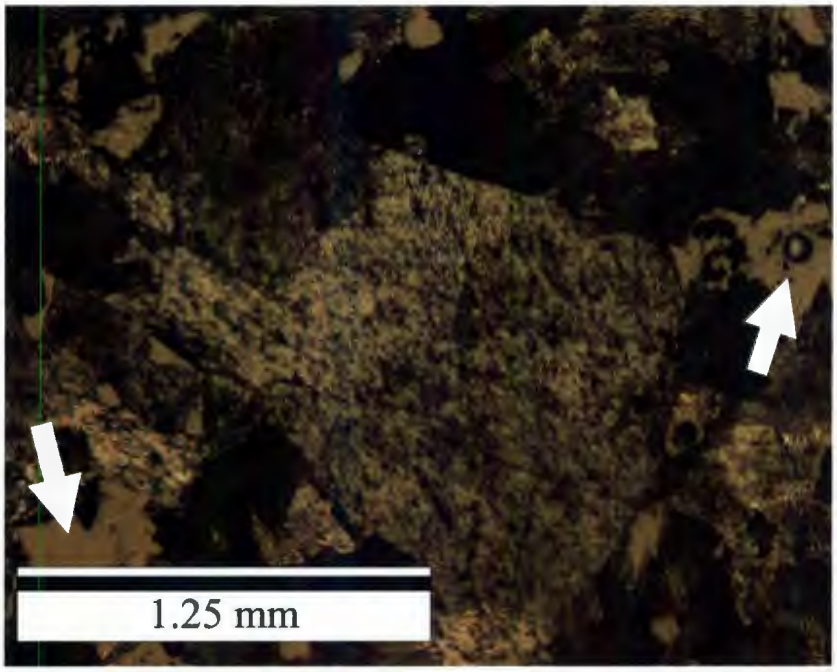

Plate 4.11. Typical coarse euhedral dolomite spar occluding pore space in the upper 40m of the Catoche Formation. Porosity is abundant (white arrows) and is considered inter-crystalline (TS MG - 13).

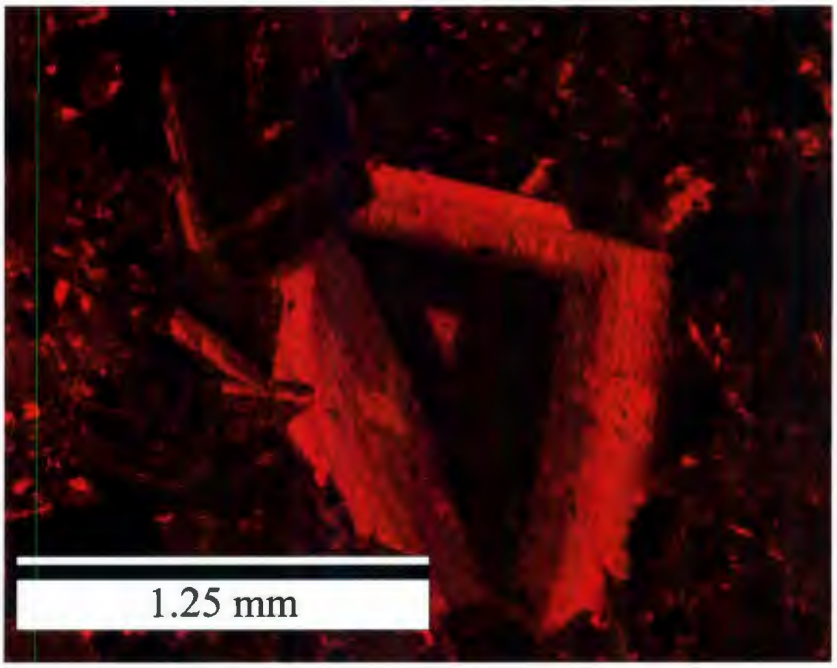

Plate 4.12. Photomicrograph of the above sample taken under cathodoluminescence. Strong zoning is apparent in the above dolomites (D4) indicating changing chemistries of the dolomitizing fluid (TS MG - 13)

the anhedral to subhedral form has occluded any remaining porosity. Cathodoluminescence shows distinct zoning (**Plate 4.12**). The outer zones may or may not display an outer dull-red luminescent band. The cathodoluminescence images clearly show some etching or dissolution around the edges of the crystals. Temperatures of homogenization for D4 range from 89.2 to 99.5 °C (**Table 4.1**).

4.3.8 Dolomite 5

Rare Fe-rich, pore-filling, milky-white crystals of saddle dolomites (D5) were observed filling bio-molds and small veins (**Plates 3.6, 3.7, and 3.8**). These cements ranged in size from 300-600 μm, have strong cleavage and wide sweeping extinction. These uniformably non-luminescent large dolomite cements differ from D4 with the strong zonations of bright and dull luminescence. No fluid inclusion data were obtained for dolomite 5 due to the very small size of primary inclusions that were not possible measure their T_h.

4.3.9 Mold-filling Cacite Spar

Coarse calcites spar (250μm to 1mm) replacing molds of body fossils and partially cementing fractures are observed within the Catoche Formation (**Plates 3.6, 3.7, 3.8, 3.9, 4.13 and 4.14**). A coarse anhedral replacement calcite (**Plates 3.5 and 3.6**) replaces bio-molds displays dull to medium, sometimes concentric, luminescence.

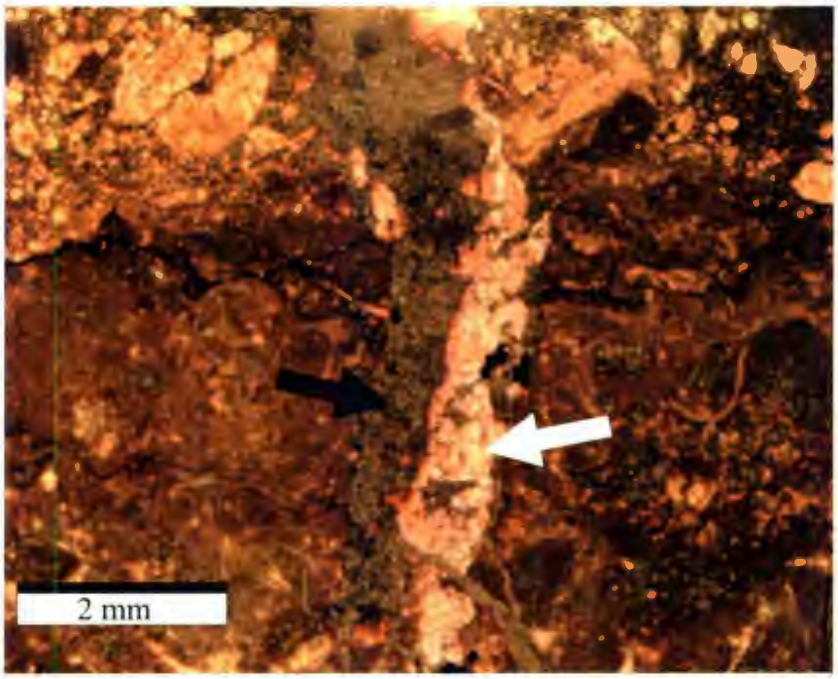

Plate 4.13. Calcite and dolomite filled vertical fracture cutting the Catoche Formation. The fracture was filled with calcite cement (white arrow) and later cemented with dolomite (black arrow) (TS MG - 100).

Plate 4.14. A magnified photomicrograph of the same thin-section as above. The dolomite clearly cross-cuts the calcite (white arrow) (TS MG - 100).

4.3.10 Fracture-filling Calcite Spar

Coarse calcite spars commonly occluded fractures and veins (Cv). Fracture-filling spars are commonly relatively of low-Fe and rarely occur as high-Fe (based on staining). In some instances, the calcite cemented fracture is cross-cut by a coarse fracture filling dolomite (**Plate 4.13 and 4.14**). Vein-filling calcite spar exhibits intense bright and dull orange zonations (**Plates 4.15 and 4.16**). Temperatures of homogenization from fluid inclusions for vein-filling calcite spars range from 115.9 to > 125°C (**Table 4.1**).

4.4 Other Elements

4.4.1 Marine Endolithic Boring and Micritization

Marine boring and partial to complete micritization of grains occurred prior to major calcite cementation and dolomitization (**Plates 3.11, 3.13. and 3.16**).

4.4.2 Stylolization

The development of solution seams and stylolites are indicators of the significance and presence of chemical compaction due to progressive burial of the Catoche Formation (**Plates 3.4, 3.9 and 3.10**). The contemperous development of localized dolomites (D3) along stylolites is common.

Sample	T_h °C
D4	89.2
D4	96.8
D4	96.1
D4	99.5
Cv	115.9
Cv	124.2
Cv	122.5
Cv	>125
Cv	117.1
Cv	121.7

Table 4.1. Temperatures of homogenization for dolomite 4 and a late vein-filling calcite.

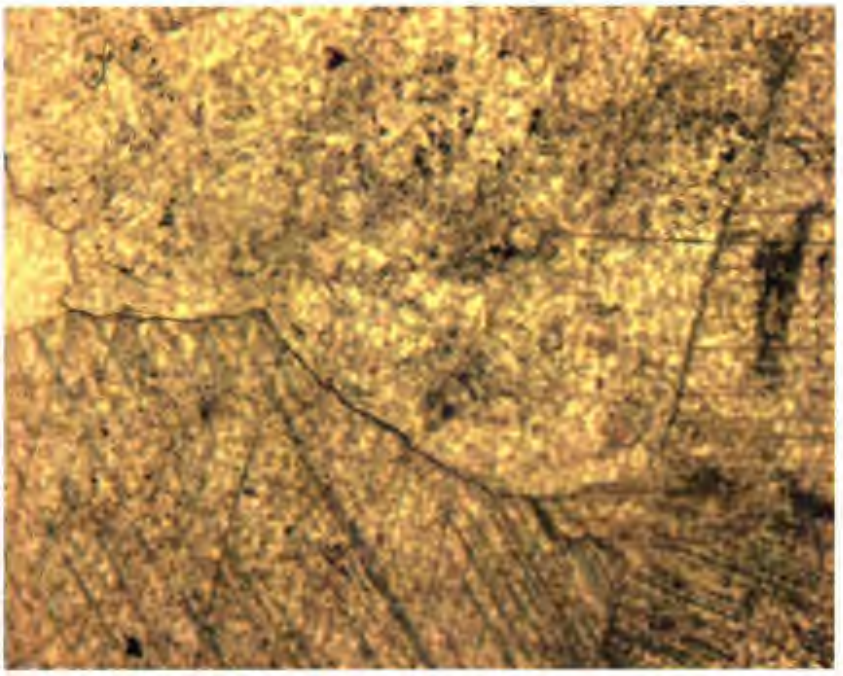

Plate 4.15. Coarse vein filling calcite spar under plane-polarized light (TS MG - 121).

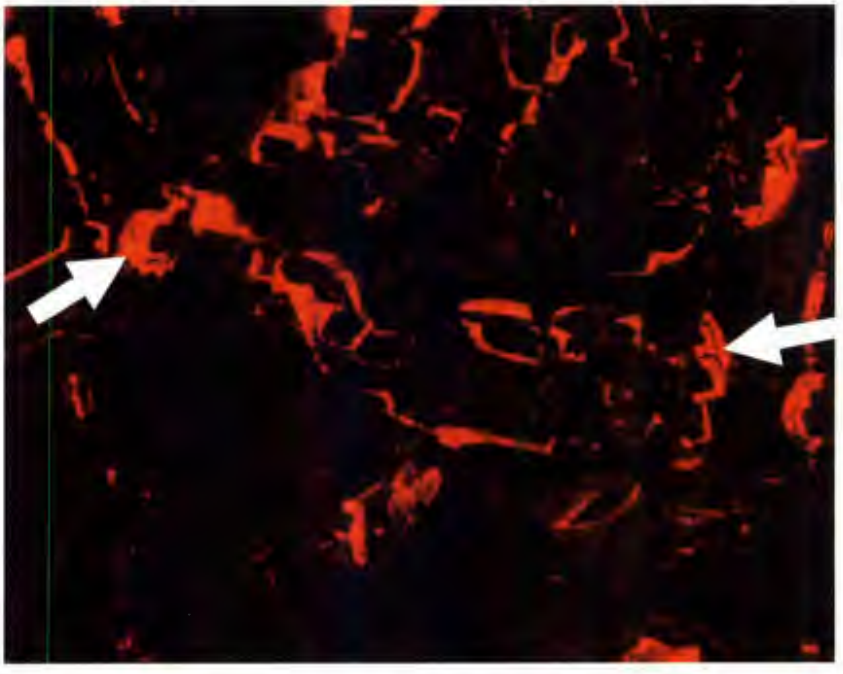

Plate 4.16. Same location as previous plate but taken under cathodoluminescence. Calcite crystals show zoning (white arrows) (TS MG - 121).

4.4.3 Faults, Fractures and Joints

Calcite and dolomite-filled vertical-subvertical fractures cut stylolites (**Plates 4.13 and 4.14**) suggesting brittle fracturing occurred after dolomitizing events D1 to D3 and post-dated chemical compaction.

Northeast trending faults and joints occur near Port au Choix and extend as much as 120m below the St. George Unconformity. Fractures are 0.5 to 3cm wide and in-filled with fine dolomite silt which resembles rock types of the overlying Aguathuna Formation. Narrow zones of dolomitization surround the joints in the Catoche (**Plates 4.17 and 4.18).** Faults and joints suggest a structural control contemperous with the creation of the St. George Unconformity and may be attributed to the evolving deformation of the lithosphere as the Taconic accretionary prism migrated westward (paleosouth) (Knight et al, 2007; Knight 1991; Baker and Knight 1993).

4.4.4 Dissolution

Dissolution in the Catoche carbonates has been previously discussed by several researchers (Haywick, 1984; Baker and Knight, 1991; and Knight et al., 1991). Pressure solution caused by burial, discussed above, dissolves grains and cements at contacts. Major dissolution has occurred during the formation of the St. George Unconformity, due to uplift and exposure of underlying rock to meteoric waters. Examples of subsurface karsting in the Catoche Formation at Port au Choix in the outcrop include caves and small voids and matrix breccias. Caves are bedding parallel and are 10 to 25 cm in height

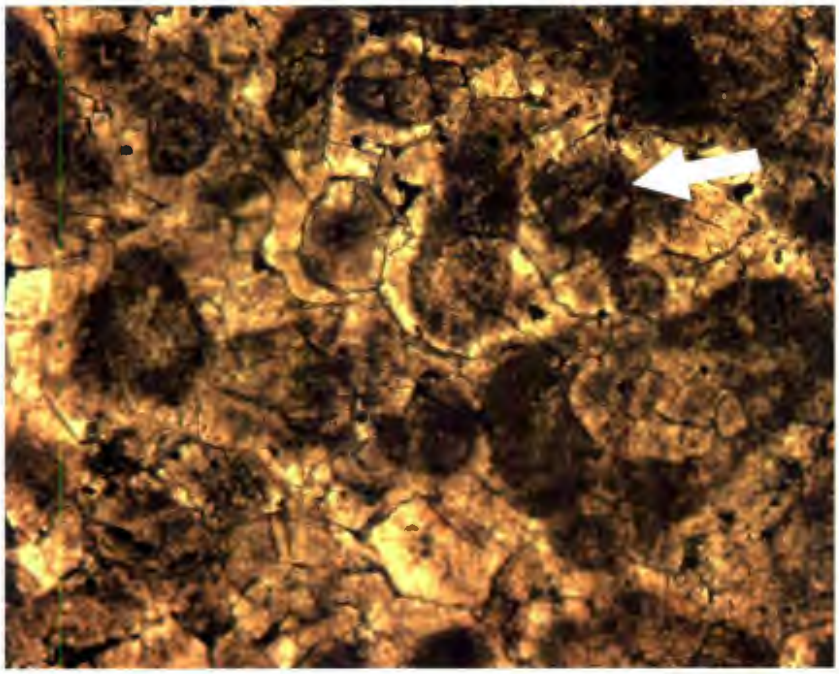

Plate 4.17. Ghosts of former grains are observed under plane-polar light (white arrow) subsequently replaced by dolomite. This sample is located adjacent to a fissure (TS MG - 402).

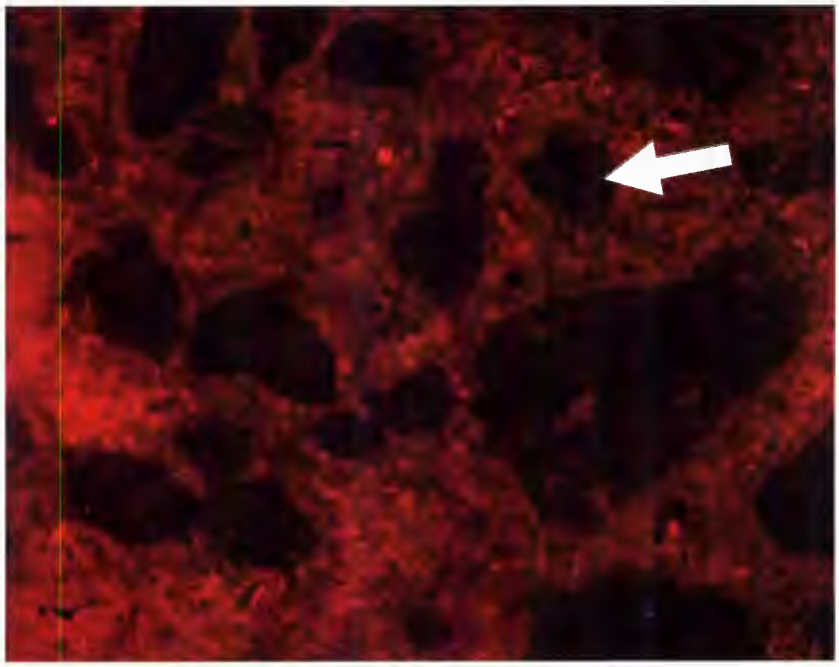

Plate 4.18. The same thin-section as above but under cathodoluminescence. The relict grains display a non to dull red luminescence while the intergranular areas have a medium to bright redish and sometimes orange luminescence. The entire sample is composed of replacement dolomite (TS MG - 402).

and commonly have solution sculptured walls (Baker and Knight, 1993). Vugs appear to have been formed prior to D4 (**Plates 4.11 and 4.12**).

4.4.5 Silicification

Silicification is very minor and rarely observed as early silicified fossils and mainly very late pore-occluding cement post dating D5. D5 is commonly post-dates late equant calcite.

4.4.6 Bitumen

Bitumen is present coating several pore walls; particularly intercrystalline pore walls (**Plate 3.21**). The emplacement of hydrocarbons may have ended the D4 dolomitization event as the D4 generation is not observed occurring after the presence of bitumen.

Table 4.2 is a summary of the approximate timing of observed petrological features within the Catoche Formation of Port aux Choix., Newfoundland.

4.5 Trace Element Distribution in Diagenetic Phases

Table 4.3 is a summary of geochemical results for the dolomites of the Catoche Formation. Chemical analysis of Dolomite 1 (D1) yields Mg (63-183 ppm), Sr (31-161 ppm), and Fe (1721-5349 ppm) concentrations. The average Mg, Sr, and Fe concentrations for D1 are 114 ppm, 72 ppm, and 3125 ppm, respectively. Chemical analysis of Dolomite 2 (D2) yields Mg (56-108 ppm), Sr (30-204 ppm), and Fe (1480-

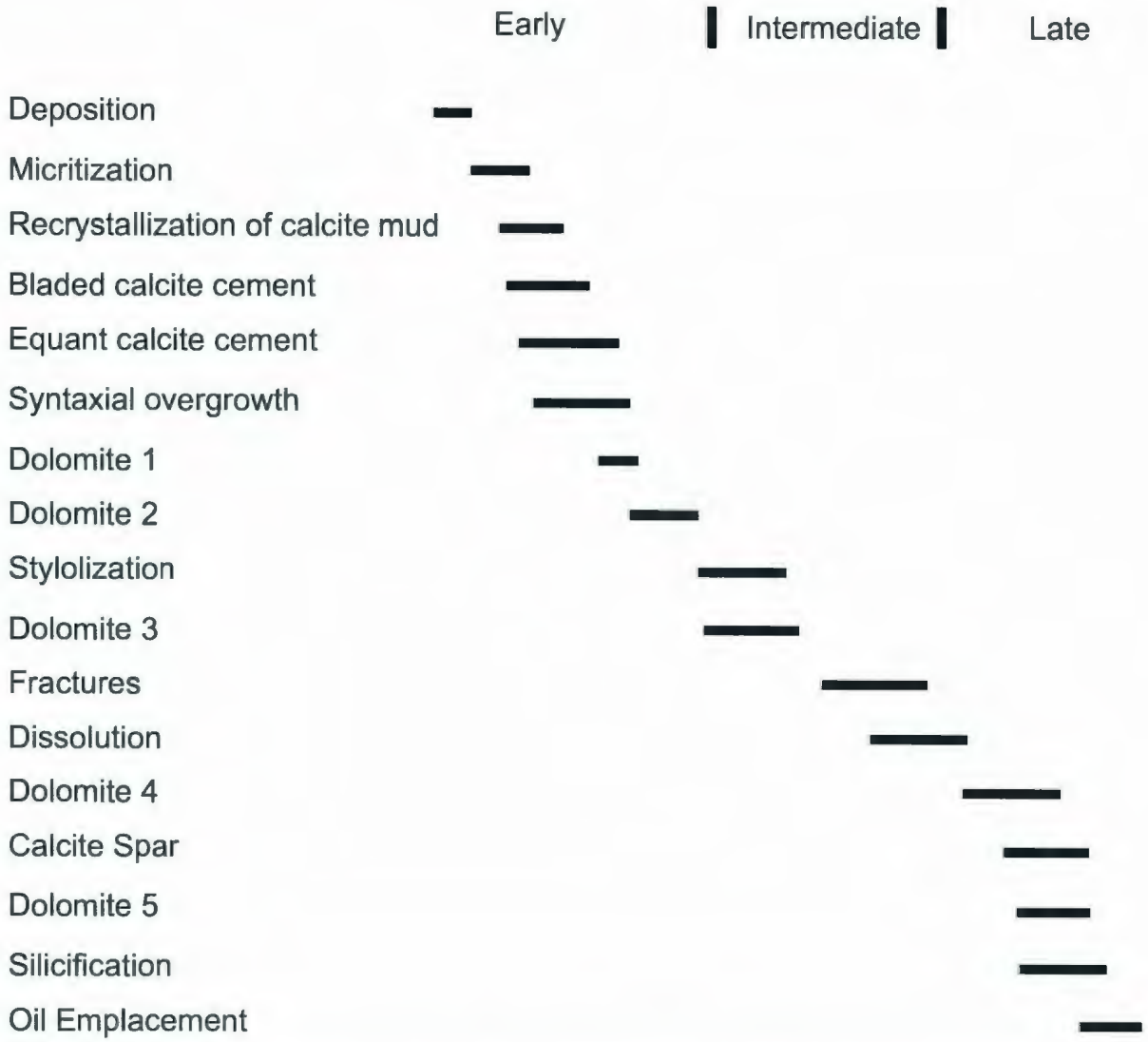

Table 4.2. Paragenetic sequence for the Catoche Formation of Port au Choix, Newfoundland.

Generation		$CaCO_3$%	$MgCO_3$%	Mn(ppm)	Sr(ppm)	Fe(ppm)	$\delta^{18}O$	$\delta^{13}C$	Sr^{87}/Sr^{86}
Dolomite 1	*n*	8	8	8	8	8	8	8	1
	Max.	60.32	45.02	183	161	5349	-6.6	-0.4	-
	Min.	54.98	39.68	63	31	1721	-9.1	-1.3	-
	Mean	57.60	42.40	114	72	3125	-7.3	-0.8	0.708867
	S.D.	1.89	1.89	45	41	1283	0.9	0.3	-
Dolomite 2	*n*	16	16	16	16	16	16	16	5
	Max.	66.74	46.46	108	204	14974	-6.1	0.1	0.710803
	Min.	53.54	33.26	56	30	1480	-10.5	-2.0	0.708989
	Mean	58.64	41.36	84	71	6126	-8.6	-0.9	0.709744
	S.D.	3.98	3.98	13	56	4433	1.3	0.5	0.000766
Dolomite 3	*n*	11	11	11	11	11	11	11	3
	Max.	64.83	44.40	257	159	13659	-8.2	-0.2	0.710206
	Min.	55.60	35.17	64	31	1259	-10.9	-1.7	0.709455
	Mean	59.41	40.59	123	74	5633	-8.3	-1.0	0.709816
	S.D.	2.78	2.78	59	43	3736	0.7	0.6	0.000376
Dolomite 4	*n*	16	16	16	16	16	16	16	3
	Max.	59.79	46.40	435	58	5600	-8.5	-0.6	0.709464
	Min.	53.60	40.21	62	26	853	-10.7	-1.5	0.708938
	Mean	55.71	44.29	206	32	1960	-9.8	-1.1	0.709149
	S.D.	1.36	1.36	86	8	1369	0.5	0.3	0.000278
Dolomite 5	*n*	4	4	4	4	4	4	4	1
	Max.	76.95	40.55	485	88	29279	-9.2	-0.7	-
	Min.	59.45	23.05	240	52	11945	-10.8	-1.5	0.708871
	Mean	65.18	34.82	363	71	20132	-9.9	-1.2	0.708871
	S.D.	8.06	8.06	115	17	8636	0.7	0.4	-

Table 4.3. A summary of the geochemical attributes of dolomite generations for the Catoche Formation.

14974 ppm) concentrations. The average Mg, Sr, and Fe concentrations for D2 are 84 ppm, 71 ppm, and 6126 ppm, respectively. Dolomite 3 (D3) yields Mg (64-257 ppm), Sr (31-159 ppm), and Fe (1259-13659 ppm) concentrations. The average Mg, Sr, and Fe concentrations for D3 are 123 ppm, 74 ppm, and 5633 ppm, respectively. Due to the overprinting nature of D3 contamination during sample collecting is likely to have occurred. Chemical analysis of Dolomite 4 (D4) yields Mg (62-435 ppm), Sr (26-58 ppm), and Fe (853-5600 ppm) concentrations. The average Mg, Sr, and Fe concentrations for D4 are 206 ppm, 32 ppm, and 1960 ppm, respectively. Chemical analysis of Dolomite 5 (D5) yields Mg (240-485 ppm), Sr (52-88 ppm), and Fe (11945-29279 ppm) concentrations. The average Mg, Sr, and Fe concentrations for D5 are 363 ppm, 71 ppm, and 20132 ppm, respectively.

4.6 Stable Isotopes

Dolomite 1, replaces lime mud, and has ranges for $\delta^{18}O$ and $\delta^{13}C$ of -6.6 to -9.1‰ VPDB and -0.4 to -1.3‰ VPDB, respectively (**Table 4.1**). Dolomite 1 has a mean $\delta^{18}O$ signature of -7.3‰ PDB.

Ranges of $\delta^{18}O$ and $\delta^{13}C$ for dolomite 2 are -6.1 to -10.5‰ VPDB and 0.1 to -2.0‰ VPDB, respectively. A mean $\delta^{18}O$ signature of -8.6‰ VPDB is further depleted than dolomite 1 suggesting dolomite 2 has formed later at relatively deeper setting of higher temperature. Dolomite 3 is associated with stylolites and has $\delta^{18}O$ and $\delta^{13}C$ signatures ranging from -8.2 to -10.9‰ VPDB and -0.2 to -1.7‰ VPDB, however due to

the nature and difficulty of sampling this dolomite generation the results are most likely contaminated with the other generations of dolomite.

The $\delta^{18}O$ and $\delta^{13}C$ values of dolomite 4 range from -8.5 to -10.7‰ VPDB and -0.6 to 1.5‰, respectively. The mean $\delta^{18}O$ signature is -9.8‰ VPDB and homogenization temperatures (Th) of primary two-phase fluid inclusions range from 89.2 to 99.5°C support a burial origin at increased temperatures for dolomite 4.

Despite having very distinct trace element contents (high Fe and Mn), D5 has isotope signatures very similar to dolomite 4. The $\delta^{18}O$ and $\delta^{13}C$ values of dolomite 5 range from -9.2 to -10.8‰ and -0.7 to -1.5‰ VPDB.

4.7 Strontium Isotopes

Dolomites were sampled and analyzed for $^{87}Sr/^{86}Sr$ signatures. One sample was obtained for D1 due to a lack of material, yeilding a $^{87}Sr/^{86}Sr$ ratio of 0.709967. $^{87}Sr/^{86}Sr$ signatures for D2 ranged from 0.708989 to 0.710803 with a mean value of 0.709744. $^{87}Sr/^{86}Sr$ signatures for D3 ranged from 0.709455 to 0.710206 with a mean value of 0.709816. $^{87}Sr/^{86}Sr$ signatures for D4 ranged from 0.708938 to 0.709464 with a mean value of 0.709149. One sample was obtained for D5 due to a lack of material, yeilding a $^{87}Sr/^{86}Sr$ ratio of 0.708871.

CHAPTER V

INTERPRETATION

5.1 Introduction

The Catoche Formation was deposited on a dominantly open-shelf, subtidal setting. The lower 80 m consists mainly of dolomitic limestones, limey dolomites and thin beds of dolostone (**Fig. 1.4**). The upper 40 m consists almost entirely of diagenetic dolostone and is interpreted to be meter scale cyclic sedimentation (Baker and Knight, 1993) (**Fig. 1.3**). Porosity within the Catoche Formation is exclusively within the diagenetic dolostone. The presence of micritic envelopes and completely micritized grains suggest an active early diagenetic effect of micro-borers. The sediments were most likely affected by marine and meteoric cementation before reaching the deep burial settings. In the following descriptions the timing for early and late dolomitization events is based on cross-cutting relationships and spatial distributions. Chemical and Isotope analysis are available as Appendix I.

5.2 Marine Diagenesis

Following deposition, marine boring around framework grains by endolithic borers occurred. After the death or vacancy of bore holes, micritic mud infilled boreholes creating micritic envelopes surrounding grains (**Plates 3.11 and 3.13**).

Rare bladed calcite cements grow normal to the substrate and range in length from 150 μm to 600 μm with length to width ratios of about 2.5:1 (**Plates 4.1 and 4.2**).

Staining suggests a low relative Fe^{+} content. Crystal faces are euhedral and terminations are prismatic suggesting marine cementation. Bladed calcite crystals were too small to sample with a microdrill for chemical analysis.

5.3 Meteoric Diagenesis

Recrystallization of lime mud occurred soon after deposition through neomorphism and transformation of aragonite and HMC components to LMC resulting in a coarsening of grain size (**Plates 3.1 and 3.2**).

Bladed cements of marine origin are followed by the more common equant cements. The equant calcite cements stain pale red to pink (Dickson, 1966) suggesting relatively Fe^{+} free calcite and precipitation in an oxidizing environment. Cementation occurred early relative to burial as evident by the low frequency of deformed framework grains.

The earliest dolomite (D1) is dolomitized lime mud and occurs sporadically throughout the succession (**Plates 4.5 and 4.6**). Dolomicrite (D1) formed from the local dolomitization of lime mud, preserving textural features of the precursor mud.

Assuming the Sr content is mainly due to D_{sr} and Sr/Ca molar ratio of the dolomitizing fluid, the latter can be calculated from equation

$$(Sr/Ca)_{dolomite} = D_{Sr}(Sr/Ca)_{fluid} \qquad \text{(Budd, 1997)}$$

where D_{Sr} varies from 0.015 to 0.06 (Banner, 1995; Budd, 1997). Values of Sr/Ca for the dolomitizing fluid of D1 are calculated to be between 0.0037 and 0.00094 when D_{sr} is equal to 0.015 and 0.06, respectively. The Sr/Ca ratio of present day seawater is about

0.0086 (Drever, 1988), which may suggest that the dolomitizing fluids that formed D1 might have contributions from fluids of non-marine origin such as meteoric waters. However, the uncertainty of D_{Sr} of dolomite may argue for caution with interpretations.

The petrographic and trace element geochemistry studies showed multiple-progressive phases of dolomitization within the Catoche Formation. The isotopic composition of the different dolomite generations reflects the isotopic composition of the different dolomitizing fluids associated with each dolomitizing phase.

The isotopic results for the Catoche dolomites and calcite components are listed in **Appendix I, Table 4.3**, and shown in **Figure 5.1**. Despite the considerable overlap, the Catoche dolomites show a decrease in the $\delta^{18}O$ values from D1 to D5 which might reflect the effect of increase of temperature with progressive burial. However, the $\delta^{13}C$ values do not exhibit a discernable trend.

The $\delta^{18}O$ signature of the dolomitizing fluid can be estimated using the $\delta^{18}O$ signature for the dolomite phase and temperature of dolomitization estimated from the homogenization temperature (Th) of primary fluid inclusions within that phase (Goldstein and Reynolds, 1994). The relationship between the dolomite mineral $\delta^{18}O$ values, the dolomitizing fluid $\delta^{18}O$ values, and the temperature of formation is reconstructed in **Figure 5.2** (Land, 1983). Due to the very small size of primary fluid inclusions within the dolomites of the Catoche Formation only four measurements from dolomite 4 and six measurements from a late vein-filling calcite were obtained (**Table 4.1**).

The near-micritic grain size of D1 suggest insignificant alteration during the exposure to meteoric environment and that dolomitization likely occurred at early stages

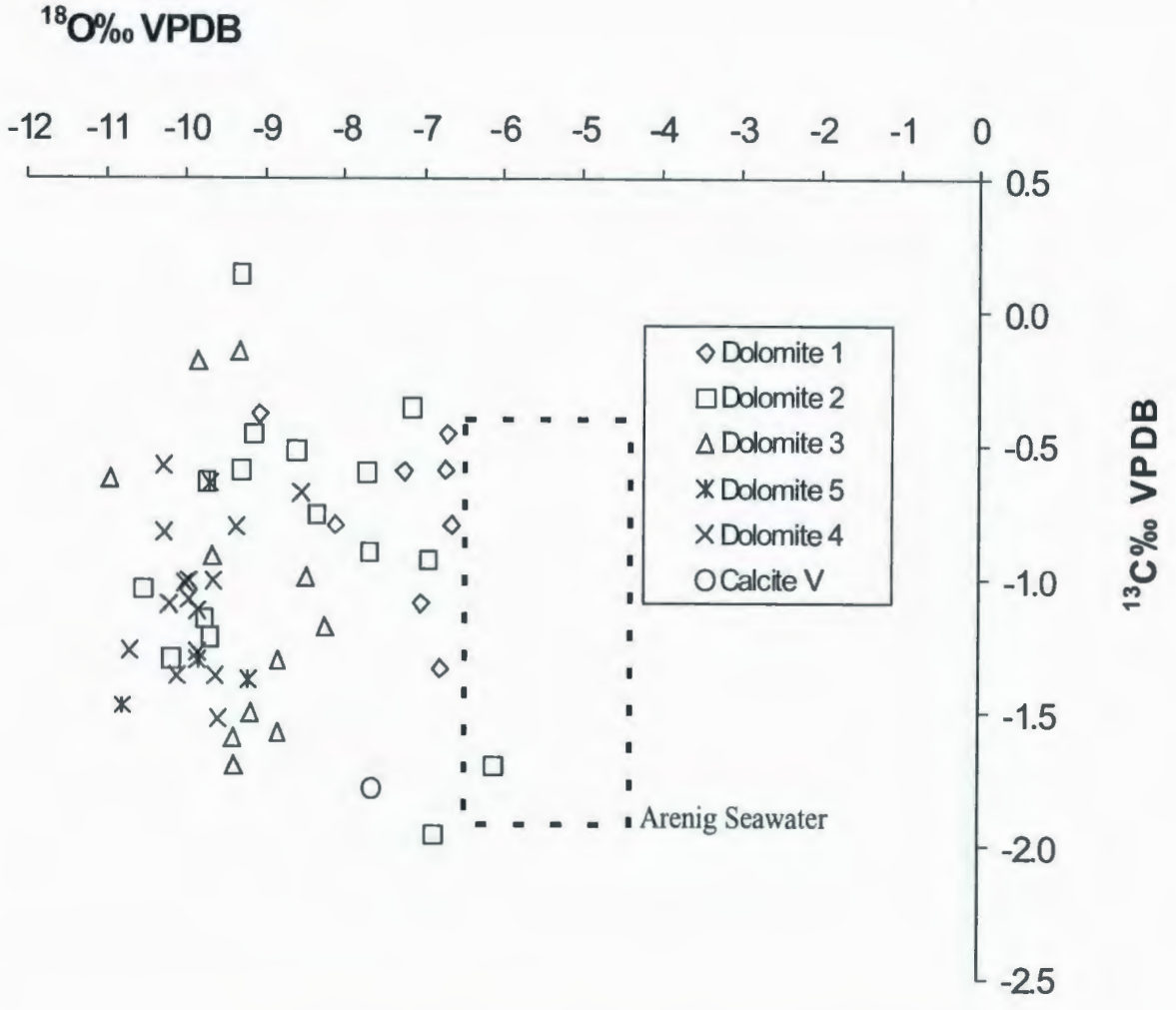

Fig. 5.1. Scatter diagram of oxygen vs. carbon isotopes for dolomite generations and late vein-filling calcite. The dashed box represents the range in isotopic composition of Arenig seawater.

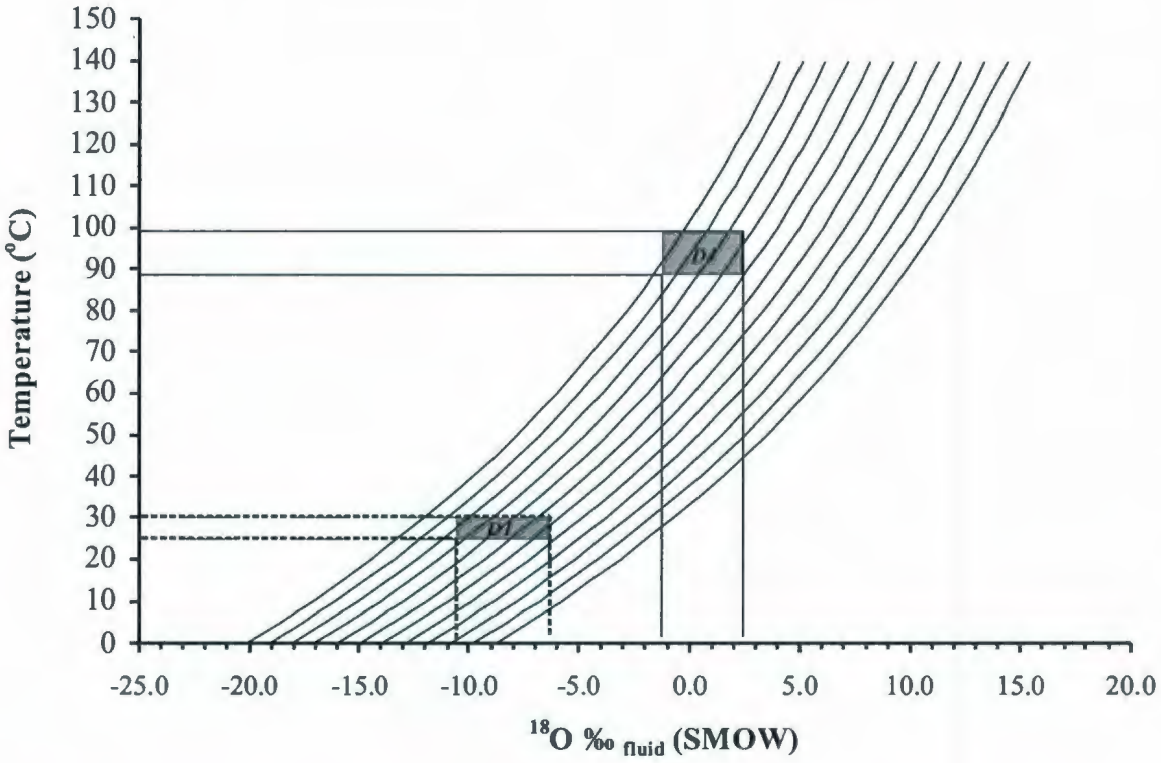

Fig. 5.2. Temperature vs. $\delta^{18}O_{diagenetic\ fluid}$ for various $\delta^{18}O_{dolomite}$ values that were reconstructed from the equation $10^3 \ln a = 3.2 \times 10^2 T^{-2} - 3.3$ (Land, 1983). The vertical bars indicate the ranges for $\delta^{18}O_{fluid}$ based on the most enriched and depleted sample for the given dolomite generation, while shaded areas mark the preferred temperature ranges.

of diagenesis at near surface conditions and temperatures possibly between 25 and 30 °C. The $\delta^{18}O$ values of D1 suggest that it might have originated from dolomitizing fluids with $\delta^{18}O$ values estimated between -10.7 to -6.4‰ VSMOW (**Figure 5.2**) which, for the most part, are slightly depleted relative to those suggested for the range of Early to Middle Ordovician seawater (Veizer et al., 1999).

The presence of boundstone stromatolite mounds and microbial limemud flats suggests that the Catoche Formation was deposited under semi-arid to possibly sub-humid, tropical conditions (Pratt and James, 1986). In similar modern day environments the $\delta^{18}O$ of seawater is about 0‰ VSMOW and that of meteoric water is depleted by about 4‰ (Clark and Fritz, 1997). Assuming that the $\delta^{18}O$ composition of the Arenig seawater and meteoric water was similar to that of today, the $\delta^{18}O$ of -10.7 to -6.4‰ VSMOW for the D1 dolomitizing fluid would suggest an origin almost entirely from meteoric type, which is simply impossible due to an inadequate source of Mg provided by meteoric waters (Land, 1992).

An alternate scenario is that $\delta^{18}O$ of ancient seawater is depleted relative to its modern counterpart (Veizer, 1999). The $\delta^{18}O$ of Arenig seawater can be calculated using well preserved brachiopods which range in $\delta^{18}O$ from -11.1‰ to -8.2‰ VPDB ("stage 2" of Table 2 in Shields et al., 2003). The mean $\delta^{18}O$ signature of tropical (~ 25 °C) early to middle Arenig seawater is about -7.7‰ VSMOW with a range of -6.6‰ to -9.5‰ VSMOW (Sheilds et al., 2003) as recorded from well-preserved brachiopod shells and calculated using the equation:

$$T = 15.7-4.36(\delta^{18}O_c-\delta^{18}O_w)+0.12(\delta^{18}c-\delta^{18}O_w)^2$$

where T is temperature in degrees Celsius, $\delta^{18}O_c$ (PDB) is the oxygen isotope signature as recorded from the brachiopod shell and $\delta^{18}O_w$ (SMOW) is the oxygen isotope signature of the diagenetic fluid (Hayes and Grossman, 1991).

Assuming that the heaviest $\delta^{18}O$ of Arenig brachiopods reflect the best preserved signal, the calculated estimate of the Arenig seawater is ~ -6.6‰ SMOW. Since the meteoric water $\delta^{18}O$ is usually 4‰ lower than that of its seawater counterpart, the estimated $\delta^{18}O$ signature of the Arenig meteoric water is ~ -10.6‰ SMOW. The calculated $\delta^{18}O$ values of the dolomitizing fluid of D1 (-10.7 to -6.4‰ SMOW) fall within the range of composition suggested for the two end-member Arenig marine (-6.6‰ SMOW) and meteoric (10.6‰ SMOW) waters, thus suggesting a mixture of marine and meteoric waters.

Dolomite 1 preserves the near-micritic size of it precursor limemud suggesting a considerable degree of preservation and minimum meteoric alteration before dolomitization. This maximizes the chance of retaining the near-primary Sr-isotope signature despite dolomitization since the $^{87}Sr/^{86}Sr$ ratio of the dolomitizing fluid is usually buffered by that of the precursor carbonate phase. Assuming that the least radiogenic $^{87}Sr/^{86}Sr$ ratio of dolomite 1 (0.708867) is a proxy for the signature of the precursor limemud, the dolomitization of the Catoche carbonate is suggested to have started during the Early to Middle Ordovician (**Figure 5.3**).

Dolomite 2 (D2) replaces grainstones, packstones and burrows in wackstones and mudstones (**Plates 4.7 and 4.8**). Dolomites 1 and 2 show a slight increase in Sr concentration with depth (**Figure 5.4**), suggesting a possible downward circulation of the

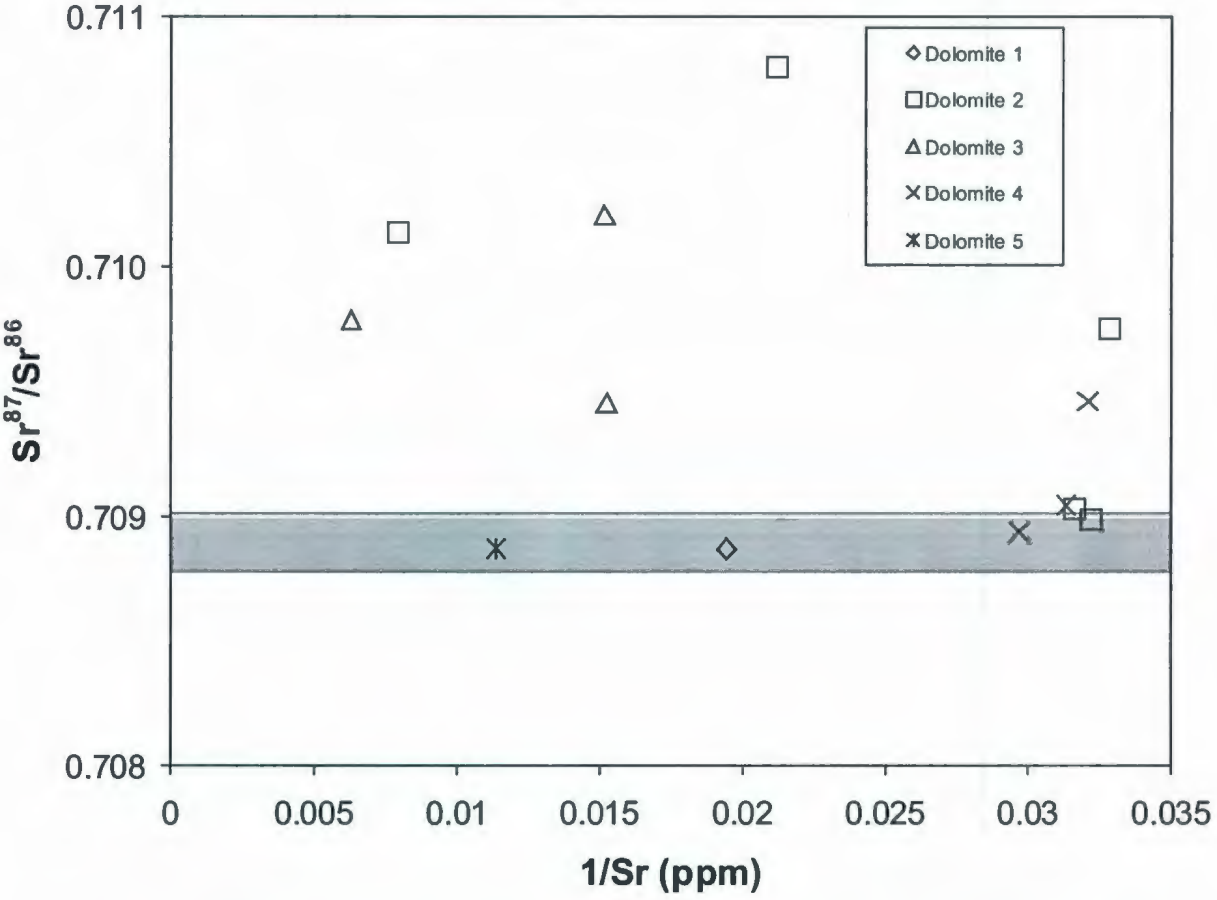

Fig. 5.3. Scatter diagram of strontium isotopes vs. Strontium. The grey shaded area represents the composition of middle Ordovician seawater (Veizer et al., 1999).

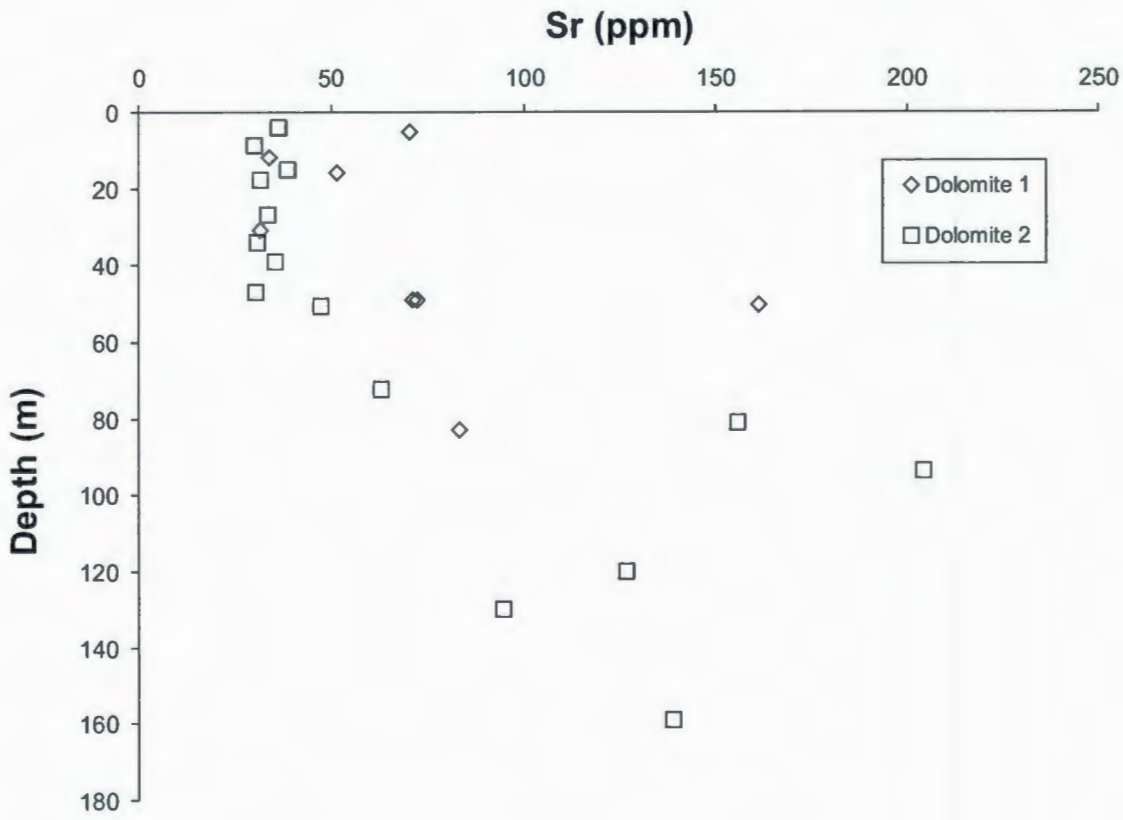

Fig. 5.4. Scatter diagram of Sr vs. Depth for dolomite generations 1 and 2.

dolomitizing fluid where such fluids became progressively enriched in Sr so that the depletion of Sr from the solid phase was inhibited with increasing depth.

5.4 Burial Diagenesis

Progressive burial of the Catoche carbonates results in chemical dissolution and the development of solution seams and stylolites (**Plates 3.4, 3.9, and 3.10**). Bounded and controlled by solution seams and stylolites are locally developed dolomites (D3). Development of D3 was contemperous with chemical compaction (**Plates 3.9 and 3.10**).

Brittle deformation is evident as fractures filled with calcite followed by dolomite spar (**Plates 4.13 and 4.14**). Fractures and fracture fills cross-cut stylolites and solution seams.

Homogenization temperatures of primary two-phase inclusions from dolomite 4 ranged from 89.2 to 99.5°C (**Table 4.1**) suggesting dolomitization at deep burial conditions or shallow conditions if fluids were hydrothermal in origin. No salinity values were obtained due to the degree of difficulty of measurement. The dolomitizing fluids associated with dolomite 4 have $\delta^{18}O$ values that range from 2.4 to -1.2 ‰ SMOW suggesting an origin of evolved diagenetic waters enriched in ^{18}O likely due to circulation in the crustal rocks at the deep burial settings.

Within the completely dolomitized top 40 m of the Catoche Formation large cm to mm sized vugs are present (**Plates 3.19 and 3.20**). Vugs have been partially occluded by euhedral pore-filling dolomites. It is possible the same fluid is responsible for both dissolution and later dolomitization and is probably of hydrothermal origin. Late

replacement dolomites are also contemperous with the formation of the pore-filling dolomite rhombs and thus are both considered as D4.

The latest dolomitization event follows the filling of bio-molds with late calcite spar and is Fe-rich saddle dolomite (D5) which formed under reducing conditions (**Plates 3.5, 3.6, 3.7, and 3.8**). There is a lack of cross-cutting relationships to relatively time the formation of this late calcite and dolomite but it appears that D5 post-dates calcite growth. The lack of availability microthermometric data of primary two-phase inclusions from D5 made it difficult to calculate estimates for the $\delta^{18}O$ values of the parent dolomitizing fluid.

5.5 Other trends in the Catoche Dolomites

Despite the overlap between the Sr and Mn contents of some of the dolomites (**Fig. 5.5**) a slight trend of decreasing Sr and increasing Mn is still generally observed in dolomites associated with progressive dolomitization and burial. Usually fine-grained dolomites have higher Sr contents than later diagenetically coarser dolomites. In general, Sr in calcite decreases with dolomitization and progressive dolomitization leads to further depletion. Manganese content typically increases with successive diagenetic episodes due to an increase in Mn concentration within diagenetic pore-waters (Warren, 2000) in burial conditions.

In terms of trace elements, Fe and Mn progressively increase, albeit considerable overlap of earlier replacement dolomites (D1 to D3) (**Fig. 5.6**). Dolomites 4 and 5 are significantly enriched in Mn and Fe contents with D5 having the highest values

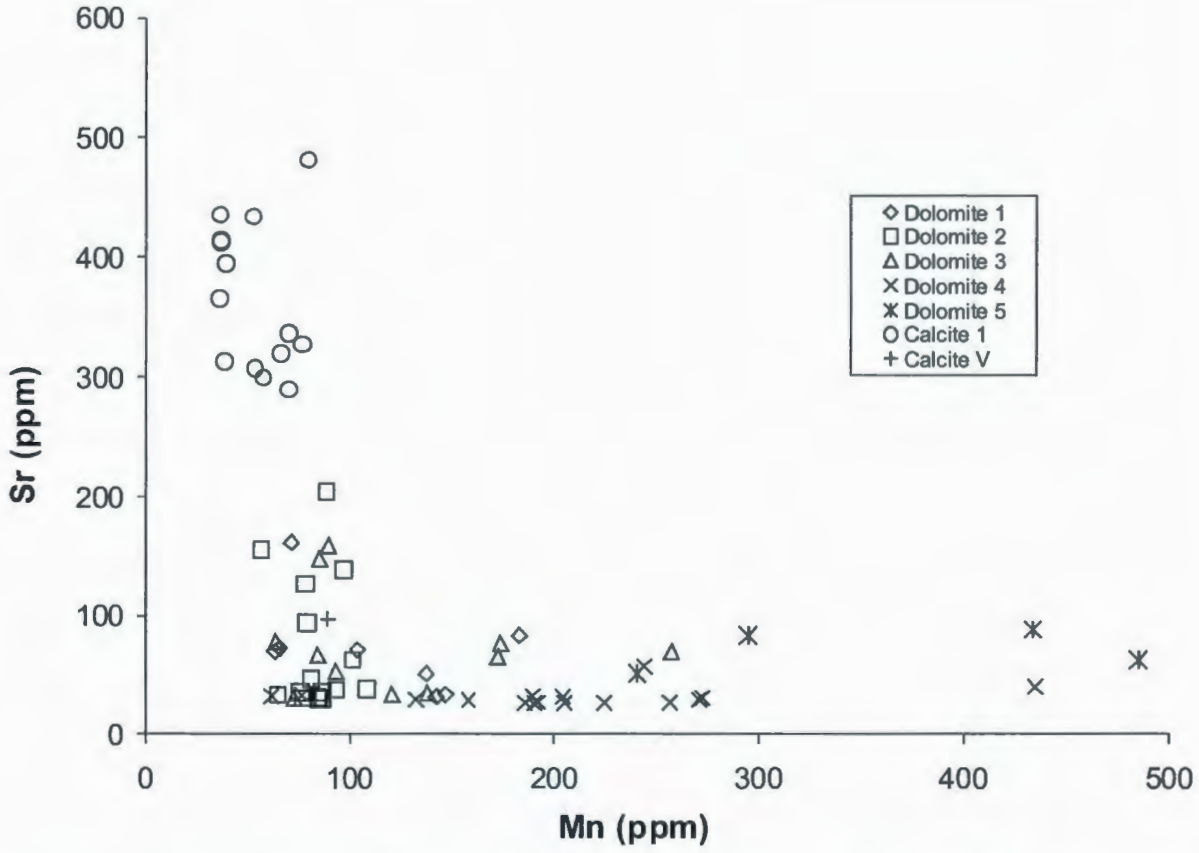

Fig. 5.5. Scatter diagram of Sr vs. Mn for dolomite generations, lime mud and late vein-filling calcite.

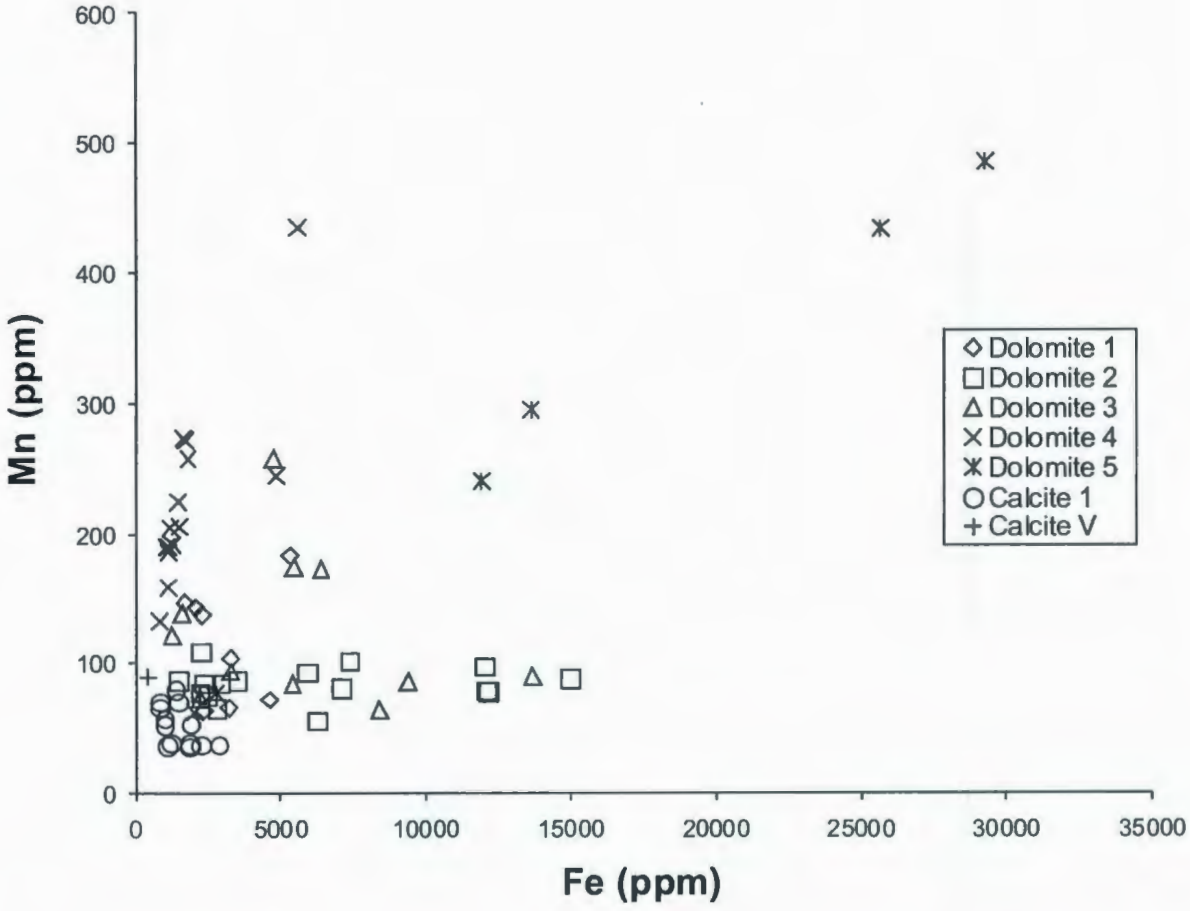

Fig. 5.6. Scatter diagram of Mn vs. Fe of dolomite generations, lime mud and late vein-filling calcite.

Iron and Mn contents (**Table 4.2, Fig. 5.6**), reflect more the redox state of the diagenetic environment than the ionic strength of the dolomitizing fluid. Considerable overlap exists in Fe and Mn content of D1 to D3 but D4 is enriched in Mn and relatively depleted in Fe, suggesting formation under significant reducing conditions with a limited supply of Fe. Dolomite 5 is enriched in both Mn and Fe with average contents of 363 ppm and 20132 ppm respectively, suggesting dolomitization most likely occurred under reducing conditions with allochthonous sources for these elements. Allochthonous sources usually indicate significant and effective fluid circulation with underlying or adjacent non-carbonate rock (Budd, 1997).

5.6 Summary

The Catoche Formation has undergone possibly 5 phases of dolomitization. The trace element geochemistry of the earliest replacement dolomites (D1), more so the Sr/Ca molar ratio, suggest an origin of mixed seawater/meteoric water for the earliest dolomitizing fluid, which is also consistent with the reconstructed $\delta^{18}O$ estimates of the dolomitizing fluids. The least radiogenic $^{87}Sr/^{86}Sr$ ratio of dolomite 1 suggests that dolomitization likely started at early stages of diagenesis during Middle Ordovician. There is some overlap of trace element concentrations of the Catoche dolomites but increased Fe contents suggest slightly more reducing conditions of deeper environment at the time of dolomitization associated with dolomite 2. Oxygen isotope signatures for dolomite 2 are depleted relative to dolomite 1 possibly due to increased temperature due to progressive burial. Strontium isotope signatures point to a more radiogenic

dolomitizing fluid for dolomite 2 than dolomite 1 suggesting a circulating fluid with some contact to siliciclastics.

The trend of slight increase of strontium with depth (**Fig. 5.4**) is possible evidence for a downward circulating fluid for dolomites 1 and possibly 2, which became progressively enriched in Sr so that the depletion of Sr from the solid phase was inhibited with increasing depth.

Dolomite 3 is associated with stylolites and difficult to sample due to significant contamination. Dolomite 4 formed at burial conditions from fluids rich in Mn and likely poor in Fe. These fluids were likely circulated through siliciclastics becoming slightly more radiogenic.

Petrographic crosscutting relationships suggest that Dolomite 5 most likely post-dates dolomite 4 and has higher Fe and Mn content. Dolomite 5 may have formed in the deepest burial setting compared.

The Catoche Formation has undergone multiple episodes of dolomitization traced by the variation in the concentrations of Mn, Sr, and Fe. The Sr/Ca molar ratio for dolomite 1 (0.0037 to 0.00094) suggest a dolomitizing fluid composed of a mixed seawater/meteoric water source of possible mixing zone environment. The low strontium contents of dolomites and a lack of evaporate layers, argues against evaporitic brines as a source for dolomitization. Both dolomites 1 and 2 show evidence of increases of Sr concentrations with depth suggesting a possible downward circulation of dolomitizing fluid in a semi-closed system.

The isotopic results for the Catoche dolomites and calcite components are listed in **Appendix I, Table 5.1**, and shown in **Figure 5.1**. Despite the considerable overlap, the Catoche dolomites show a decrease in the $\delta^{18}O$ values from D1 to D5 which might reflect the effect of increase of temperature with progressive burial. However, the $\delta^{13}C$ values do not exhibit a discernable trend.

The petrographic and trace element geochemistry studies showed multiple-progressive phases of dolomitization within the Catoche Formation. The isotopic composition of the different dolomite generations reflects the isotopic composition of the different dolomitizing fluids associated with each dolomitizing phase.

The subsequent phases of dolomites have variable $^{87}Sr/^{86}Sr$ ratio that cannot be related to seawater since progressive dolomitization led to an increased $^{87}Sr/^{86}Sr$ ratio which resulted from dolomitizing fluids that circulated though siliclastics in deep burial environments.

CHAPTER VI

POROSITY EVOLUTION IN THE CATOCHE FORMATION

6.1 Introduction and Theoretical Concept

The evolution of porosity within carbonate rocks during diagenesis is important for the evaluating reservoir properties. Primary and secondary porosity of carbonate rocks are at times facies-controlled and further altered through processes involved in diagenesis (e.g., Moore, 2001). Primary porosity forms during the syndepostional stage, which may include pores within forams, corals, or ooids and secondary porosity is a product of diagenesis which may occur after deposition. Processes that can be constructive to porosity development during diagenesis include dissolution, dolomitization, fracturing and brecciation. Porosity can be destroyed through processes such as cementation and progressive dolomitization (Flugel, 2004).

Porosity is the percentage of a volume of rock that is occupied by interstices, without regard to the connectivity of the pore system. The effective porosity is the percentage of the total rock volume that consists of interconnected pores. Effective porosity is controlled more by the pore throats then the pore volumes, and is key to an effective permeable reservoir system.

6.2 Porosity Types in Carbonates

Choquette and Prey (1970) classification for porosity in carbonate rocks is the most widely used. This classification distinguishes porosity based on fabric-selective

porosity which includes interparticle, fenestral, intraparticle, shelter, growth framework, intercrystal, and moldic porosity, and non-fabric selective porosity which includes fracture, channel, vug, and cavern porosities. Breccia, boring, burrow and shrinkage porosity can be classified as either fabric selective or not.

6.3 Porosity in the Catoche Formation

The porous diagenetic dolostone of the Catoche Formation were originally deposited as upward shoaling, meter scale, peloidal grainstones following a significant textural shift from the muddy packstones and wackstones of the lower 120m of the succession (Baker and Knight, 1993). It is probable that the peloidal grainstones were more open to pervasive dolomitization due to increased primary porosity over the less porous muds and restricted meteoric cementation. The upper ~40 m of diagenetic dolostone was most likely open to such pervasive dolomitization possibly due to the original (and since destroyed) permeable fabric inherent in peloidal grainstone shoals and/or the early diagenetic pore system developed by dissolution through the karstification caused by the major St. George Unconformity. The main very significant, type of porosity within the Catoche Formation is entirely secondary in origin and all of the porosity is located within the completely dolomitized Costa Bay Member (cyclic peloidal grainstones). The most common type of porosity are large vugs (commonly of 1mm scale or greater), followed by a significant proportion of intercrystalline porosity (associated with D2), and lesser amounts of stylo-porosity.

Visual estimations of porosity from thin sections in this study yield a range of 0 to >20 % with the effective or connected porosity of most samples varying greatly. Porosity values ranging from 6.8 to 9.6 % were documented for the Pointe Blanche section on the Port aux Choix Peninsula with permeability values ranging from 0.02mD to 317mD (Baker and Knight, 1993). There exists a strong lateral petrophysical variation in single porous dolomite beds over short distances (Baker and Knight, 1993).

6.3.1 Types of Porosity in the Catoche Formation

Three types of porosity occur within the Catoche Formation; intercrystalline, vuggy and stylo-porosity. Intercrystalline porosity features significant effective porosity and is commonly associated with dolomite 2 within the Costa Bay member (**Plates 3.21, 6.1 and 6.2**). Intercrystalline pores typically range from 20 to 200 μm in size and are usually polyhedral to tetrahedral in shape. Pores are commonly but not always connected creating an effective permeable network. The presence of intercrystalline porosity suggests dolomitization occurred under a closed or semi-closed system with local and limited sources for Mg and CO_3^{2-}. The incorporation of Mg into the crystal lattice of the mineral phase resulted in a reduction in the volume of the mineral phase. The decrease in volume of rock is thus accompanied by an increase in porosity (cf. Warren 2000). If the diagenetic system was open with unlimited sources of Mg and CO_3^{2-}, the results may have been total occlusion of open pore space due to uninhibited dolomite growth (Lucia and Major, 1994).

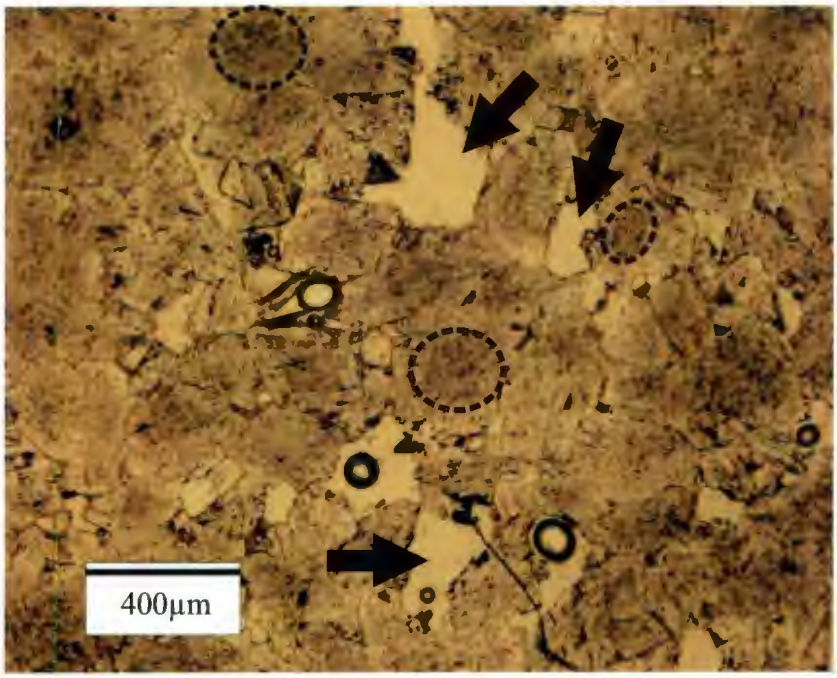

Plate 6.1. Intercrystalline porosity (black arrow) developed in dolomite 2. Ghosts of precursor peloids are present (black dashed circle) (TS MG - 27).

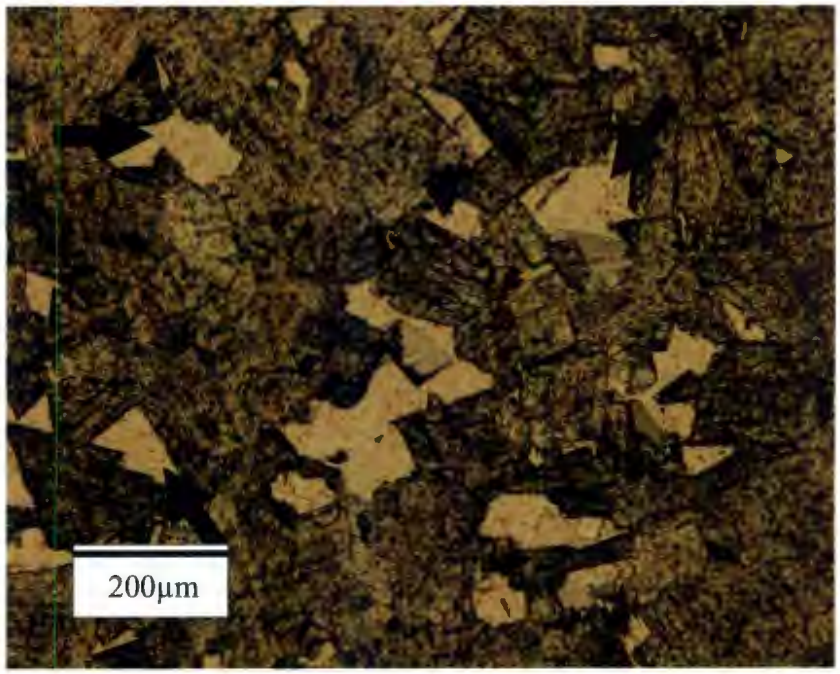

Plate 6.2. Intercrystalline porosity (black arrow) developed in dolomite 2. Porosity within this sample may be effective (TS MG - 20).

Vuggy porosity is also significant within the Catoche Formation, sometimes constituting 20 to 25% of a sample (**Plates 3.19, 3.20, 4.11, 4.12, 6.3 and 6.4**). Vugs typically range in size from 500 μm to a few millimeters and are separated from other vugs (**Plates 6.3 and 6.4**). Vugs may or may not be connected by intercrystalline porosity present within the matrix dolomite. Coarse dolomite crystals (D4) line vugs partially occluding pores and rare saddle dolomite (D5) post-dates D4. These vugs likely formed through aggressive dissolution by the earlier diagenetic fluids. It is possible that acidic basinal brines formed from the maturation of organic matter might have contributed to the development of the vugy pores (Feazel and Schatzinger, 1985) in the Catoche dolomites. Fluid inclusion data for D4 (Chapter 4) suggests temperatures of formation between 89.2 and 99.5°C and petrographical cross-cutting relationships indicate dissolution and formation of vugs post-dated stylolization suggesting that meteoric waters were not responsible for the formation of vuggy porosity but possibly the hot basinal brines.

Stylo-porosity is minor within the diagenetic dolostone of the Catoche Formation but appear to form effective porous conduits which theoretically might have aided in fluid flow (**Plate 3.22**). Stylolites form prior to the latest phases of dolomitization (D4 and D5) and locally appear to be flushed of stylo-cumulate producing channel-style porosity.

The occlusion of pores was halted with the termination of growth of D4 and D5. If the dolomitizing fluid became undersaturated with respect to Mg, a cessation in dolomite growth may have occurred. However, the presence of bitumen present within

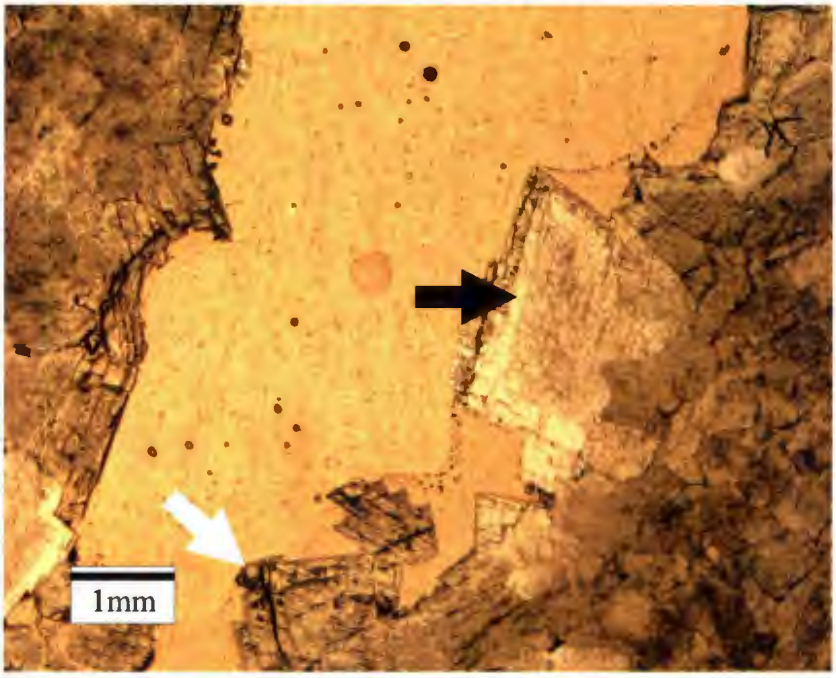

Plate 6.3. A photomicrograph of a large vug within the Catoche Formation. Dolomite 4 lines the pore wall (black arrow) and minor saddle dolomite is present (white arrow) (TS - MG 35).

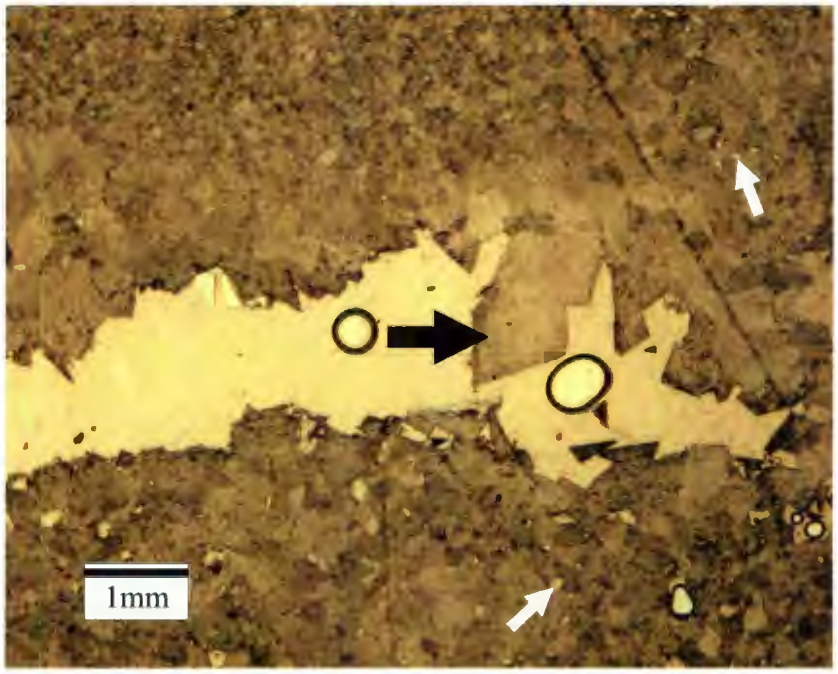

Plate 6.4. A photomicrograph of a large vug within the Catoche Formation. Dolomite 4 lines the pore wall (black arrow) and intercrystalline porosity (white arrow) is present in matrix dolomite (white arrow) (TS - MG 35).

some intercrystalline porosity and vugs might suggest that a hydrocarbon emplacement might have inhibited growth of late occluding dolomite cements.

6.4 Summary

Within the Catoche Formation of the St. George Group, porosity occurs mainly in the upper ~40m of diagenetic dolostone. Types of porosity present include intercrystalline porosity, vuggy porosity and stylo-porosity. Vugs make up the highest percentage of porosity (20 to 25% in some samples) but are not frequently interconnected and in many instances are isolated. Intercrystalline porosity (~10%) is usually less abundant than the vuggy porosity; however they are significantly better connected and thus forming effective porosity. The stylo-porosity, although rare, creates effective channels for fluid flow.

The preservation of porosity in the Catoche dolomites is likely related to restricted sources of late diagenetic fluids so that they did not occlude all pores. The emplacement of hydrocarbons likely inhibited further dolomitization and pore-space occlusion.

CHAPTER VII

CONCLUSIONS

The Catoche Formation of the St. George Group was deposited on an open-shelf subtidal setting and consists mainly of shallow water platform sediments. It consists of lower tidal muds, storm-generated gravel bars and/or tidal deposits, and tidal muds. The upper Costa Bay Member has been significantly affected by extensive dolomitization resulting in the development and preservation of porosity.

About 5 episodes of dolomitization have affected the Catoche Formation. The first episode (D1) formed from mimic replacement of limemud early in the diagenetic history. Trace elements, in particular the Sr/Ca molar ratio suggest an origin of mixed seawater/meteoric water for the earliest dolomitizing fluid. Stable and radiogenic isotopes support a mixed source origin for dolomite 1.

Dolomite 2 replaces burrows and packstone/grainstone. Dolomite 2 crystals have a bimodal size distribution with sizes ranges of 50 to 120 μm for a subhedral to euhedral form and an anhedral to euhedral ranging 150 to 250 μm. Cloudy cores are common in many D2 crystals and are usually surrounded with clear rims. Stable isotopes are depleted relative to D1 and the radiogenic strontium isotope signatures suggest that dolomitizing fluid may have circulated through siliciclastics prior to dolomitization. Strontium concentration patterns show an increase with depth suggesting a downward circulation of the dolomitizing fluid. Intercrystalline porosity is most commonly

associated with the euhedral and well developed D2 where dolomitization ceased prior to total occlusion of pore space.

Dolomite 3 is localized throughout the Catoche Formation and only occurs in association with stylolites and stylo-cumulate.

Dolomite 4 lines and partially occludes vugs in the upper ~40m of the Catoche Formation. Crystal sizes for D4 range from about 200 μm to several millimeters and are most commonly euhedral in shape. Fluid inclusion data yields homogenization temperatures from 89.2 to 99.5°C for D4 while the oxygen isotope signature of the dolomitizing fluid was calculated to range from 2.4 to -1.2 ‰ VSMOW which is consistent with an origin of evolved diagenetic waters enriched in ^{18}O likely due to circulation in the crustal rocks at deep burial settings. The associated dolomitizing fluids for D4 most likely migrated laterally through permeable beds that were deposited as peloidal shoals.

Dolomite 5 is saddle dolomite, minor in abundance and is relatively Fe-rich with respect to all other generations of dolomite within the Catoche Formation. Dolomite 5 occurs as fracture and biomold filling as well as very minor amounts lining vugs.

The most significant types of porosity within the Catoche dolostone are intercrystalline and vuggy porosity. Intercrystalline porosity is most often associated with D2 and suggests dolomitization occurred with a limited supply of Mg and/or CO_3^{2-}. Vugs may occur up to several millimeters in size and are only effective when adjacent to intercrystalline pores. Dissolution occurred prior to D4 and D4 commonly lines vugs.

Although partially occluded, dolomitization terminated early either due to a limited supply of Mg or the emplacement of hydrocarbons.

REFERENCES

Al-Aasm, I.S., Azmy, K., 1996. Diagenesis and evolution of microporosity of Middle-Upper Devonian Kee ScarpReefs, Norman Wells, Northwest Territories, Canada: petrographic and geochemical aspects. AAPG Bull., 80: 82–100.

Al-Aasm I.S., and Veizer J., 1986b. Diagenetic stabilization of aragonite and low-Mg calcite. II. Stable isotopes in rudists. J Sediment Petrol., 56: 763–770

Anderson, T. F., and Arthur, M. A., 1983, Stable isotopes of oxygen and carbon and their application to sedimentologic and paleoenvironmental problems, in Arthur, M. A., and Anderson, T. F., eds., Stable isotopes in sedimentary geology: Society of Economic Paleontologists and Mineralogists Short-Course 10, p. 1.1–1.151.

Azmy, K., Veizer, J., Misi, A., Oliveira, T.F. de, Sanches, A.L., Dardenne, M.A., 2001. Dolomitization and isotope stratigraphy of the Vazante Formation, São Francisco Basin, Brazil. Precambrian Res., 112: 303 - 329.

Azmy, K., Veizer, J., Wenzel, B., Bassett, M.G., Copper, P., 1999. Silurian strontium Isotope stratigraphy.GSABull., 111: 475–483.

Baker, D. and Knight, I., 1993. The Catoche dolomite project, Anticosti Basin, eastern Canada: CERR Report, Memorial University of Newfoundland, St. John's Newfoundland.

Banner, J.L., 1995. Application of the trace element and isotope geochemistry of strontium to studies of carbonate diagenesis. Sedimentology 42: 805–824

Bathurst, R. G. C., 1975. Carbonate Sediments and their Diagenesis, Developments in Sedimentology 12. Elsevier, Amsterdam: 658p.

Boggs, Jr., S., and Krinsley, D., 2006. Application of Cathodoluminescence Imaging to the study of Sedimentary Rocks. Cambridge University Press, New York, p 165.

Brand, U. and Veizer, J., 1980. Chemical diagenesis of a multicomponent carbonate system: 1. Trace elements. J. Sediment. Petrol., 50: 1219–1236

Brand, U. and Veizer, J., 1981. Chemical diagenesis of a multicomponent carbonate system: 2. Stable isotopes. J. Sediment. Petrol., 50: 987–997

Budd, D.A., 1997. Cenozoic dolomites of carbonate islands: their attributes and origin. Earth Sci. Rev., 42: 1–47.

Cawood, P.A., Dunning, G. R., Lux, D. and van Gool, J. A. M., 1994. Timing of peak metamorphism and deformation along the Appalachian margin of Laurentia in Newfoundland: Silurian, not Ordovician. Geology., 22: 399-402.

Choquette, P.W. and James, N.P., 1987. Limestones — the burial diagenetic environment. In: McIlreath, I.A., Morrow, D.W. (Eds.), Diagenesis. Geosci. Can. Repr. Ser., 4: 75–112.

Choquette, P.W., and Pray, L.C.,1970. Geologic nomenclature and classification of porosity in sedimentary carbonates. Bull. Am. Ass. petrol. Geol., 54: 207–250.

Clark, I.D. and Fritz, P., 1997. Environmental Isotopes in Hydrogeology. Lewis publisher, Boca Raton: 328p

.

Cooper, M., Weissenberger, J., Knight, I., Hostad, D., Gillespie, D., Williams, H., Burden, E., Porter-Chaudhry, J., Rae, D., and Clark, E. 2001. Basin evolution in western Newfoundland: new insights from hydrocarbon exploration. American Association of Petroleum Geologists, Bulletin, 85: 393–418. Dickson, J. A. D., 1966. Carbonate identification and genesis as revealed by staining. J. sedim. Petrol., 36: 491–505.

Diener, A., Ebneth, S., Veizer, J., Buhl, D., 1996. Strontium isotope stratigraphy of the Middle Devonian: brachiopods and conodonts. Geochim. Cosmochim. Acta, 60: 639–652.

Drever, J.I., 1988. The Geochemistry of Natural Waters. Prentice Hall, Englewood Cliffs, NJ, p. 437.

Faure G., and Mensing T. M., 2005. Isotope principles and applications. 3rd edn. John Wiley & Sons, NJ.

Flugel, E., 2004. Microfacies of Carbonate Rocks. Springer, Berlin: 976p.

Folk R.L., 1974. Petrology of sedimentary rocks. Hemphill, Austin, Texas, USA.

Goldstein, R.H. and Reynolds, T.J. 1994. Systematics of fluid inclusions in diagenetic minerals. SEPM Short Course, 31.

Hays, P.D., and Grossman, E.L., 1991. Oxygen isotopes in meteoric calcite cements as indicators of continental paleoclimate: Geology, 19: 441-444.

Haywick, D.W., 1984. Dolomite within the St. George Group (Lower Ordovician), western Newfoundland: M.Sc. thesis, Memorial University of Newfoundland.

Hoefs, J., 1997. Stable Isotope Geochemistry. 4th edn. Springer-Verlag, Berlin.

James, N.P., Choquette, P.W., 1988. Limestones - the meteoric diagenetic environment. In: McIlreath, I.A., Morrow, D.W. (Eds.), Diagenesis. Geosci. Can. Repr. Ser., 4: 35–73.

James,N.P. & Choquette,P.W., 1990. Limestones - the sea floor diagenetic environment. In: McIlreath, I.A., Morrow, D.W. (Eds.), Diagenesis. Geosci. Can. Repr. Ser., 4: 13–34.

James, N.P., and R.K. Stevens, 1986. Stratigraphy and correlationof the Cambro-Ordovician Cow Head Group, western Newfoundland:Geological Survey of Canada Bulletin, 366: 143.

Kerans, C., 1989. Karst-controlled reservoir heterogeneity in Ellenburger Group carbonates of West Texas: American Association of Petroleum Geologists Bulletin, 72: 1160-1183.

Knight, I., 1978. Platformal sediments on the Great Northern Peninsula: stratigraphic studies and geological mapping of the north St. Barbe district. In Gibbons, R. V. (ed.), Report of activities for 1977, Newfoundland Dept. Mines and Energy, Mineral Development Division, Rept. 78-1.

Knight, I., 1987. Geology of the Roddickton (12I/16) map area. In: Blackwood, R.F., Walsh, D. G., and Gibbons, R. V. , (eds.) , Current Research: Newfoundland Dept. Mines and Energy, Mineral Development Division, Rept. 87-1: 343-357.

Knight, I., 1991, Geology of Cambro-Ordovician in the Port Saunders (NTS 12I/ 1 1), Castors River (NTS 12I/15), St. John Island (NTS 12I/14) and Torrent River (NTS 12I/10) map areas: Newfoundland Department of Mines and Energy, Geological Survey Branch, Report 91-4.

Knight I. 1997. Ordovician dolomite reservoirs of the Port aux Choix area, Western Newfoundland: Report to Hunt Oil and Pan-Canadian Petroleum. 88 p.

Knight, I., Azmy, K., Greene, M.G. and Lavoie, D., 2007. Lithostratigraphic setting of diagenetic, isotopic, and geochemistry studies of Ibexian and Whiterockian carbonate rocks of the St. George and Table Head Groups, Western Newfoundland. Current Research: Newfoundland and Labrador Dept. of Natural Resources, Geological Survey, Report 07-1: 55-84.

Knight, I., and James, N.P., 1987. Stratigraphy of the St. George Group (Lower Ordovician), western Newfoundland; the interaction between eustasy and tectonics. Can. Jour. Earth Sci., 24: 1927-1952.

Knight, I., James N. P., and Lane, T. E., 1991. The Ordovician St. George unconformity, northern Appalachians: the relationship of plate convergence at the St. Lawrence Promontory to the Sauk/Tippecanoe sequence boundary. Geological Society of America Bulletin, 103: 1200-1225.

Land, L.S., 1983. The application of stable isotopes to studies of the origin of dolomite and to problems of diagenesis of clastic sediments. In: Arthur, M.A., Anderson, T.F.,Kaplan, I.R., Veizer, J., Land, L.S. (Eds.), Stable Isotopes in Sedimentary Geology. SEPM Short Course Notes 10, 4-1–4-22.

Land, L.S., 1992. The dolomite problem: stable and radiogenic isotope clues. In: Clauer, N., Chaudhuri, S. (Eds.), Isotopic Signature of Sedimentary Records. Lecture Notes in Earth Science 43: 49–68.

Lane, T .E., 1990. Dolomitization, Brecciation and Zinc Mineralizaiton and Their Paragenetic, Stratigraphic and Structural Relationships, Upper St. George Group (Ordovician) Daniel's Harbour, Western Newfoundland. Unpubl. Ph.D. thesis, Memorial University of Newfoundland, St. John's, Newfoundland: 565p.

Langdon, G. S., and Mireault, R. 2004, Revised exploration model for the inversion fairway, western Port au Port, Penensula, Newfoundland: A report for Canadian Imperial Venture Corp., St. John's, Newfoundland: 50 p.

Lavoie, D. and Morin, C, 2001. Hydrothermal dolomitization in the Lower Silurian Sayabec Formation in northern Gaspe-Matapedia (Quebec); constraint on timing of porosity and regional significance for hydrocarbon reservoirs: Bulletin of Canadian Petroleum Geology, 52, p. 256-269.

Lucia, F. J., and Major R. P., 1994. Porosity evolution through hypersaline reflux dolomitization, in B. Purser, M. Tucker, and D. Zenger, eds., Dolomites: International Association of Sedimentologists Special Publication 21: 325-341.

Machel, H-G. & Burton, E. A., 1991. Factors governing cathodoluminescence in calcite and dolomite, and their implications for studies of carbonate diagenesis. In: Luminescence Microscopy: Quantitative and Qualitative Aspects (Ed. by C. E. Barker & O. C. Kopp), Soc. econ. Palaeont. Miner., Dallas, Short Course, 25, 37–57.

Machel, H-G., Mason, R., Mariano, A. N. & Mucci, A., 1991. Causes and emission of luminescence in calcite and dolomite. In: Luminescence Microscopy: Quantitative and Qualitative Aspects (Ed. by C. E. Barker & O. C. Kopp), Soc. econ. Palaeont. Miner., Dallas, Short Course, 25, 9–25.

Milliman, J.D., 1974. Marine Carbonates. Springer-Verlag, New York.

Moore, C.H., 2001. Carbonate Reservoirs: Porosity Evolution and Diagenesis in a Sequence Stratigraphic Framework. Developments in Sedimentology, 55. Elsevier, Amsterdam: 444 p.

Ozawa, L., 1990. Cathodoluminescence: Theory and Applications, VCH, Basel, Switzerland.

Pagel, M., Barbin, V., Blanc, P., and Ohnenstetter, D., 2000. Cathodoluminescence in geosciences. Springer, Berlin Heidelberg New York Tokyo, 514 p

Shields, G.A., Carden, G.A.F., Veizer, J., Meidla, T., Rong, J.-Y. and Li, R.-Y., 2003. Sr, C, and O isotope geochemistry of Ordovician brachiopods: a major isotopic event around the Middle–Late Ordovician transition. Geochim. Cosmochim. Acta 67, pp. 2005–2025.Stenzel, S.R., and James, N.P., 1987: Death and destruction of an early Paleozoic carbonate platform, western Newfoundland. Abstr., SEPM Annual Mtg., Austin, Texas, p. 80.

Tucker, M.E., 2001. Sedimentary Petrology. Third Edition. Blackwell Publishing: 261p

Tucker, M. E., and Wright, V. P., 1990. Carbonate sedimentology. Blackwell Scientific Publications, 482 p.

Pratt, B.R., James, N.P., Cowan, C.A., 1992. Peritidal carbonate. In: Walker, R.G., James, N.P. (Eds.), Facies Models, Response to Sea Level Change. Geol. Assoc. Can.: 303–322.

Pratt, B.R., and James, N.P., 1982. Cryptalgal-metazoan bioherms of Early Ordovician age in the St. George Group, western Newfoundland. Sedimentology, 29: 543-569.

Pratt, B.R., and N.P. James, 1986: The tidal flat island model for peritidal shallow-upward sequences; St.George Group, western Newfoundland. Sedimentology, 33: 313-344.

Vahrenkamp, V.C., and Swart, P.K., 1990. New distribution coefficient for the incorporation of strontium into dolomite and its implications for the formation of ancient dolomites. Geology, 18: 387-391.

Veizer, J., 1983. Chemical diagenesis of carbonates: theory and application of trace element technique: AAPG Continuing Education course note series, no. 10, p. 3.1-3.100.

Veizer, J., Ala, D., Azmy, K., Bruckschen, P., Bruhn, F., Buhl, D., Carden, G., Diener, A., Ebneth, S., Goddris, Y., Jasper, T., Korte, C., Pawellek, F., Podlaha, O., Strauss, H., 1999. $^{87}Sr/^{86}Sr$, ^{18}O and ^{13}C evolution of Phanerozoic seawater. Chem. Geol. 161: 59–88.

Warren, J., 2000. Dolomite: occurrence, evolution and economically important associations. Earth-Sci. Rev. 52: 1–81.

APPENDIX I

CHEMICAL AND ISOTOPIC RESULTS

Chemical data are represented by concentrations of the studied trace elements recalculated on the total carbonate basis. Ca is in %; Mg, Sr, Mn, and Fe are in ppm; $\delta^{18}O$ and $\delta^{13}C$ are in ‰ relative to PDB. The abbreviations used are as follow: **C1** lime mud, **D(1 through 5)** dolomite generations 1 through 5, and **Cv** vein/biomold filling calcite cement.

Sample	Formation	Cement	Depth (m)	$\delta^{18}O$	$\delta^{13}C$	$CaCO_3$%	$MgCO_3$%	Mn(ppm)	Sr(ppm)	Fe(ppm)	Sr^{87}/Sr^{86}	±2σ
1	Catoche	C1	58.37	-	-	96.12	3.88	79	482	1392		
5	Catoche	C1	51.4	-	-	94.56	5.44	77	328	2220		
103	Catoche	C1	163.95	-	-	98.73	1.27	53	307	1904		
106	Catoche	C1	158.9	-	-	98.82	1.18	70	337	1486		
108	Catoche	C1	140.5	-	-	98.64	1.36	57	300	1001		
110	Catoche	C1	129.85	-	-	97.31	2.69	39	395	1224		
113	Catoche	C1	119.85	-	-	98.46	1.54	38	313	1890		
115	Catoche	C1	113	-	-	97.98	2.02	36	366	1889		
117	Catoche	C1	102.5	-	-	98.51	1.49	36	415	2254		
123	Catoche	C1	81	-	-	98.81	1.19	36	436	1106		
125	Catoche	C1	73.4	-8.63	-1.79	93.91	6.09	37	413	2874		
129	Catoche	C1	57.6	-	-	94.02	5.98	70	290	827		
131	Catoche	C1	50.2	-	-	98.71	1.29	66	320	822		
9	Catoche	D1	49	-6.71	-0.60	57.45	42.55	103	71	3288		
9	Catoche	D1	49	-6.63	-0.8	56.20	43.80	66	72	3237		
27	Catoche	D1	30.9	-9.05	-0.38	58.02	41.98	143	31	2096		
40	Catoche	D1	15.9	-8.09	-0.8	54.98	45.02	138	51	2304	0.708867	0.000008
44	Catoche	D1	11.9	-7.2	-0.6	56.18	43.82	147	34	1721		
49	Catoche	D1	5.3	-7.02	-1.09	57.51	42.49	63	70	2378		
MG-401-Df	Catoche	D1	83	-6.78	-1.34	60.32	39.68	183	83	5349		
131A	Catoche	D1	50	-6.69	-0.46	60.13	39.87	72	161	4631		
7	Catoche	D2	50.4	-9.72	-0.64	57.05	42.95	81	47	7063	0.710803	0.000007
11	Catoche	D2	46.9	-9.30	-0.59	56.96	43.04	87	30	1480	0.709757	0.000026
19	Catoche	D2	38.9	-9.13	-0.46	54.78	45.22	75	36	2482		
24	Catoche	D2	33.9	-8.6	-0.52	53.54	46.46	77	31	2221	0.708989	0.000010
29	Catoche	D2	26.9	-9.3	0.14	56.49	43.51	65	34	2812		
38	Catoche	D2	17.9	-8.34	-0.76	53.64	46.36	84	32	2379	0.709036	0.000008
41	Catoche	D2	14.9	-7.7	-0.6	57.26	42.74	108	39	2280		
46	Catoche	D2	8.6	-10.16	-1.3	56.25	43.75	85	30	2949		
50	Catoche	D2	4.1	-9.67	-1.22	57.10	42.90	86	37	3518		
106	Catoche	D2	158.9	-6.93	-0.93	63.61	36.39	97	139	12030		
119	Catoche	D2	93.6	-6.86	-1.96	66.74	33.26	88	204	14974		
113	Catoche	D2	119.85	-7.67	-0.9	64.34	35.66	78	127	12164	0.710137	0.000009
110	Catoche	D2	129.85	-7.15	-0.36	62.08	37.92	79	95	12110		

Sample	Formation	Cement	Depth (m)	$\delta^{18}O$	$\delta^{13}C$	$CaCO_3$%	$MgCO_3$%	Mn(ppm)	Sr(ppm)	Fe(ppm)	Sr^{87}/Sr^{86}	±2σ
126	Catoche	D2	72.2	-9.75	-1.15	59.59	40.41	101	63	7389		
123	Catoche	D2	81	-6.1	-1.7	62.12	37.88	56	156	6233		
53	Catoche	D3	0.7	-9.6	-0.9	56.90	43.10	138	34	1628		
31	Catoche	D3	24.9	-9.31	-0.15	57.03	42.97	121	33	1259		
31	Catoche	D3	24.9	-9.83	-0.19	55.60	44.40	73	31	2254		
126	Catoche	D3	72.2	-9.15	-1.50	62.24	37.76	173	66	6400	0.709455	0.000012
117	Catoche	D3	102.5	-8.46	-1	64.83	35.17	89	159	13659	0.709787	0.000007
122A	Catoche	D3	82.5	-9.37	-1.7	61.65	38.35	64	78	8393		
124	Catoche	D3	76.9	-8.81	-1.58	61.49	38.51	85	147	9389		
126	Catoche	D3	72.2	-8.23	-1.18	58.11	41.89	84	66	5431	0.710206	0.000008
130	Catoche	D3	51.2	-10.94	-0.63	58.19	41.81	93	53	3292		
402-DA	Catoche	D3	83	-9.38	-1.6	58.73	41.27	257	69	4774		
402	Catoche	D3	83	-8.81	-1.31	58.74	41.26	174	77	5481		
32	Catoche	D4	23.9	-9.83	-1.12	55.58	44.42	189	32	1056		
28	Catoche	D4	27.9	-9.94	-1.08	56.25	43.75	225	26	1494		
43	Catoche	D4	12.8	-10.08	-1.37	56.28	43.72	271	30	1736		
53	Catoche	D3 and D4	0.7	-10.18	-1.1	53.82	46.18	77	34	2775	0.708938	0.000009
34	Catoche	D4	21.9	-9.82	-1.28	55.73	44.27	186	27	1138		
53	Catoche	D4	0.7	-10.68	-1.27	56.44	43.56	257	27	1833		
33	Catoche	D4	22.9	-10.24	-0.83	55.00	45.00	204	32	1202	0.709044	0.000013
23	Catoche	D4	34.9	-9.94	-1.01	55.63	44.37	273	31	1641	0.709464	0.000018
15	Catoche	D4	42.9	-10.26	-0.58	53.60	46.40	62	33	2042		
13	Catoche	D4	44.9	-9.64	-1.01	55.91	44.09	435	40	5600		
17	Catoche	D4	40.9	-9.64	-1.01	54.63	45.37	192	27	1311		
19	Catoche	D4	38.9	-9.34	-0.81	55.38	44.62	158	29	1135		
24	Catoche	D4	33.9	-8.53	-0.68	55.85	44.15	132	29	853		
35	Catoche	D4	20.9	-9.99	-1.02	55.83	44.17	205	26	1510		
402		D4	83	-9.57	-1.53	59.79	40.21	244	58	4881		
46	Catoche	D4	8.6	-9.6	-1.37	55.63	44.37	190	26	1144		
108	Catoche	D5	140.5	-9.83	-1.31	63.84	36.16	295	83	13629		
114	Catoche	D5	115	-9.67	-0.65	60.49	39.51	485	62	29279		
108	Catoche	D5	140.5	-9.19	-1.38	76.95	23.05	434	88	25677	0.708871	0.000008
121A	Catoche	D5	83.5	-10.77	-1.48	59.45	40.55	240	52	11945		
401-Cv	Catoche	Cv	83	-7.64	-2	98.94	1.06	89	97	446		